UNIVERSITA' DEGLI STUDI DI NAPOLI FEDERICO II

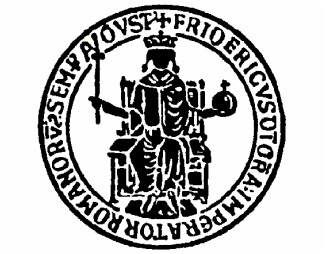

Dottorato di Ricerca in Ingegneria Chimica
(XXI Ciclo)

Catalytic microcombustion for portable electric power generation

Scientific Committee:
Prof. Gennaro Russo
Prof. Paolo Ciambelli
Prof. Francesco Gioia

Author:
Andrea Scarpa

ABSTRACT

In this Ph. D. thesis the main issues in catalytic micro-combustion will be explored with the conclusive aim to develop efficient combustors exhibiting a operating window wide enough to make possible their application in portable power generation.

Particular attention will be devoted to the preparation of catalytic micro-structured reactors for the combustion of C_3H_8, H_2, CH_4 and H_2-CH_4. A preparation method is developed to depose efficaciously the active phase on inert substrates of different materials (Cordierite, α-Al_2O_3 and FeCralloy) and in the form of both monoliths and platelets. Cheap and stable active phase constituted by supported perovskite, γ-Al_2O_3/$LaMnO_3$ has been prevalently considered. However, the effect of promoting perovskite with a little amount of platinum has been taken into account and, thus, Pt/Al_2O_3 catalyst are prepared and tested as reference material too.

A novel single channel planar catalytic reactor (SSR) is developed for the study of diluted combustion of H_2, CH_4 and H_2-CH_4 up to a maximum temperature of 800°C. Such a reactor gives the possibility to modulate the combustion chamber height thus allowing to study in depth the particular interaction between heterogeneous and homogeneous combustion. In particular, SSR will show its maximum relevance in understanding the chemical synergy in H_2 assisted CH_4 combustion.

Combustion under auto-thermal conditions has been studied too. In particular, ignition and quenching of C_3H_8, H_2, CH_4 and H_2-CH_4 combustion have been investigated in a large spectrum of operating conditions. Particular attention has been devoted to novel heat-recirculation reactors. In particular, in order to experimentally verify the role of heat recovery on combustion stability, a quartz reactor easy to run both in heat-recirculation and in no-recirculation reactor modes is developed. The simple geometry of the proposed reactor enables to obtain fundamental understanding of the effect of heat recirculation and on the instability mode in the limit of low conductive reactor walls.

Micro power generators have been developed by coupling catalytic combustors with thermoelectric modules. In particular, an innovative solution consisting on the integration of multiple pass heat-recirculating combustors with TEs is proposed.

Part of the present work and specifically the study on heat recirculation combustors and electricity generators (discussed in the chapters 6 and 7) has been performed at University of Delaware in the research group of Professor Vlachos.

INDEX

CHAPTER 1

INTRODUCTION

1.1 Portable power generation using catalytic combustion

The remarkable advances experienced in the last few years in high precision techniques allow the development of smaller and smaller electronic devices for portable use like mobile phone and laptops (Fernandez-Pello, 2002). Moreover, the growing trend in the miniaturization of electro-mechanical engineering systems till to a characteristic dimension of the order of micron has given rise to a novel technological area named MEMS (micro electro-mechanical systems) mainly involved in the fabrication of sensors and actuators but also of more complex systems like pumps and motors (Fernandez-Pello, 2002). In the future, at the same time as the development of such systems it is expected a rise in the demand of high energy density power sources for portable use with small-size, low weight and long duration.

The power of interest in such applications ranges from milliwatts to watts but may be of the order of kilowatts in the automotive field. Conventional power supply in all these cases is constituted by batteries. However, the low energy density of this kind of systems contributes to the excessive weight and bulk of portable equipment and severely limit the duration of operations using portable electronic devices. This aspect is very critical in the case of MEMS where the power source may constitute a large fraction of both mass and volume of the entire device.

Alternatively to batteries technology it has been recently proposed the use of electric portable power sources based on combustion (Fernandez-Pello, 2002). The concept behind this emerging research field is the higher specific energy of a liquid fuel compared to that of a battery. By the comparison of propane and iso-octane energy density with that of a Lithium ion battery, reported in Figure 1.1, it results that a fuel is 13 and 40 times energetically denser as regards the unit of volume and of weigh respectively. It follows that combustion is able in theory to overcome the current State-of-the-Art in portable power production by slashing the weight and size of the ultimate electronic device.

The high combustion potential in micro-power generation is driving the research efforts towards the development of conversion system of the thermal power into electricity suitable for portable applications. However, based on the values of energy density above reported, in order to equal battery performances a quite low thermal to electrical conversion efficiency, $\eta=2.5\div7.5\%$ is

required. Moreover, in many applications even a lower efficiency may result successful considering that a fuel based generator could be much more easy to recharge not requiring any electric power cost. In particular, the latter aspect points out the relevance of the proposed technology in overcoming any barrier to the use of portable technologies in remote places. As a result efficiency doesn't constitute the key parameter in the development of these new conception generators for the benefit of other ratings such as compactness, operation flexibility, durability, the maintenance requested.

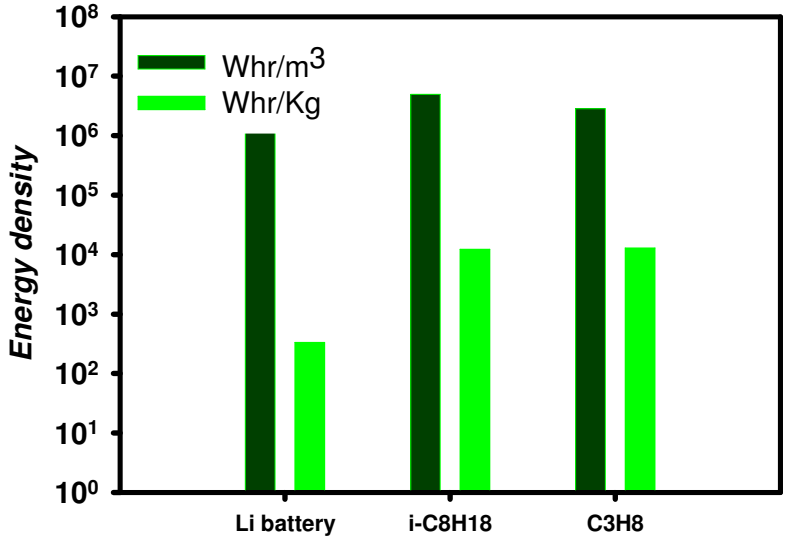

Figure 1.1 *Specific energy for iso-octane, propane and Lithium polymer battery. Data reported both in the units of weight and volume. Data for propane and iso-octane derived from Perry and Green (1997). Energy density in the unit of weight of a Li battery are derived from Palo et al. (2002). Energy density of a Li battery in the unit of volume derived from that in the unit of weight by considering the typical weight and the volume of a mobile phone battery.*

The necessity of miniaturized electro-mechanical devices places at micro-scale the major interest in combustion. Despite of the great technological interest, combustion application in portable electricity generation field stays within the ambit of research involving some serious problems far from being solved. In particular, the characteristic length scale involved in this application is typically below the millimeter and is strongly unfavourable to the propagation of flame being of the same order of the quenching diameter of the most common fuels (see Table I.1). Basically, by decreasing the combustor size the surface-to-volume ratio increases thus exalting the wall-effects on the process. More specifically, reactor wall behaves as a sink for the heat and the radicals released via combustion causing either thermal or radical quenching of the process (Miesse et al., 2004).

However, it is possible to sustain a flame below quenching distances. Careful materials choice and high temperature annealing treatment may minimize radical quenching (Miesse et al., 2004). Still, a proper thermal management may further prevent quenching involving an increase in the combustion temperature. Such an intent is pursued in literature through the development of novel combustors based on heat-recovery (Vican et al., 2002, Ronney, 2003, Kaisare and Vlachos, 2007, Kuo and Ronney, 2007, Kim et al., 2007, Ahn et al., 2007, Federici and Vlachos, 2008, Federici et al., 2009). The principle lies in recovering part of the sensible heat of the exhaust gas to preheat the cold incoming; as a result, combustor can operate at super adiabatic temperatures reducing wall quenching (Vican et al., 2002).

Table I.1 *Quenching diameters of combustion of different fuel/air mixtures under stochiometric conditions (Barnard e Bradley, 1985).*

Combustibile	***D_Q [mm]***
H_2	0.6
CH_4	2.5
C_3H_8	2.1
i-C_8H_{18}	2.1

Even if it is theoretically possible to sustain combustion in the gas phase at the micro-scales material life time is strongly compromised by the high required temperatures. Moreover, gas phase combustion at the micro-scales exhibit a very narrow operating window (Kaisare and Vlachos, 2007, Kaisare et al., 2008). On the contrary, the use of a catalyst may easily overcome these disadvantages (Vican et al., 2002, Karagianidis et al., 2007, Ahn et al., 2007, Kaisare et al., 2008). The use of a catalyst, in fact, allows combustion to occur in faster and non-inhibited way, while also enlarging the range of the process operability and allowing high combustion efficiency even in lean conditions. As a result, catalytic microcombustion may be sustained at significantly lower temperature compared to its homogeneous counterpart thus minimizing concerns as regards materials durability. Moreover, a catalyst allows a better distribution of power released via combustion thus increasing the efficiency of thermal to electrical conversion system (Yang et al., 2005). Finally, catalytic combustors are more safe compared to their homogeneous counterparts and it is commonly reported that the presence of a catalyst inhibits flame (Wang et al., 2001, Veser, 2001, Karagiannidis et al. 2007, Norton et al., 2004).

Based on these considerations catalytic combustion is very appealing in micro-generation field. However, even if the use of a catalyst undoubtedly enhances combustion performances it cannot

avoid instabilities due to the pronounced dissipative nature of microsystems (Norton and Vlachos, 2005, Ahn et al., 2007, Karagianidis et al., 2007, Kaisare et al., 2008, Federici et al., 2009).

Moreover, the typical low electric power at stake requires to minimize the gas pumping cost. As a results, minimum pressure drops are required in gas flowing through the system thus making more technologically valid structured catalysts compared to a packed bed reactors. However, development of micro-structured reactors for combustion applications and energy production is not a trivial matter. Deposition techniques of catalytic layers are well-established in the case of honeycomb monoliths (Zwinkels et al., 1999, Cimino et al., 2001, Valentini et al., 2001, Fabbrini et al., 2005). However, in microcombustion field a growing interest is devoted to planar substrates like platelets. The scientific literature on preparation of catalyst in the form of platelets is relatively young thus leaving unexplored many practical aspects. For this kind of substrates the only investigated active phase is constituted by noble metals and specifically by platinum (in the most of cases, Kusakabe et al., 2001, Vican et al., 2002, Spadaccini et al., 2003, Norton et al., 2004, Suzuki et al., 2004, Yang et al., 2005, Norton et al., 2006) and palladium (Wang et al., 2001). In few cases active phase has been supported by an high specific surface support constituted by a washcoat of γ-Al_2O_3 (Wang et al., 2001, Vican et al., 2002). Alternatively, γ-alumina is formed through anodic oxidation of aluminum (Suzuki et al., 2004, Norton et al., 2006). The active phase is often unsupported and deposed directly on the substrate through electro beam deposition (Spadaccini et al., 2003), sputtering (Kusakabe et al., 2001) and wet impregnation (Yang et al., 2005, Norton et al., 2004). In all the case no information is provided concerning the repeatability of deposition method, catalyst anchoring on the substrate and eventual chemical/thermal de activation of the catalyst.

1.2 Instabilities in small scales combustion: heat recovery strategies

Loss of combustion stability occurs either via extinction or blowout (Norton and Vlachos, 2004, Kaisare et al., 2008, Ronney, 2003, Karagianidis et al., 2007). In extinction, stability is lost due to large heat losses compared to the power provided via combustion. In blowout, quenching occurs because of low residence time, resulting in incomplete fuel conversion and a considerable shift of the reaction front downstream. As a results, in microscales stable combustion occurs in a limited operating window and the challenge is to adopt a careful combustor design to enlarge it.

The wall thermal conductivity certainly plays a relevant role. Particularly, it needs to be sufficiently high to provide ignition of the cold incoming gas but it is responsible, at the same time, for the heat losses exhibited by the system. As a results, wall thermal conductivity needs to be balanced in order to provide enough preheating such as to avoid blowout but limit heat losses to prevent extinction.

Similar considerations are valid in the case of gas velocity. Particularly, it is suggested a tradeoff regarding the total flow rate that needs to be balanced in order to generate sufficient power to prevent extinction but avoid blowout.

As already reported, an approach to enhance microcombustion stability is based on heat recovery. Heat-recovery systems include the reverse flow reactor and the heat recirculation reactor, whose effectiveness in enhancing combustion stability has been studied theoretically and experimentally (Vican et al., 2002, Ronney, 2003, Kaisare and Vlachos, 2007, Kuo and Ronney, 2007, Kim et al., 2007, Ahn et al., 2007, Federici and Vlachos, 2008, Federici et al., 2009). In reverse flow reactor the flow direction is periodically reversed to trap a hot zone within the reactor (Kaisare and Vlachos, 2007). A heat-recirculation combustor is equipped with a counter-current heat exchanger that transfers the heat from the hot exhaust gas to the in-coming reactants (Ronney, 2003, Federici and Vlachos, 2008, Federici et al., 2009). One of the most effective heat-recovery configuration for micro-combustor is constituted to date by the swiss-roll, where the counter-current heat recirculation reactor is coiled up allowing a combustion chamber at its center (Vican et al., 2002, Kuo and Ronney, 2007, Kim et al., 2007, Ahn et al., 2007).

Many theoretical studies report heat recovery strategy is effective in preventing blowout (Kaisare and Vlachos, 2007, Federici and Vlachos, 2008). Compared to a single channel reactor (without heat recirculation) a heat-recovery based reactor allows a strong decrease in the optimum reactor wall thermal conductivity thus involving a much more efficient heat transfer of the power released by combustion towards the cold reactants (Norton and Vlachos, 2004, Kuo and Ronney, 2007). It is theoretically found that a more efficient heat transfer in heat recirculation reactors is due to a change in the pre-heating mechanism of incoming gas. As already reported, in a single channel combustor the latter occurs via axial heat transfer through the reactor walls. On the contrary, in a heat recirculation reactor the pre-heating of incoming reactants occurs through transverse heat transfer from countercurrent recirculation gases (Federici and Vlachos, 2008, Ronney, 2003). However, from theoretical studies, such an enhancement in heat transfer rate is effective only in the limit of low conductive reactor walls. In the case of highly conductive wall, in fact, it is reported that the rate of axial heat transfer through the reactor wall may be faster than that ruled by the transverse thermal gradiend (Federici and Vlachos, 2008, Ronney, 2003). Similar results are obtained in the case of reverse flow reactor: even is this case, in fact, heat recovery is effective only in the limit of low conductivity materials (Kaisare and Vlachos, 2007).

Despite the important ramifications for microcombustion, theoretical results concerning the effects of heat recovery on combustion stability as well as the effect of wall conductivity are not satisfactorily experimentally validated. Experiments with metallic (stainless steel) heat recirculation

reactor have indeed confirmed the marginal improvement in stability with heat recirculation (Federici et al., 2009). However no direct experimental validation still exists for the most exciting regime of low conductivity materials. Low conductivity materials, in fact, cannot easily be machined thus making the fabrication of micro-reactor extremely difficult.

1.3 Catalyst for combustion applications

Noble metals, in particular platinum and palladium, are the most active catalysts for catalytic combustion of hydrocarbons; their high activity at low temperatures has made possible their applications as catalytic converters (Seiyama, 1992). Nevertheless noble metals are very expensive and their use is not suitable in high temperature applications. It is known, in fact, these catalytic systems lose activity at high temperature, because of sintering and volatilization phenomena. Moreover, palladium, less volatile than platinum, exhibits a pronounced chemical instability at high temperatures in consequence of which the activity is considerably reduced. The active phase for combustion is palladium oxide which however tends to decompose in metallic phase: generally PdO is stable at temperatures lower than 1055 K and beyond this temperature the reduction to the metallic phase takes place (Lyubovsky et al., 2003). The transition from oxide phase to metal phase is reversible but re-oxidation is a very slow phenomenon and, besides, is characterized by hysteresis.

These restrictions justify the employment of noble metals just when high activity is required at very low temperatures (Gélin et al., 2003); in many applications, as micro-combustors, cheaper and more thermally and chemically stable materials are preferred, despite of a lower activity. In catalytic combustion, transition metals meet these requests; they may be used as simple oxides (Liu and Stephanopoulos, 1995, Bozo et al., 2000, Choudhary et al., 2002, Kirchnerova et al., 2002, Wierzba and Depiac, 2004,), but also as mixed oxides in structures as perovskites and as dopant substances in exa-aluminate for employment at temperatures higher than 1000°C (Zwinkels et al., 1999).

In particular, a growing interest in catalysis concerns perovskites-type oxides. They are ternary compounds, characterized by an ABO_3 structural formula. B cations are constituted by a transition metal and are octahedrally coordinated by oxygen; A cations are lanthanoid elements placed in the lattice vacancies (Tejuca et al., 1989, Seiyama, 1992, Forni and Rossetti, 2002). The transition metal gives to the structure high catalytic activity, whereas A cation is responsible for thermal stability of the material. Both two cations may be partially substituted by other cations, causing the formation of structural defects which influence catalytic activity of the material (Seiyama, 1992). The activity of perovskites in oxidation reactions is ascribed to structural defects involving cation

vacancies in their lattice. As a result, an extra oxygen may be accommodated in these systems thus causing their typical nonstochiometry (Tejuca et al., 1989). Indeed, such extra oxygen plays a determinant role in high temperature Mars-Van-Krevelen oxidation mechanism being much more reactive than that transferred to the surface from the gas phase (Forni and Rossetti, 2002).

Among the most studied perovskites there are those constituted by lanthanum; whereas among transition metals chrome (Saracco et al., 1996, Zwinkels et al., 1999, De Collongue et al., 1991), cobalt (Fabbrini et al., 2005, O'Connel et al., 1999; Alifanti et al. 2005; Kirchnerova et al., 2002), manganese (Saracco et al., 1999, Arnone et al., 1998; Cimino et al., 2000; Cimino et al., 2001; Cimino et al., 2003) and iron (Kirchnerova and Klvana., 2003) have been proposed. Among different perovskites $LaMnO_3$ is one of the most active (Saracco et al., 1999, Marchetti e Forni, 1998).

Perovskites are very cheap and thermally stable; moreover, under particular conditions, they have the same activity of a noble metal based catalysts (Seiyama et al., 1992, Alifanti et al., 2005). The use of perovskites is limited because of their low specific area (De Collongue et al., 1991). In order to improve this property it is possible to disperse perovskite on a support such as to enhance the specific area and the mechanical resistance of the material (Cimino et al., 2000). One of the most employed support is γ-Al_2O_3, characterized by a specific area of about 200 m^2/g. Nevertheless, close to 1000°C, γ-alumina undergoes a phase transition to α-alumina, which exhibits a lower specific area. In order to overcome such an inconvenient, it has been proposed to kinetically inhibit γ to α phase transition, by adding small quantities (typically 5wt % as regards the total amount of support is considered enough) of lanthanum oxide to the γ-alumina lattice (Arai e Machida., 1996).

In order to increase perovskites activity in combustion reactions, the use of bi-functional catalysts has been proposed, in which perovskite phase is promoted by small quantities of noble metal (Cifà et al., 2003, Kucharczyk and Tylus, 2004, Cimino et al., 2004, Civera et al., 2005, Uenishi et al., 2005, Petrovic et al., 2005, Cimino et al., 2007, Giebeler et al., 2007). Perovskite, besides exhibiting its own catalytic activity, may be an ideal environment to host noble metals involving an high dispersion of the active phase such as to avoid noble metal volatilization and sintering. Moreover, particular synergies may occur especially due to eventual interactions of the noble metal with the extra oxygen in perovskites lattice. On the other hand, the noble metal, even if in small quantities but well-dispersed, may increase catalyst activity at low temperature. Despite numerous studies concerning catalytic combustion on Pd-perovskite catalysts (Cimino et al., 2004, Cimino et al., 2007, Uenishi et al., 2005, Petrovic et al., 2005, Cifà et al., 2003, Kucharczyk e Tylus, 2004, Civera et al., 2005), Pt-perovskites are almost unexplored. However platinum is the

most active catalyst for combustion of hydrogen, propane and butane fuels (Choudhary, 2002), widely investigated in microcombustion, making interesting its application as perovskites dopant.

Based on the few published data (Giebeler et al., 2007) platinum promoting is not effective in enhancing perovskites activity in methane combustion at least on oxidized samples. However, a more detailed investigation is needed to evaluate the activity of mixed phase catalyst with respect to single phase, both perovskites and platinum catalysts for different fuels combustion.

1.4 Considerations as regards fuel choice

Specific energies of different fuels are reported in Figure 1.2.

Heating value of liquid fuel in the unit of volume is higher than that of a gas fuel up to three magnitude orders. Consequently, liquid fuels are very appealing in small scale, portable application where the overall size of the electricity generators is the key parameter. However, the use of a liquid fuel shows some disadvantages in microcombustion applications, mainly due to the need to obtain its atomization and mixing with oxygen at micro-scales. At this proposal, complex atomizing and micro-mixing systems have been proposed in literature (Deng et al.,2007). In order to overcome such a drawback the use of condensable fuels like propane and butane may be preferred. Actually, they may be stocked in liquid phase at relatively low pressure (2÷3 bar) while are gaseous at atmospheric pressure. From a technological point of view the stocking pressure may be employed for gas pumping without additional electrical costs.

Due to the attempt of controlling CO_2 emissions, it is to be hoped the use of fuels exhibiting high H/C ratios, especially in applications (like automotive one) involving a developed power of the order of kilowatts. Gaseous fuels meet such a requirement exhibiting a $H/C \geq 3$ further showing high specific power for mass unit. Among gas fuels methane is the widest used fuel in energy production field because it is abundant and well-distributed all over the planet. However methane is also a very stable molecule and, consequently, very difficult to burn. On the other hand, the interest in hydrogen is very strong too. It is one of the most reactive and intrinsically clean fuel; on the contrary, safety issues makes its distribution, stocking and employing in industrial applications a very complex matter. In the last years the scientific interest is moving towards the study of CH_4-H_2 mixtures combustion. CH_4-H_2 fuel couples synergistically the properties of hydrogen and methane thus constituting a fuel that is reactive and clean but also safe and well-distributed.

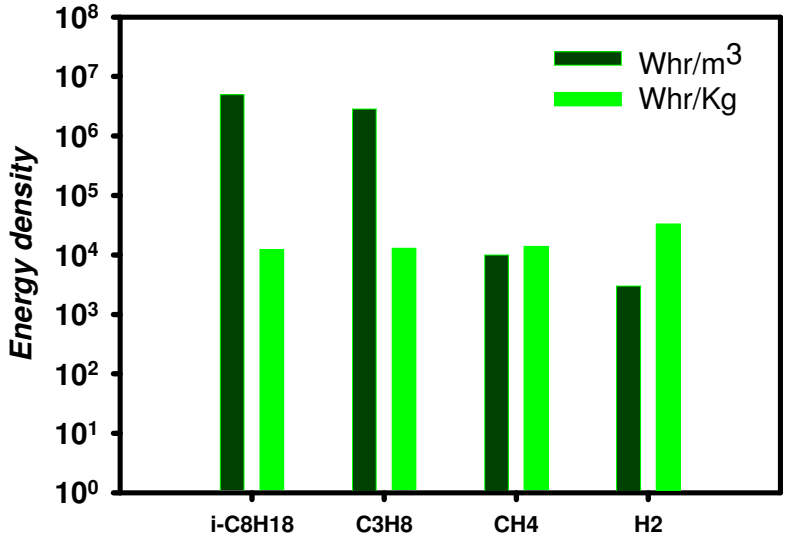

Figure 1.2 *Specific energy for iso-octane, propane, methane and hydrogen. Data reported both in the units of weight and volume and derived from Perry and Green (1997).*

Hydrogen may promote methane combustion due to both thermal and chemical effects. In particular, H_2 burning at significantly lower temperatures, may assist thermally CH_4 combustion by decreasing its light-off temperature. Deutschmann et al. (2000), through a comparative experimental/theoretical study on CH_4-H_2 mixtures combustion on platinum has shown that in order to obtain light-off of methane the quantity of hydrogen to introduce in the mixture has to determine a rise in the catalyst temperature sufficiently high to encourage oxygen desorption and methane adsorption.

Moreover, hydrogen addiction to methane fuel may involve a change in the chemical nature of the catalyst modifying its active sites and its oxidation state and thus affecting the catalytic activity. These considerations are confirmed by a study performed by Demoulin et al. (2006) on combustion of CH_4-H_2 fuel on supported palladium. The authors in part have recognized the role of hydrogen combustion in assisting thermally methane ignition, as reported by Deutschmann et al. (2000); however, they have shown that the catalyst temperature rise produced by H_2 combustion and necessary to methane light-off is higher than that considered sufficient to determine methane adsorption on catalyst. The hydrogen added in mixture causes, in fact, the partial reduction of palladium from oxide form to metal, less active for methane combustion; consequently, the heat to adduce has to increase to compensate for the enhanced light-off temperature.

Still, hydrogen may promote chemically methane combustion by activating reactive paths in the homogeneous phase. Actually, hydrogen combustion may adduce a quantity of $OH^{\cdot}$ radicals such as

to ignite methane in the gas phase at relatively low temperatures (Schefer et al., 2002, Dagaut e Nicolle, 2005, Sabia et al., 2007, Derudi et al., 2007).

The high potential of hydrogen in increasing methane reactivity has the maximum resonance in microcombustion where the use of methane has been prohibited to date.

1.5 Combustion to electrical power converters at small-scales

A possible approach to convert combustion power into electricity is to reproduce at the small scales gas turbine large scale plants, characterized by a very high overall efficiency (of about 40%). This kind of solution based on thermodynamics cycles has been stimulated by the advances in MEMS allowing the fabrications of micro-turbines and micro-pumps and is pursued mainly by MIT (Massachusetts Institute of Technology, Spadaccini et al., 2003 and Mehra et al., 2000). However the hypothetical advantage arising from high theoretical efficiency has to be re-evaluated by considering the life time of this kind of devices. Actually, even if novel fabrication technique allows to scale down power production plants the friction losses are hardly scalable and component usury strongly reduces the durability of these devices at the micro-scale.

An alternative approach is based on system converting combustion power directly into electricity without including thermal cycles and moving parts. In such a case conversion system is coupled with combustor constituting an heat source for the process. Several conversion principles have been proposed and among these the most studied are thermoelectric, TE (Federici et al., 2006, Karim et al., 2008, Qiu and Hayden, 2008) and thermophotovoltaic, TPV (Yang et al., 2002). Nowadays, TE and TPV exhibit a theoretical efficiency maximum of 10%, significantly lower than that of fuel cell and micro-turbine based generators. However they are characterized by high compactness, operation flexibility, durability, low cost and maintenance requested.

In particular, a great attention is recently devoted to thermoelectric conversion system based on Seebeck effect (Riffat and Ma, 2002, Dughaish, 2002, Wagner et al., 2007, Boukai et al., 2008, Hochbaum et al., 2008, Vining, 2008, Goncalves et al., 2008). The great diffusion of this kind of systems is mainly due to the great life time, higher than 10^5h (Riffat and Ma, 2002) and the capability of converting to electricity any low-grade waste heat (Muhtaroglu et al., 2008).

Based on Seebeck principle, when a temperature differential is established between the hot and colds ends of a semiconductor material an electrical potential is developed. This voltage is called Seebeck voltage and is directly proportional to the temperature differential, as it is expressed in the equation Eq. 1.1. Such a constant of proportionality is known as the Seebeck coefficient. In Figure 1.3 is shown a schematic of the operation mode of thermoelectric. In particular, n and p type semiconductors are electrically connected in series with a resistive device; in consequence of the

heat supplied to the device T_{HOT}-T_{COLD}>0 and an electric current flows in the circuit thus delivering an electrical power. A single couple of n and p semiconductors constitutes a thermocouple. Generally a single thermocouple generates very low voltage. In order to increase the electric potential an high thermocouple density is required and more thermocouples need to be connected in series thus constituting a thermoelectric module. In a module thermocouples are thermally connected in parallel in the sense that they are joined such as to have common hot and cold junctions.

Thermoelectric efficiency, η_{TE} is the ratio between the generated electric power and that transferred to the device. As it is reported in Eq. 1.3, η_{TE} increases by increasing the undimensional figure of merit, ZT, that is a specific quantity of each considered material. ZT is a function of the Seebeck coefficient and of electrical and thermal conductivities as reported in the equation Eq. 1.2. Maximizing ZT is a challenging because of the difficulty in increasing electrical conductivity without simultaneously increasing the thermal conductivity (Dughaish, 2002, Wagner et al., 2007, Boukai et al., 2008, Hochbaum et al., 2008). Moreover, another obstacle is constituted by the low thermal stability of thermoelectric materials mainly due to their typically low melting point, high vapour pressure and low chemical (Dughaish, 2002). Moreover, by increasing temperature the eventual mobility of dopant substances increases too thus changing thermoelectric properties of the materials (Dughaish, 2002).

Several thermoelectric materials have been proposed (Dughaish 2002) and among these the most promising are Bismuth and Lead telluride (respectively Bi_2Te_3 and PbTe) and Silicon-germanium . Despite of the very promising properties of Si-Ge and PbTe materials in terms of maximum allowed operation temperature and figure of merit, their application is up to now in a feasibility stage. On the contrary, bismuth-telluride semiconductors are well-established thermoelectric materials and provide a ZT≈0.7÷1 (Goncalves et al., 2008, Vining, 2008). Such materials allow a maximum operation temperature of 250÷300°C thus exhibiting a maximum efficiency of 5÷7%. However, it is worth mentioning the new technological frontiers consist in producing thermoelectric materials in nano-structured form (Goncalves et al., 2008, Boukai et al., 2008, Hochbaum et al., 2008). Actually, this strategy allows to enhance thermoelectric efficiency by determining a reduction of thermal conductivity without affecting electrical conductivity (Hochbaum et al., 2008). Furthermore, new exciting opportunities derive form the possibility to structure on the same substrate thermoelectric and catalytic materials; in such a way thermoelectric is constituting part of the combustor thus enhancing efficiency and compactness.

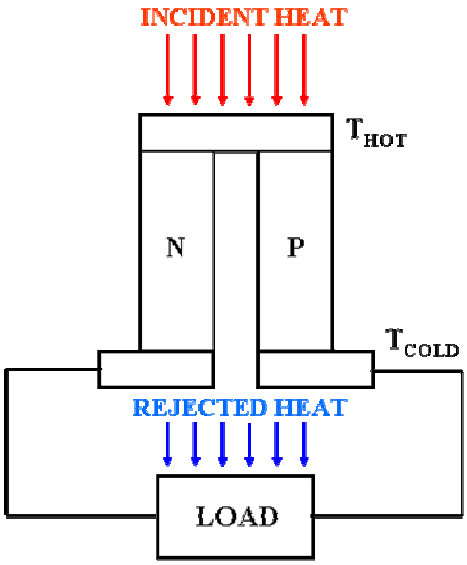

Figure 1.3 *Schematic of Seebeck effect in thermoelectric conversion system*

$$V = \alpha \cdot \Delta T = \alpha \cdot \left(T_{HOT} - T_{COLD}\right) \qquad \textit{Eq. 1.1}$$

$$ZT = \frac{\alpha^2 \sigma T}{\lambda} \qquad \textit{Eq. 1.2}$$

$$\eta_{te} = \frac{P_{EL}}{P_{TR}} = \frac{T_{hot} - T_{cold}}{T_{hot}} \left[\frac{\sqrt{1+ZT} - 1}{\sqrt{1+ZT} + T_{cold}/T_{hot}} \right] \qquad \textit{Eq. 1.3}$$

V	Seebeck voltage
α	Seebeck coefficient
Z	figure of merit
ZT	undimensional figure of merit
T_{HOT}	hot junction temperature
T_{COLD}	cold junction temperature
T	mean temperature between T_{HOT} and T_{COLD}
ZT	figure of merit
α	Seebeck coefficient
σ	electrical conductivity
λ	thermal conductivity
η_{TE}	thermoelectric efficiency
P_{EL}	electric power
P_{TR}	transferred power to thermoelectric

The overall efficiency of an electric generator based on combustor/thermoelectric coupling is equivalent to η_{TE} only if ideally the chemical fuel is completely transferred to thermoelectric. However, as already reported, combustion efficiency is questionable at the micro scale and even if fuel is totally converted the power transferred to thermoelectric is only a part of the total released power due to the heat lost via both exhausted gas and reactor wall. Propane fueled generator developed by Federici et al. (2006) exhibited an overall efficiency of 0.5%. In details, the energy balance executed on the entire system revealed that only 20% of the total combustion power is transferred to thermoelectric.

Based on these considerations, it is pointed out the need to study particular engineering solutions assuring high combustion efficiency and an optimal combustor/thermoelectric coupling. As already reported, heat regeneration constitutes a promising strategies to enhance combustion efficiency at the microscale. However, heat recovery is the key parameters to improve the efficiency of combustor/thermoelectric coupling too. Weinberg (Weinberg et al., 2002, Weinberg, 2004) calculated the efficiency of thermoelectric converter coupled with heat recirculating combustors in the case of a configuration based on the recovery of the thermoelectric heat wasted via cold junction. In Figure 1.4 it is shown the schematic of the proposed configuration: thermoelectric module is external to the combustion chamber and the unconverted heat through thermoelectric is transferred to the cold incoming gas. In this configuration the temperature difference provided by combustion is approximately equal to that established between the thermoelectric junctions and it is possible to show that it should be low (250°C) to allow an efficient operation of the system. As a consequence, the use of such a thermoelectric/combustor coupling is optimized under combustion diluted conditions.

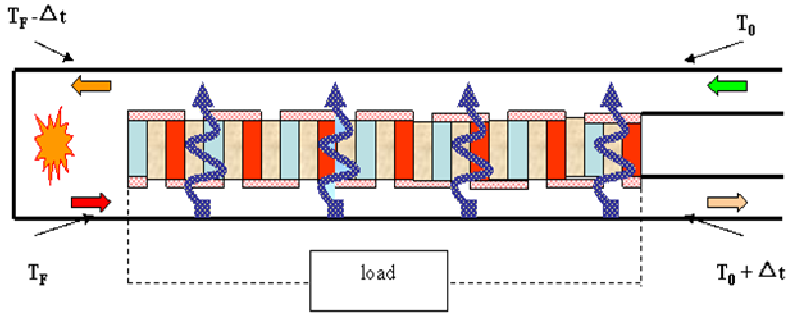

Figure 1.4 *Schematic of combustor/heat-exchanger/converter proposed by Weinberg (2004)*

Despite the great relevance, no experimental studies are found in literature concerning the combustor/thermoelectric coupling neither regarding the configuration proposed by Weinberg nor for any other alternative solution.

1.6 Aim of the thesis

In this Ph. D. thesis the main issues in catalytic micro-combustion will be explored with the conclusive aim to develop efficient combustors exhibiting a operating window wide enough to make possible their application in portable power generation.

Particular attention will be devoted to the preparation of catalytic micro-structured reactors for the combustion of C_3H_8, H_2, CH_4 and H_2-CH_4. A preparation method is developed to depose efficaciously the active phase on inert substrates of different materials (Cordierite, α-Al_2O_3 and FeCralloy) and in the form of both monoliths and platelets. Cheap and stable active phase constituted by supported perovskite, γ-Al_2O_3/$LaMnO_3$ has been prevalently considered. However, the effect of promoting perovskite with a little amount of platinum has been taken into account and, thus, Pt/Al_2O_3 catalyst are prepared and tested as reference material too.

A novel single channel planar catalytic reactor (SSR) is developed for the study of diluted combustion of H_2, CH_4 and H_2-CH_4 up to a maximum temperature of 800°C. Such a reactor gives the possibility to modulate the combustion chamber height thus allowing to study in depth the particular interaction between heterogeneous and homogeneous combustion. In particular, SSR will show its maximum relevance in understanding the chemical synergy in H_2 assisted CH_4 combustion.

Combustion under auto-thermal conditions has been studied too. In particular, ignition and quenching of C_3H_8, H_2, CH_4 and H_2-CH_4 combustion have been investigated in a large spectrum of operating conditions. Particular attention has been devoted to novel heat-recirculation reactors. In particular, in order to experimentally verify the role of heat recovery on combustion stability, a quartz reactor easy to run both in heat-recirculation and in no-recirculation reactor modes is developed. The simple geometry of the proposed reactor enables to obtain fundamental understanding of the effect of heat recirculation and on the instability mode in the limit of low conductive reactor walls.

Micro power generators have been developed by coupling catalytic combustors with thermoelectric modules. In particular, an innovative solution consisting on the integration of multiple pass heat-recirculating combustors with TEs is proposed as alternative to that reported by Weinberg (Weinberg et al., 2002, Weinberg, 2004). In the configuration the temperature difference provided by combustion is independent by that established between the thermoelectric junctions and the combustor is run under autothermal conditions.

Part of the present work and specifically the study on heat recirculation combustors and electricity generators (discussed in the chapters 6 and 7) has been performed at University of Delaware in the research group of Professor Vlachos.

CHAPTER 2

CATALYST PREPARATION AND CHARACTERIZATION

This chapter concerns the preparation and the characterization of the catalysts tested in this Ph. D. research activity.

In particular, the first section is devoted to the description of the catalyst preparation methods; $LaMnO_3/\gamma\text{-}Al_2O_3$, $Pt/\gamma\text{-}Al_2O_3$ and $Pt\text{-}LaMnO_3/\gamma\text{-}Al_2O_3$ based catalysts have been prepared both in the powder and in structured form. As regards structured catalysts, a procedure to coat monoliths and platelets is presented.

The second section is devoted to the characterization of the prepared catalysts. In particular, specific surface area measurements, SEM and EDS analysis are discussed.

2.1 Catalysts preparation

2.1.1 Preparation of the platelet substrates

Alumina platelets, characterized by an elevated thermal (maximum working temperature as high as 2000°C), mechanical and chemical resistance, have been prepared starting from products supplied by Cotronics Corp.. Preparation technique includes the preparation of a slurry constituted by a liquid activator used as binder and by $\alpha\text{-}Al_2O_3$ pure powder. The slurry is dried overnight at room temperature and it is further fired at 950°C in air. The platelets are prepared in the required shape and dimensions through the use of specific home-made flexible and impermeable moulds; in particular they are made in the shape of a parallelepiped, 0.5 cm thick, 1.5 cm wide and 3.0 cm long. The manufacturing tolerance on the finished product is 0.1 mm. A detailed description of the preparation technique is below reported.

In order to prepare the mould, a plate in the required shape and dimensions is realized in a piece of brass by means of a milling machine. A silicone-like slurry is poured inside the block and it is dried overnight at room temperature. The silicone part, removed from the block, is the mould employed for preparing the platelets (Figure 2.1c).

According to the recipe supplied by Cotronics, a specific amount of alumina powder (Cotronics Corp., Rescor 780) and liquid activator are poured in a beaker and properly mixed until obtaining a slurry provided with a certain consistency. The slurry is then poured in the formerly prepared

mould. The mould is successively stirred for about 15 min in order to take out from the slurry the remaining air bubbles, thus avoiding the occurrence of cracks in the further thermal treatments. After about 20 min the slurry in excess is removed by the mould using a shovel, in order to obtain the platelet in the required dimensions in the limit of the manufacturing tolerance. Slurry workability is about 20 min, then acquiring a significant mechanical resistance. The slurry inside the mould is dried at room temperature for about 20h. After such operation the mechanical resistance is high enough to allow the removal of the platelet from the mould and the sample is further fired at 950°C for 5 h. Such thermal treatment determines a further increase in the substrate mechanical resistance besides allowing the removal of the organic part present in the liquid activator. However, thermal treatment may causes over pressure because of the air still present in the platelet and the thermal decomposition of the organic part. So, in order to avoid cracks in the finished product, a very low heating rate (1°C/min) has been considered. In Figure 2.1a, b, d some pictures of the prepared plates are reported.

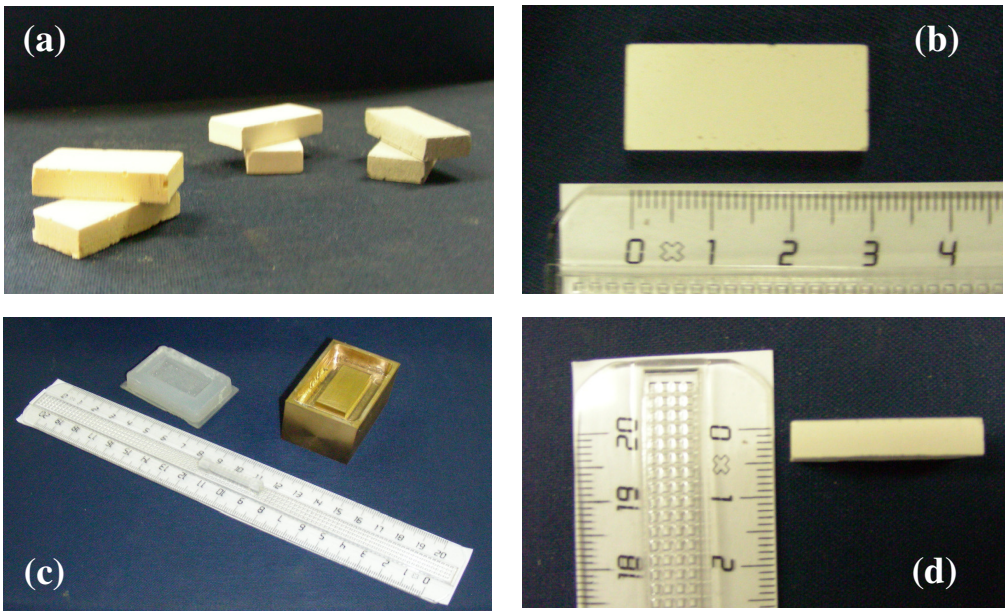

Figure 2.1 *Preparation of the alumina platelets; (a),(b),(d): platelets shape and dimension; (c) mould used in the preparation.*

2.1.2 Pre-treatment of the FeCralloy platelets

Catalytic substrates are prepared starting from FeCralloy foils (Good Fellow), characterized by a thickness comprised between 1 and 5 mm. The foils are properly cut in order to obtain 1.5 cm wide and 3.0 cm long samples. Before performing the deposition of the catalytic film, the metallic plates undergo a specific treatment whose aim is to improve the anchoring of the layer subsequently

deposed. Actually, processing residual oil, still present on the untreated sample, needs to be removed otherwise catalyst deposition success could be seriously compromised. Furthermore, it is reported that a specific thermal treatment in air allows the growth of γ-alumina layer on the FeCralloy surface (Valentini et al., 2001, Zhao et al. 2003). Ceramic structures, the so-called whiskers, interposing between the FeCralloy surface and the catalytic layer, improve the anchoring because of their greater chemical affinity with the deposed film respect to the metallic substrate.

The specific treatment performed on FeCralloy platelets is reported below.

Metallic substrates are first cleaned in ethanol for approximately 30min.; successively, in agreement with the procedure reported by Zhao et al. (2003), the samples are treated for 15 min. in a solution of NaOH (1 M) and successively for 15 min. in a solution of HCl (0.5 M). After these chemical treatments, FeCralloy substrates are calcined in air for 10h at 950°C, decisive for the formation of the surface alumina.

2.1.3 Preparation of powder catalysts

Powder catalysts have been prepared by supporting on γ-Al_2O_3 the active phase constituted by Pt, $LaMnO_3$ and Pt-$LaMnO_3$. The preparation procedure of the samples includes several stages. In the first step alumina in the form of powder (CK300, Akzo) is finely ground by means of a "ball milling" machine till the mean diameter of the particles is less then 2 μm. In order to shift γ- to α-alumina transition at temperatures higher than 1000°C, a stabilization procedure is needed and carried out by inserting some amount of lanthanum oxide (5wt%) into the structure, thus inhibiting the mobility of oxygen and aluminium atoms and, as consequence, the transition to the alpha phase (Arai e Machida, 1996). After being stabilized, γ-Al_2O_3 is loaded up by the active phase.

The active phase and La_2O_3 are deposed on alumina through an "incipient wetness impregnation" method in a rotary vapour (Laborota 4002, Heidolph). According to this method the inert alumina powder is suspended in an aqueous solution constituted by the precursors of the stabilizer or of the active phase. The precursors are added to the solution in a such amount as to have the desired load and formulation of the catalysts. The prepared suspension is fed into the rotary vapour rotating at 75 rpm and it is dried under vacuum conditions (100 mbar) at 50°C. The dried impregnated powder is consequently calcined at 800°C for 3h in air.

An impregnation solution constituted by lanthanum nitrate has been prepared in order to stabilize γ-Al_2O_3. About active phase, in the case of Pt/γ-Al_2O_3 systems an impregnation solution constituted by a diluted chloroplatinic acid solution (Sigma Aldrich) has been prepared. A solution constituted by manganese acetate (Manganese acetate tetraydrate, Aldrich) and lanthanum nitrate (Lanthanum nitrate Hexahydrate, Fluka) has been prepared in the case of $LaMnO_3$/γ-Al_2O_3 based catalyst.

Finally, in the case of the mixed active phase, Pt-$LaMnO_3$/γ-Al_2O_3 catalysts, a solution constituted at the same time by the precursors of Pt, Mn and La has been considered.

Table II. 1 provides details and the nomenclature of the catalysts prepared. Twelve samples are prepared characterized by a different loading of $LaMnO_3$ e Pt. The amount of perovskite deposed on γ-Al_2O_3 varies from 10 to 30 wt% as regards the total weight of catalysts. Moreover, platinum based catalysts are characterized by a Pt amount comprised between 0.15÷1 wt % as regards the total weight of catalysts.

The prepared catalysts constituted "fresh" samples while if pretreated constituted "aged" samples. Powder catalysts before being tested are subjected to an ageing treatment at 900°C in air lasting maximum 3h.

ICP analysis is employed to measure Mn, Pt and La content in the prepared catalysts. The analysis is performed on fresh samples; in Table II. 1 the obtained results are resumed. Concerning supported perovskites, by measuring Mn and La amount is easy to derive indirectly the loading of $LaMnO_3$; according to measured values a maximum discrepancy of about 10% is revealed by comparing the nominal and the actual $LaMnO_3$ loading. Even in the case of Pt the discrepancy between nominal and actual loading is maximum 10%.

Table II.1 *Summary of powder catalysts prepared: active phase loading in terms of nominal and measured values. Catalyst code (column 1) notation: the first number refers to the % (wt) of Pt (if any) and the symbol to the catalyst employed (Pt, LM=$LaMnO_3$,Pt-LM=Pt/$LaMnO_3$).*

Catalyst Code	**Loading, %**			
	$LaMnO_3$		**Pt**	
	Nominal	Actual	Nominal	Actual
LM10	10	9.0	0	-
LM20	20	18.5	0	-
LM30	30	32.0	0	-
0.15PtLM10	10	9.0	0.15	0.16
0.35PtLM10	10	9.0	0.35	0.36
0.9PtLM10	10	9.0	0.90	0.93
0.15PtLM20	20	18.5	0.15	0.16
0.35PtLM20	20	18.5	0.35	0.36
1PtLM20	20	18.5	1.00	1.04
0.35PtLM30	30	32.0	0.35	-
0.35Pt	0	-	0.35	0.34
1Pt	0	-	1.00	1.11

2.1.4 Deposition of a catalytic film on platelets

The deposition of a catalytic layer on FeCralloy and alumina platelets is carried out through two main preparation steps. In particular, catalysts is formerly prepared in the form of powder following the preparation method described before and it is successively deposed on the substrates.

In order to depose the catalytic film on the FeCralloy and alumina substrate, a "slurry" constituted by the fresh powder catalysts is prepared. At this proposal the powder samples, prepared according to the procedure as above reported, is mixed with Boehmite (Disperal, Sasol), used as binder. The solid mixture is thus suspended in an aqueous solution of nitric acid. The recipe of the slurry used for the coating of the FeCralloy and alumina plates is reported in Table II.2.

Table II.2 *Composition of the slurry used for coating FeCralloy and alumina platelets*

	Quantity [mg/(ml, H_2O)]
HNO_3 (65% wt)	21.6
Boehmite	58.8
Powder catalyst	250

The slurry is spread on the plates through a paintbrush and it is, successively, dried at 120°C for 20min. It is, finally, calcined at 800°C for 3h, in order to anchor the catalytic film on the substrate.

Moreover, the slurry used in the preparation of the catalytic platelets is further calcined; the resulting powder catalyst is used as reference in the kinetic measurements in order to evaluate the effectiveness of the deposition technique.

Some details of the structured catalyst prepared are reported in Tab. II.3. The first eight samples are FeCralloy and alumina catalytic plates. They are constituted by a loading of perovskite (if applicable) of 20wt% as regards the total amount of catalysts deposed on the substrate. The loading of Pt (if applicable) corresponds to 1wt%. The sample A5 is a blank platelets. Finally, PwLM is the powder sample obtained by calcining the slurry employed to prepare perovskite supported structured catalysts.

ICP analysis has not been performed for the catalytic film deposed on the platelets. However, its formulation is known being equivalent to that of the powder catalysts.

As-coated samples constituted "fresh" catalysts while if pretreated constituted "aged" samples. Catalytic platelets before being tested are subjected to an ageing treatment at 800°C in air lasting maximum 30h.

2.1.5 Preparation of monolith catalysts

Structured catalysts, constituted by Pt/γ-Al_2O_3, $LaMnO_3$/γ-Al_2O_3, Pt-$LaMnO_3$/γ-Al_2O_3, have been prepared by coating cordierite honeycombed monoliths (NGK), characterized by a cell density of 400 and 900 cpsi. Considered substrates are either in the shape of a cylinder or of a parallelepiped. The monoliths are previously cut in order to obtain the desired shape and dimension. Specifically, rectangular reactors are 5 cm long with a cross section made up of 2x5 channels in the case of 400 cpsi or 3x8 in the case of 900 cpsi; while circular reactors are 1.2 cm long and have a diameter equal to 1.7 cm, corresponding to 317 channels if 900 cpsi substrates are considered.

Table II.3 *Summary of catalytic plates prepared: active phase loading in terms of nominal values. Catalyst code (column 1) notation: the first number refers to the platelet thickness (if applicable), the second number refers to the % (wt) of Pt (if any) and the symbol to the catalyst employed (F=FeCrAlloy, A=Alumina, Pw=Powder, Pt, LM=$LaMnO_3$); the number after hyphen is a sequence number in the preparation.*

Code	Substrate	Amount of catalyst	Active phase loading, %		Height, mm	
		mg	$LaMnO_3$	Pt	plate	gap
F5LM	FeCralloy	16	20	-	5	1
F5Pt1LM	FeCralloy	17	20	1	5	1
F5Pt1	FeCralloy	17	0	1	5	1
F2LM	FeCralloy	14	20	0	2	4
F5LM-2	FeCralloy	18	20	0	5	1
A5LM	Alumina	19	20	0	5	1
A5LM-2	Alumina	18	20	0	5	1
A5Pt1LM	Alumina	32	20	1	5	1
A5	Alumina	0	0	0	5	1
PwLM	**powder**	**-**	**20**	**0**	**-**	**-**

The blank monolith are wash-coated with a γ-Al_2O_3 thin layer (approximately 50μm thick) through modified dip-coating technique (Cimino et al., 2001). According to this technique, the sample is dipped in a suspension made of diluted nitric acid and a solid content, equal to 20 wt%,

constituted by a mixture of small size alumina (80 wt%, Alfa Aesor) and commercial boehmite (Disperal, Sasol) powder. After few minutes, enough to fill the channels with the slurry, the monolith is removed from the suspension and the excess is blown-out by means of compressed air. The sample is dried for 20 minutes at 120°C and afterwards calcined at 550°C for 2 h. A certain number of cycles are needed to depose the desired amount of alumina, approximately equal to 20 wt% of the final weight of the monolith and once got it the sample is calcined at 800°C for 3 h in order to anchor the layer to the substrate.

In the case of cylindrical monoliths, γ-Al_2O_3 has been stabilized by adding lanthanum oxide after monolith washcoating; the loaded amount of stabilizer is 5-7 wt% respect to the total washcoat weight (lanthanum and aluminium oxide weight). Impregnation technique is used to disperse La_2O_3 in the alumina structure. At this proposal, the wash-coated sample is dipped in a solution of diluted lanthanum nitrate (Lanthanum nitrate Hexahydrate, Fluka) until the monolith channels are filled with the solution. The sample is thus removed from the solution, the excess of solution is blown-out and the monolith is dried at 120°C for 20 min and calcined at 800°C for 3h. This procedure is repeated until the desired loading of La_2O_3 is obtained.

Impregnation technique is also used to load the active phase. In the case of Pt/γ-Al_2O_3 catalysts, the wash-coated sample is dipped in a solution of diluted chloroplatinic acid (Sigma Aldrich), corresponding to 0.1wt% of Pt. After the sample is removed from the solution and the excess is blown-out, it is calcined at 800°C for 3h. This procedure is repeated until the desired loading of Pt is obtained. The same procedure is followed in the case of perovskite based catalysts. In particular for preparing $LaMnO_3$/γ-Al_2O_3, the wash-coated monoliths are dipped in an aqueous solution made of lanthanum nitrate (Lanthanum nitrate Hexahydrate, Fluka) and manganese acetate (Manganse acetate tetraydrate, Aldrich), corresponding to 1.7 wt% of La and 0.7wt% of Mn. In the case of Pt-$LaMnO_3$/γ-Al_2O_3, only one solution containing both perovskite and Pt precursors is prepared. In particular the aqueous solution, made starting from lanthanum nitrate, manganese acetate and chloroplatinic acid, contains 1.7 wt% of La and 0.7wt% of Mn and 0.1wt % of Pt.

As-coated samples constituted “fresh” catalysts while if pretreated constituted “aged” samples. Catalytic monoliths before being tested are exposed to combustion environment, at T=800÷900°C and at a carbon dioxide and water concentrations of about 6÷10vol%, for about 5-10hr.

In Table II. 4 a summary of the monolith catalysts prepared is reported.

The Pt content was measured through Atomic Adsorption (AA) on “aged” samples, after they were subjected to several hours of combustion. The results, reported in Table II.4, indicate overall reasonable agreement between expected and measured noble metal loading on the catalyst. In the case of Pt-$LaMnO_3$, AA was also performed on the “fresh” catalyst: no difference was observed on

the noble metal loading, indicating good anchoring of the catalytic layer on the cordierite substrate and no measurable Pt volatilization.

Table II. 4 *Summary of monolith catalysts prepared: washcoat and active phase loading in terms of nominal and measured values. Catalyst code (column 1) notation: the first number refers to the % (wt) of Pt (if any), the last number to the monolith porosity in cpsi, and the symbol to the catalyst employed (Pt, LM=$LaMnO_3$,Pt-LM=Pt/$LaMnO_3$).*

Catalyst code	**Reactor Shape**	**Porosity, cpsi**	**Catalyst Loading, g**	**Nominal Loading, %**		**Actual Pt loading, %**
				$LaMnO_3$	*Pt*	
R1Pt400	rectangular	400	0.116	-	1.00	1.06
R0.5Pt900	rectangular	900	0.220	-	0.50	0.59
R1Pt900	rectangular	900	0.217	-	1.00	1.05
R0.5PtLM900	rectangular	900	0.272	20	0.5	0.62
R0.5PtLM400	rectangular	400	0.156	20	0.5	-
RLM900	rectangular	900	0.287	20	-	-
C1PtLM900	Circular	900	1.103	20	1	-

2.2 Catalysts characterization

2.2.1 BET measurements on powder catalysts

Specific surface (S.S.) of the prepared catalysts is evaluated by N_2 adsorption at 77K according to the BET method using a Quantachrome Instruments Autosorb 1-C apparatus.

Analyses have been performed on aged samples (as already reported powder is treated in air at T=900°C for 3h) after oxidation tests, performed at a maximum temperature of 800°C.

In Table II.5 the results of the analyses are reported. The specific surface exhibited by the catalysts, evaluated for unit of the sample weight, is strongly lower than that of γ-Al_2O_3 (S.S.≈200m^2/g) constituting the support of the active phase in each considered case. In particular, all the considered catalysts exhibit a S.S.<100m^2/g. The lower specific surface of the prepared catalysts compared to that of the starting γ-alumina powder is partially due to the ageing thermal treatment performed on the samples. Such a treatment, in fact, may cause a phase transformation of part of γ-alumina to α phase (Arai and Machida, 1996, Cimino et al., 2001). However, the decrease in the specific surface is also due to the solid-solid interactions of γ-Al_2O_3 with the loaded phase

and it becomes more significant by increasing the amount of active phase on the catalyst. In confirming with that, S.S. of the samples decreases by increasing the perovskite loading. S.S. decreases also by increasing the platinum loading on the samples but maintaining the same amount of deposed perovskite. In the case of LM10, for example, the specific surface is 109 m^2/g; by considering Pt promoted catalysts, S.S.=103 and S.S.=99 are measured respectively if 0.15 and 0.35wt% of Pt is added to perovskite. It is worth mentioning that this outcome, concerning the decrease in the specific surface in the case of Pt promoted $LaMnO_3$ compared to that of unpromoted perovskite, is in agreement with the results reported by Giebeler et al. (2007)

Table II.5 *BET measurements on powder catalysts*

Catalyst	**S.S. m^2/g**
LM30	74.7
LM20	91.2
LM10	108.9
0.15PtLM20	81.3
0.35PtLM20	79.1
0.15PtLM10	102.8
0.35PtLM10	99.2

2.2.2 SEM analysis on catalytic platelets

SEM analysis was performed on catalytic platelets using a Philips XL30 instrument equipped with an EDAX detector for EDS analysis.

2.2.2.1 Surface modification of FeCralloy.

SEM analysis is performed on 1mm thick FeCralloy platelets before and after the pre-treatment described in the previous section. Moreover, an image of the washcoated substrate is also shown.

The thermal treatment in air performed on the substrates allows the growth of γ-alumina layer on the FeCralloy surface, the so-called whiskers (Valentini et al., 2001, Zhao et al. 2003). Such a ceramic micro-structures are pointed out by comparing the SEM images performed on the untreated (Figure 2.2a) and treated (Figure 2.2b) substrates. In particular, it is evident that the latter exhibits a much more wrinkled and brighter surface compared to the former. Moreover, in Figure 2.2c a more

magnified front view on the substrate is shown and the typical shape of γ-alumina whiskers is thus highlighted (Valentini et al., 2001, Zhao et al. 2003).

As already reported, the whiskers, interposing between the FeCralloy surface and the catalytic layer, improve the anchoring of the deposed ceramic film to the metallic substrate. In order to the evaluate the effect of the FeCralloy pre treatment on the adhesion between the washcoat and the metallic support, a γ-Al_2O_3 washcoat is deposed by the technique discussed in the previous section (such a technique is actually modified: in the specific γ-Al_2O_3 powder is considered instead of catalyst powders). In Figure 2.2d is shown a front view of a pre-treated FeCralloy plate washcoated by γ-Al_2O_3. Even if the deposed layer is slightly fractured a total covering of the substrate is obtained. Moreover, the as-coated sample has been exposed to adherence tests by ultrasonic vibrations. Such a test has revealed a weigh loss of maximum 5wt% as regards the total amount of γ-Al_2O_3 deposed after exposure to ultrasonic for 30min.

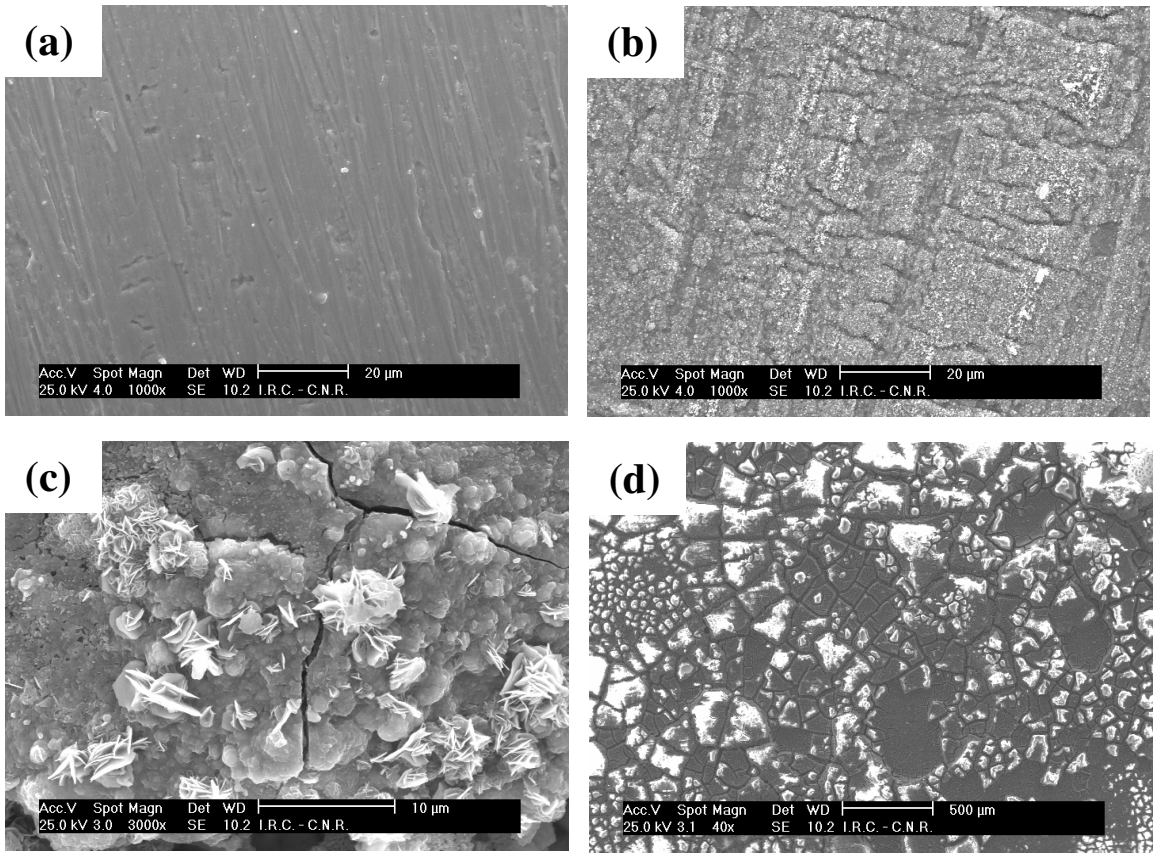

Figure 2.2 *SEM images of FeCralloy substrates (front view). (a) substrate before being treated; (b) and (c) substrate after treatment; (d) substrate coated by γ-Al_2O_3.*

In order to further confirm the formation of γ-Al_2O_3 on the surface of FeCralloy in consequence of the described treatment in Table II.6 the results of EDS analysis on the untreated and treated substrates are reported. In particular, it is reported that the chemical composition of the starting FeCralloy foils is 72.1wt% of Fe, 20.3wt% of Cr and 7.6wt% of Al. Such a FeCralloy composition is consistent with that supplied by Good Fellow and with that reported in literature for other FeCralloy substrates (Zhao et al., 2003). After the treatment a strong alteration of FeCralloy chemical compositions is observed. In particular, the treated sample exhibits a much higher content of aluminum; more specifically, the percentage of Al is 7.6 and 45.2wt% respectively in the case of untreated and treated substrate. The increase in Al percentage in the surface composition indicates the existence of Al_2O_3 outer layer consisting of the alumina whiskers (Valentini et al., 2001, Zhao et al. 2003).

Table II.6 *EDS analysis on the surface of FeCralloy substrate before and after the treatment*

	Fe, wt%	Cr, wt%	Al, wt%
Untreated sample	72.1	20.3	7.6
Treated sample	40.8	14.0	45.2

2.2.2.2 Catalytic layer deposed on α-alumina plates

In Figure 2.3 SEM images of "fresh" A5LM catalyst are shown. In particular, two different magnifications of both the front view and the cross section of the as-coated substrate are presented.

The platelets exhibits an homogeneous distribution of the of the catalytic layer on the surface. The deposed film, in fact, totally covers the substrate even if some cracks are observed (see Figure 2.3c). The film deposed is constituted by blocks of particle whose size is ranged from 5 to 20μm. (see Figure 2.3a). Moreover, the thickness of the catalytic layer is quite uniform with a value of about 80μm (see Figures 2.3b and d).

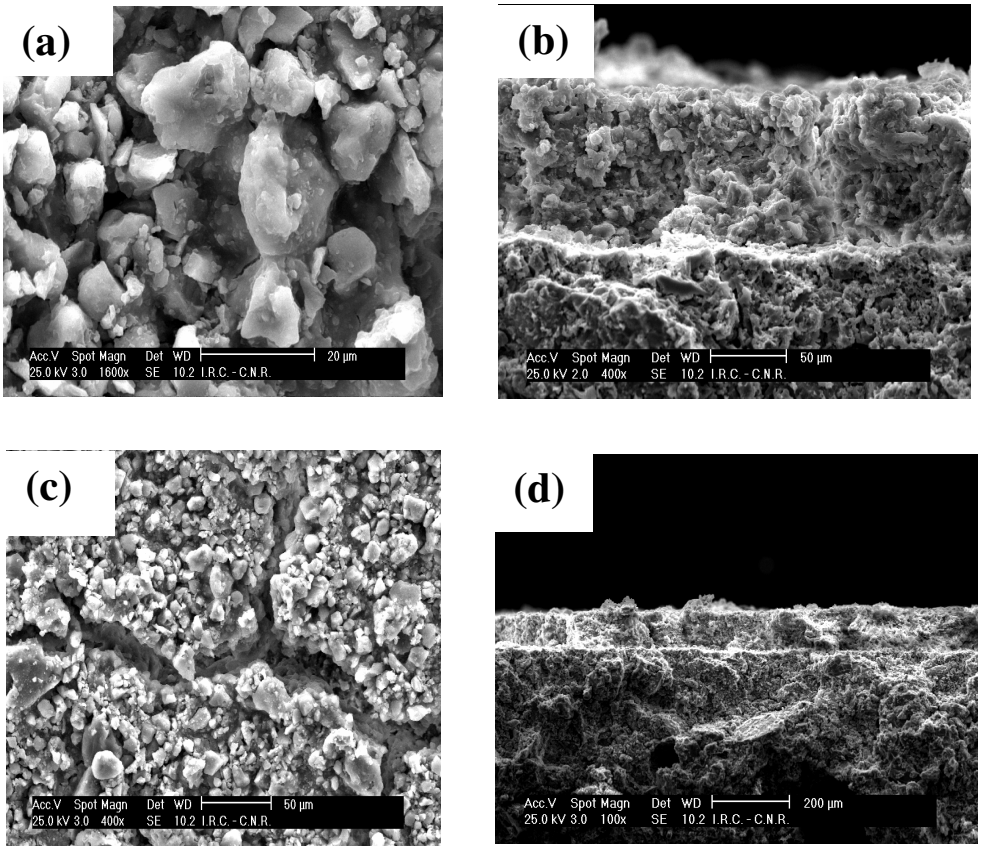

Figure 2.3 *SEM images of the catalytic layer deposed on A5LM sample. (a) and (c) front view on the substrate; (b) and (d) transverse section.*

CHAPTER 3

EXPERIMENTAL SET-UP

In this chapter the reactors and the experimental set up developed in this Ph. D. research activity are described.

The first section is devoted to the description of the different catalytic reactors employed in the reaction tests. Different solutions are presented in terms of reactor wall materials, manufacturing details, flow configuration and catalytic systems.

Finally, in the third section the experimental apparatus and all the employed equipments are reported.

3.1 Reactor design

3.1.1 Quartz reactors for combustion tests on powder catalysts

A quartz reactor (PwQR) has been developed to carry out combustion tests on powder catalysts. In Figure 3.1 a descriptive picture of the reactor is reported.

The reactor is constituted by a quartz tube whose external (OD) and internal (ID) diameters are respectively 11.0 mm and 9.0 mm. A ceramic porous septum provided with a circular section and with a mesh comprised between 70 and 120 μm and welded at a certain height of the quartz tube, holds up the powder catalyst.

A smaller blind quartz tube is inserted axially inside the larger one. This second tube is mounted such as to have the closed end strictly in contact with the septum while the open one is outside the reactor. A thermocouple (0.5mm thick) is inserted in this tube allowing the measure of the thermal profile inside the catalytic bed. The resulting section for the gas flowing is annular with an I.D. equal to 6.0 mm.

The particular reactor configuration allows temperature measurements along all the length of the bed by moving the thermocouple axially through the internal tube. Moreover, the placement of the thermocouple longitudinally respect to the flow direction rather than transversally allows to measure temperatures reducing perturbations on the fluid dynamics.

3.1.2 Stainless steel reactor for combustion tests on catalytic plates.

High thermal resistance stainless steel (AISI 310S) reactor, SSR is used in the combustion tests on catalytic plates. In Figure 3.2a a picture of the SSR is reported.

A particular attention has been devoted to the reactor design that has to respond to the requirements reported below:

- the reactor has to be gastight until a relative pressure equal at least to 500 mbar;
- reactant by-passing has to be avoided
- uniform distribution of the gas residence time inside the reactor has to be achieved
- dead volume has to be reduced
- a simple placement and displacement of the platelets is needed
- thermal profile measurement along the axial length needs to be detected.

The main body of the reactor (Figure 3.2b) is constituted by a flanged barrel where a chamber for the placements of the catalyst has been realized. The chamber is 6 mm high, 15 mm wide and 50 mm long. The catalytic plate is inserted in this cavity leaving a determined gap (varying in the range of 1-4mm) and thus constituting the combustion chamber. The main body of the reactor shows an annular cavity (Figure 3.2b) for the placement of a metal-plastic gasket. A flange is used to sandwich the gasket that is properly pressed by means of six bolts and nuts.

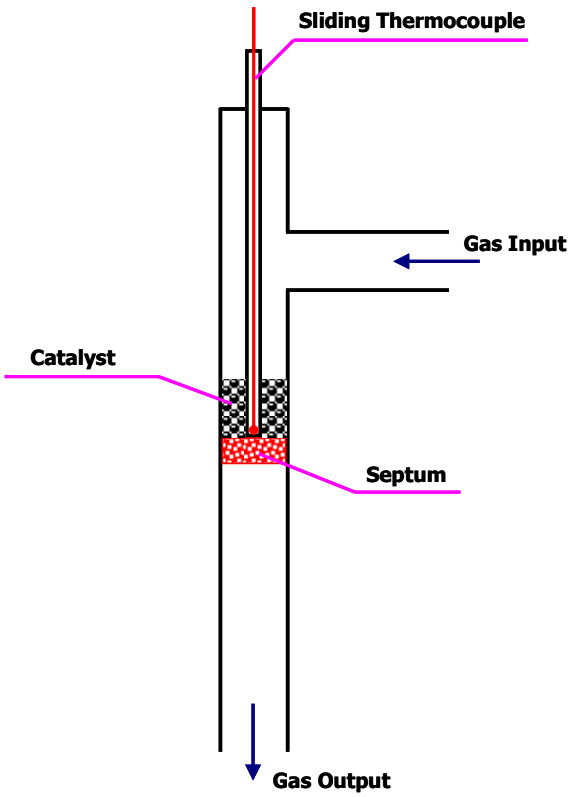

Figure 3.1 *Quartz reactor for combustion tests on powder (PwQR); flow direction, catalyst, thermocouple and septum placement.*

Several blind holes are realized on the axial length of the reactor in order to house the thermocouples (Figure 3.2a). The holes are 7mm spaced and their end is 0.5 mm far from the combustion chamber. The most part of the holes are on the axis of the reactor while one of them is outside the axis in order to allow temperature measurement on the transverse direction (Figure 3.2a). Tubes for the reactant feed and for the exhausted are properly connected to the reactor through Swagelok unions (Figure 3.2a). In Figure 3.2c it is reported the placement of the SSR in the oven during the reaction tests.

In Figure 3.3 the flow configuration in the SSR is showed. The gas enters the reactor and flows tangentially with respect to the catalytic platelet. Two silicon carbide foams are placed before and after the catalysts in order to well distribute the mass flow of the gas in correspondence with the inlet and the outlet of the catalyst.

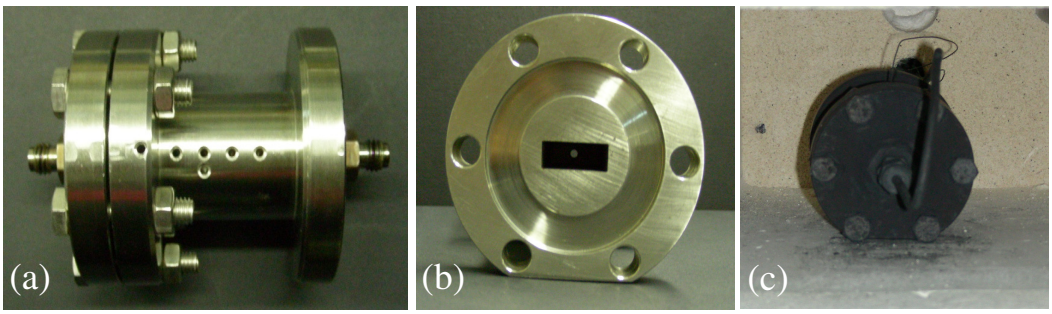

Figure 3.2 *Some images of SSR; (a) coupling flange, bolts and nuts, holes housing the thermocouples, Swagelok unions for the connection of inlet and outlet tubes; (b) holes for bolts, annular cavity for the gasket, combustion chamber; (c) SSR placement in the oven during reaction tests.*

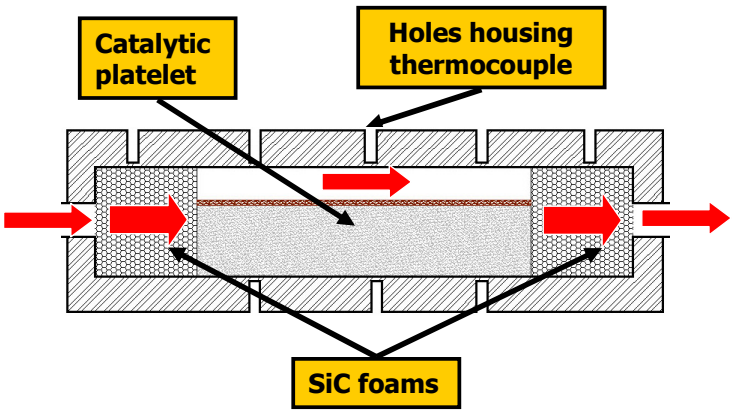

Figure 3.3 *Flow configuration in SSR; catalytic platelet, holes housing thermocouples and SiC foams placements*

3.1.3 Quartz reactor for combustion tests on monoliths

A quartz reactor has been developed for the study of auto-thermal combustion on monolith catalysts. A reactor drawing is reported in Figure 3.4. It consists of a cylindrical quartz tube whose external and internal diameters are respectively 2.54 and 2.39 cm. The monolith catalyst (C1PtLM900), 12mm long and having a diameter of 17mm, is inserted inside the tube. Two ceramic foams (2.5 cm long) are placed upstream and downstream of the catalyst acting as thermal shields. In order to avoid reactants bypass through the gap between the quartz and the catalytic substrate, monolith and foams are wrapped in a thin alumina blanket before being inserted in the quartz tube.

A particular attention is devoted to make possible the temperature measurement inside the channels of the monolith. In particular, a second and smaller quartz tube is mounted coaxially with the previous one and is used to house thermocouples (K type). The tube has one end outside the reactor, in a cold zone, and the other in contact with the upstream foam. The thermocouples pass through the upstream foams and enter one channel of the monolith. Actually, because of the eventual catalytic role of the metals forming thermocouples (Chromel-Alumel), the channel devoted to the temperature measurements is closed at its end with ceramic wool, avoiding its participation to the reaction. Three thermocouples are inserted inside the catalyst monolith; specifically, temperature is detected at the inlet (approximately 3 mm far from the inlet), at the middle and at the end (approximately 3 mm far from the outlet) of the catalyst.

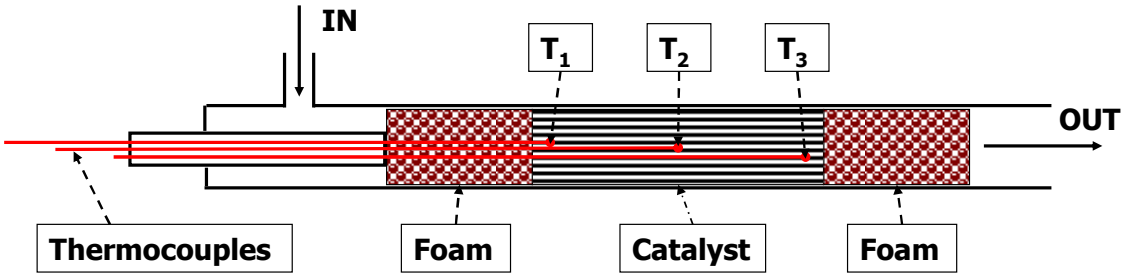

Figure 3.4 *Quartz reactor for combustion test on monolith (MQR). Flow configuration. Placement of monolith catalyst and of ceramic foams. Thermocouples position.*

3.1.4 Heat-recirculation quartz reactors

A quartz reactor easy to run both in heat recirculation (2-passes, HRR) and no-recirculation (single-pass, NRR) mode has been developed.

The quartz reactor consists of two rectangular tubes that are coaxially mounted one inside the other. The larger tube's cross section is 14.6 mm x 10.6 mm and the smaller one's is 10.6 mm x 6.6 mm. The wall thickness of both tubes is 1.3 mm. The catalyst (a 5 cm long monolith) is set in the

smaller, inner tube; two blank monoliths (2.5 cm long) are set upstream and downstream of the catalytic one to shield the heat. In order to avoid reactants bypass through the gap between the quartz and the monolith, the catalyst is wrapped in a thin alumina blanket before being inserted in the quartz tube. Figure 3.5 shows the flow configuration of the HRR. The inlet gas, pumped into the inner tube passes through the upstream blank monolith, enters the catalyst and reacts. The exhaust gas then goes through the downstream blank monolith and turns back through the bigger tube along the channel gap (700 μm thick) between the two tubes (a two-pass HRR).

The tilted (red) arrows in Figure 3.5 show the expected direction of the transverse heat flux in the HRR. Downstream of the reaction zone, heat flows from the inner to the outer tube. Upstream of the reaction front, some of the sensible heat of the exhaust gas preheats the incoming reactants.

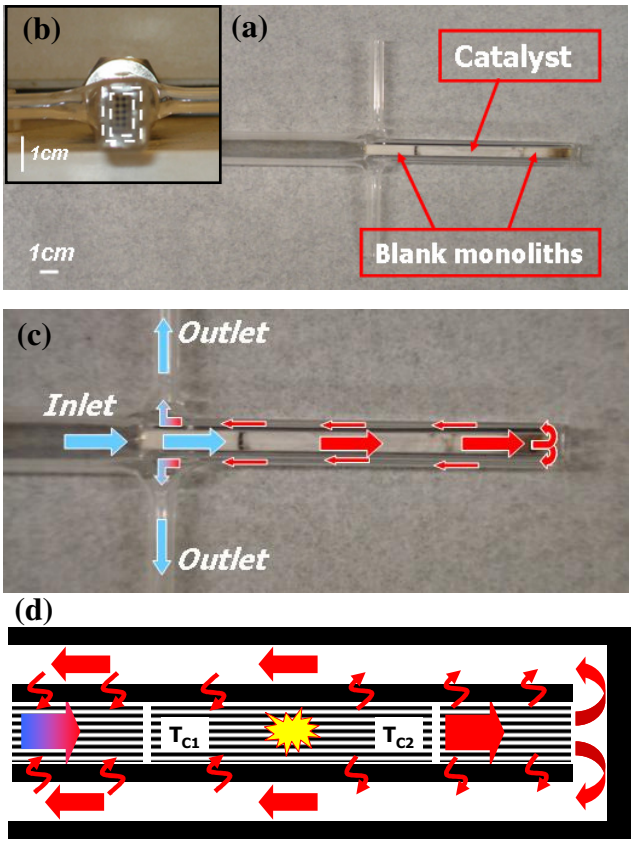

Figure 3.5 *Quartz heat recirculation reactor (HRR). (a) Catalyst and thermal shields position. (b) Cross-section of the reactor. (c) Flow direction in HRR mode. (d) Schematic of HRR mode: heat flux direction and thermocouple positions.*

The described reactor is run in no-recirculation (single-pass) mode simply by removing the external tube. In this configuration the exhausted gas exits from the reactor through the downstream blank monolith after reaction takes place and is not forced in the heat recirculation channel.

As already reported in the previous paragraph, temperature measurements is carried out inside one channel of the reactive monolith. Even in this case a quartz tube is used to house the thermocouples. Specifically, two thermocouples (K type) are inserted inside the catalyst monolith; specifically, temperature is detected at the inlet (approximately 5 mm far from the inlet) and at the end (approximately 5 mm far from the outlet) of the catalyst.

3.1.5 Electricity micro-generators

HRR combustor is integrated with a thermoelectric module (HZ-2, Hi-Z Technology, Inc.) thus constituting an electricity generator. Such a coupling is realized taking the procedure reported by Federici et al. (2006) as a starting point.

In Figure 3.6 a schematic of the cross-sectional view of 2pTER generator is shown. In particular, the main parts constituting the generator are highlighted so making clear the coupling procedure.

A HHR combustor, not equipped with thermal shields, is inserted coaxially in a rectangular aluminum tube. In order to fill the gap between the walls of quartz reactor and Al tube, HRR combustor is previously wrapped up in a very thin copper foil (500μm thick). Actually, the presence of an air layer in the interspace is very detrimental for the heat transfer from the combustor to thermoelectric module. On the contrary, a promoting effect is expected by using an highly conductive metal as copper.

The HZ-2 module is approximately 2.9cm wide x 2.9cm long x 0.5cm thick and weigh 13.5g. It consists of 97 thermocouples arranged electrically in series and thermally in parallel. The thermocouples consists of "Hot Pressed", Bismuth Telluride based, semiconductors. The bonded metal conductors enable the HZ-2 module to operate continuously at temperatures as high as 250°C and intermittently as high as 400°C without degrading the module. Moreover, the device exhibits an internal electrical resistance R_{int}=4Ω (data supplied by Hi-Z Technology, Inc.). The thermoelectric module is mounted on one side the combustor such as to have its hot junction on the aluminum tube. The latter is a good support for the thermoelectric module; in fact, it exhibits a sufficiently high thermal conductivity to efficaciously spread the heat released by combustion thus guaranteeing an uniform temperature on its surface. Moreover, Al shows a lower density compared to that of copper such as to allow a strong decrease in the final device weight.

A finned copper heat sink, CoolWave CPU Cooler from Spire, is placed on top of thermoelectric, in correspondence of cold junction, to enhance convective cooling efficiency.

In order to prevent electrical shorting two pieces of α-alumina wafers are placed between the thermoelectric and the aluminum tube and between the thermoelectric and the copper heat sink.

To improve the thermal contact, thermal grease supplied by Hi-Z is placed between the thermoelectric and the alumina wafers and between the alumina wafers and the aluminum tube.

The part of HRR combustor not taken up by thermoelectric is devoted to the pre heating of the fuel mixture. This reactor section, in fact, is wrapped up in a high temperature heating tape and is successively insulated with Pyrogel (Aspen Aerogels).

To further improve the thermal contact, the entire HRR combustor/Al tube/thermoelectric/heat sink/ stack is placed under compressive force of a coventional C-clamp (≈30lb).

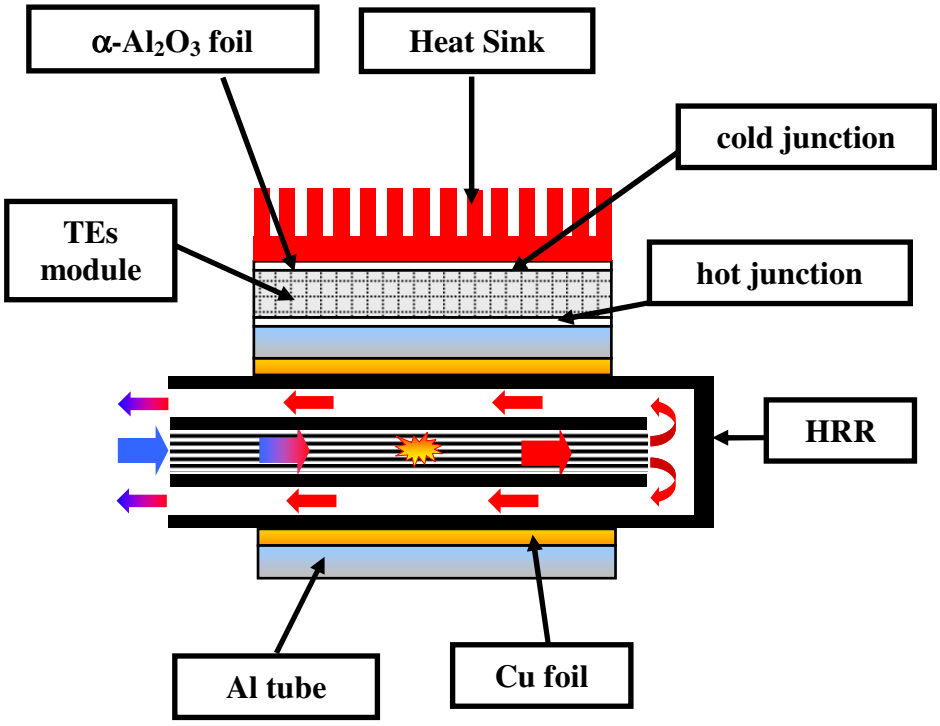

Figure 3.6 *Schematic representation of 2pTER. The main constituting parts are highlighted: Al tube, copper foils, HRR combustor, thermoelectric module (hot and cold junctions), heat sink, α-Al_2O_3 foils.*

In Figure 3.7 a schematic of the cross-sectional view of 3pTER generator is shown.
The coupling procedure of the thermoelectric module with the combustor is exactly the same as that employed in the case of 2pTER but differently from this generator, 3pTER is formed by a 3-pass heat recirculation reactor whose external wall is constituted by the aluminum tube. In other word, in 3pTER Al tube is not only a support of thermoelectric module but is a part of the reactor. As a consequence in the 3-pass generator the Al tube is much bigger than that employed in the case of 2-

pass generator. In Figure 3.8 a picture of 3pTER is shown. In particular, it is highlighted the presence of Swagelok-type fittings to mount the aluminum tube on HRR.

In Figure 3.9 a picture of the as-mounted 3pTER generator is reported. In particular, it is highlighted the presence of two external thermocouples employed to measure the hot and cold junctions temperatures. Moreover, the two electric wires exiting from thermoelectric module are shown. Actually, as it will be clear later, these wires constitute part of the electric circuit considered to test generator performances. In Figure 3.9 are also shown other generator elements like the C-clamp, the heating tape and the heat sink/thermoelectric stack.

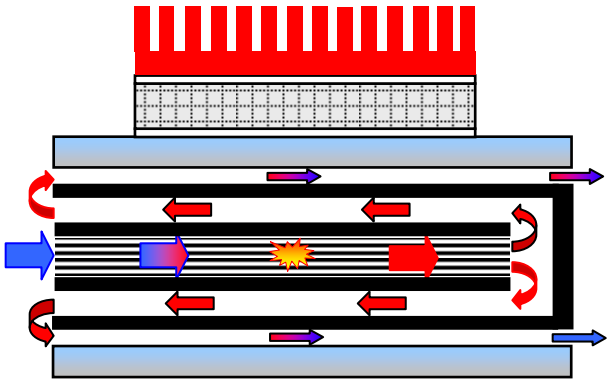

Figure 3.7 *Schematic representation of 3pTER. The main constituting parts are derived by comparing this drawing with that reported in Figure 3.5: Al tube, HRR combustor, thermoelectric module (hot and cold junctions), heat sink, α-Al_2O_3 foils.*

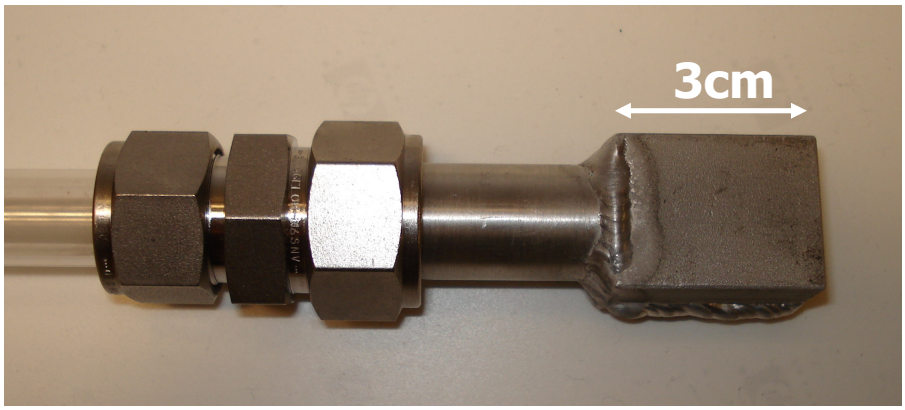

Figure 3.8 *Picture of 3pTER generator.*

3.2 Experimental apparatus

3.2.1 Diluted combustion tests

Reaction tests have been carried out in the experimental apparatus reported in Figure 3.10. Overall, it is divided into a gas feed, reactive and analysis sections, whose details are reported below.

Gas is stored in high purity cylinders; specifically, methane (IP 4.5), oxygen (IP 2.7), nitrogen (IP 4.8) and H_2/N_2 mixture (2Vol% H_2) have been used. Moreover, pure hydrogen has been provided by a generator (HG2400, Claind) based on water electrolysis.

Gas flow rates have been controlled through mass flow controllers (MFC 5850E, Brooks), communicating with a computer by means of a serial interface. Gas cylinders are provided with specific regulators adjusting the delivery pressure to the MFCs at their working value, (4 bar).

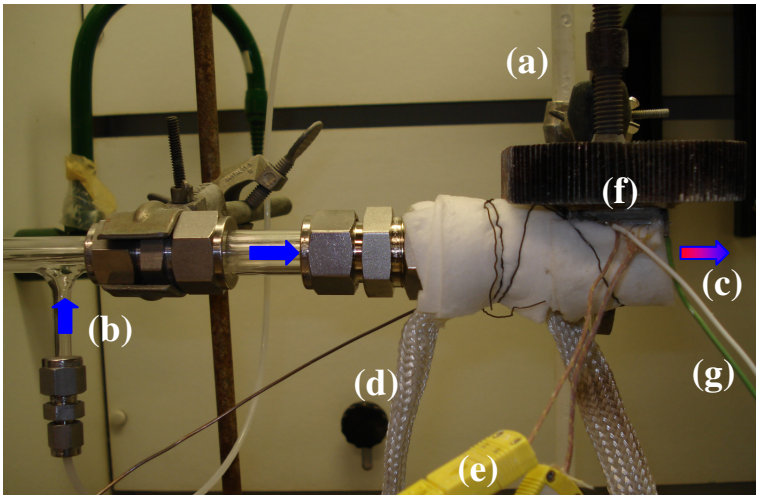

Figure 3.9 *Picture of as mounted 3pTER generator. (a) C-clamp; (b) gas inlet; (c) exhausted gas; (d) heating tape; (e) k-type thermocouples; (f) heat sink/thermoelectric stack; (g) electric wire exiting from TEs.*

Reactant gas passes through a four way valve and in dependence of the valve position enters the reactor or by-passes it. By-passing the reactor is necessary to measure the inlet gas composition.

In order to carry out combustion test under temperature controlled conditions, electric heating elements are employed. Specifically, a tubular furnaces (Lenton), working at a maximum temperature equal to 1200°C, is considered in the case of PwQR. In the case of SSR it is employed a muffle (AAF1100, Carbolite) working at maximum 1100°C. Both the furnaces are provided with a PID-type controller.

CH_4, CO, CO_2, H_2 and O_2 concentrations are measured continuously by means of an analyzer (NGA2000, Fisher-Rosemount). In particular, an infrared detector is employed for CH_4, CO, CO_2 analysis, a TCD provides hydrogen measurement while a para-magnetic cell is considered in the case of O_2 analysis. A software internal to the analyzer allows a concentration measurement corrected from eventual interferences in real time; in the specific, it is needed to take in account interferences in hydrogen measurement through TCD. Finally, the right use of the analyzer is guaranteed at a total flow rate comprised in the range of 12 and 90 slph.

In order to avoid water condensation inside the measurement cells of the analyzer, thus falsifying the analysis, exhausted gases are dried in a chemical trap constituted by a calcium chloride bed and placed downstream of the reactor. This kind of trap is effective and selective in adsorbing vapor while it is inert with respect to the other reaction reactants and products (particularly CO_2).

Moreover, the experimental apparatus allows flow rate measurements by means of a bubble flow meter.

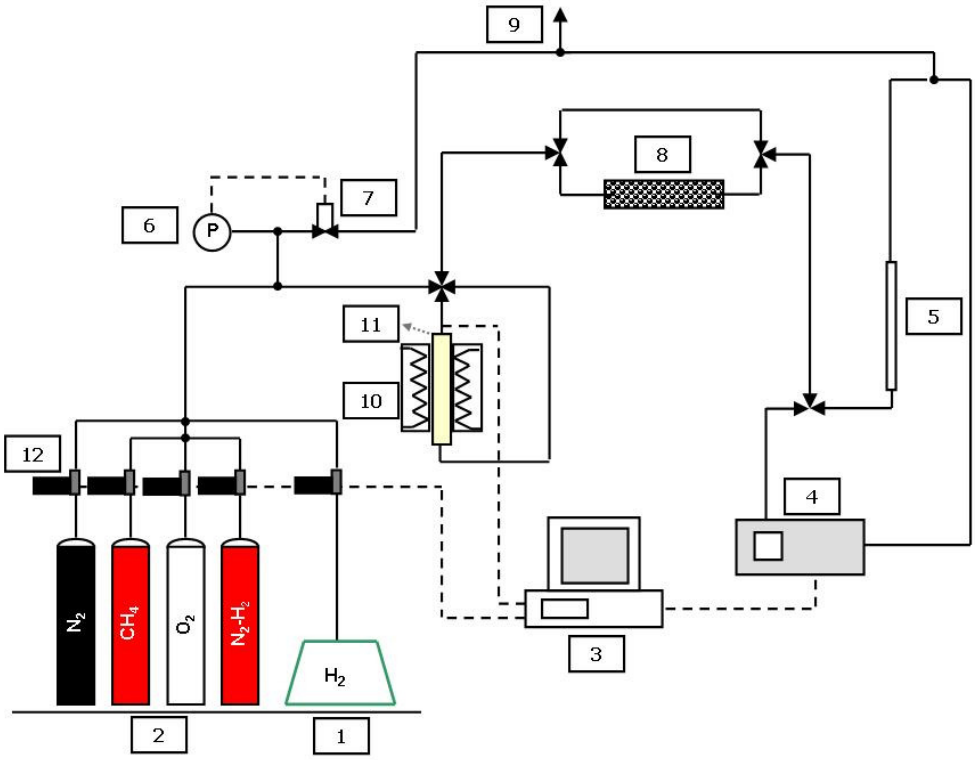

Legend:

1. ***H_2 Generator***
2. ***Gas cylinders***
3. ***Computer provided with a data acquisition board***
4. ***Analyzer***
5. ***Bubble flow meter***
6. ***Pressure transductor***
7. ***Electro valve***

8. ***$CaCl_2$ trap***
9. ***Venting***
10. ***Heating elements***
11. ***Reactor***
12. ***Mass flow controller***
--- ***Data lines and electrical signals***

Figure 3.10 *A description of the experimental apparatus for temperature controlled reaction tests.*

Relative pressure is detected upstream of the reactor by means of a transductor (ROSEMOUNT 2088). In order to vent eventual over pressure, an On-Off electrovalve (ASCO 8263) with a threshold value equal 0.5 bar is employed.

National Instruments data acquisition board (NI PCI-6229, M series DAQ) is used to acquire signals from thermocouples, transductor and analyzer. The data are collected, visualized, recorded and elaborated by means of a P.C. using a home-made software developed in Lab View environment.

3.2.2 Auto-thermal combustion tests

Combustion tests under auto-thermal conditions are carried out in the experimental apparatus reported in Figure 3.11.

As in the experimental apparatus described previously, a gas feed, a reactive and an analysis sections are present. Gases are stored in high purity gas cylinder; specifically, propane (IP 4.5), methane (IP 4.5), oxygen (IP 2.7), nitrogen (IP 4.8) and helium (IP 4.8) (the latter not reported in Figure 3.11) have been used; moreover the hydrogen generator (HG2400, Claind) is used. Gas flow rates are controlled throgh mass flow controllers (MFC 5850E, Brooks) and enters the reactors through a four way valve.

Actually, a total flow rate comprised between 40 and 150 slph is considered in the case of auto-thermal experiments but, as already stated before, maximum 90 slph could be sent to the analyzer for avoiding malfunction. So the experimental ring in this case has to provide for a splitting of the current into two part downstream of the reactor. Specifically, a part of the total flow rate goes through a needle valve and exits; only the remaining part goes to the analysis section. The needle valve has the aim of changing the pressure drop thus controlling the total flow rate sent to the analysis section.

High fuel concentration required for achieving auto-thermal condition brings about a vapor partial pressure in the exhausted higher than vapor pressure at room temperature. An ice bath based condenser is placed upstream of the trap in order to avoid its fast saturation.

As already described in the previous paragraph, Fisher-Rosemount NGA2000 analyzer is used to measure continuously CH_4, CO, CO_2, H_2 and O_2 concentrations.

In the case of propane combustion gas is analyzed using an HP 6890 Series Gas Chromatograph: CO_2 and O_2 are detected using a TCD detector, while C_3H_8 using both TCD and FID detectors.

Fuel mixtures are ignited by means of electric heating elements. Specifically, a tubular furnaces (Lenton), provided with a PID-type controller and working at a maximum temperature of 1200°C, is considered in the case of MQR reactor. A one-zone-controlled heating tape is instead employed in the case of HRR and NRR.

In order to reduce heat dissipation the reactors are thermally insulated with either ceramic wool or pyrogel (Aspen Aerogels).

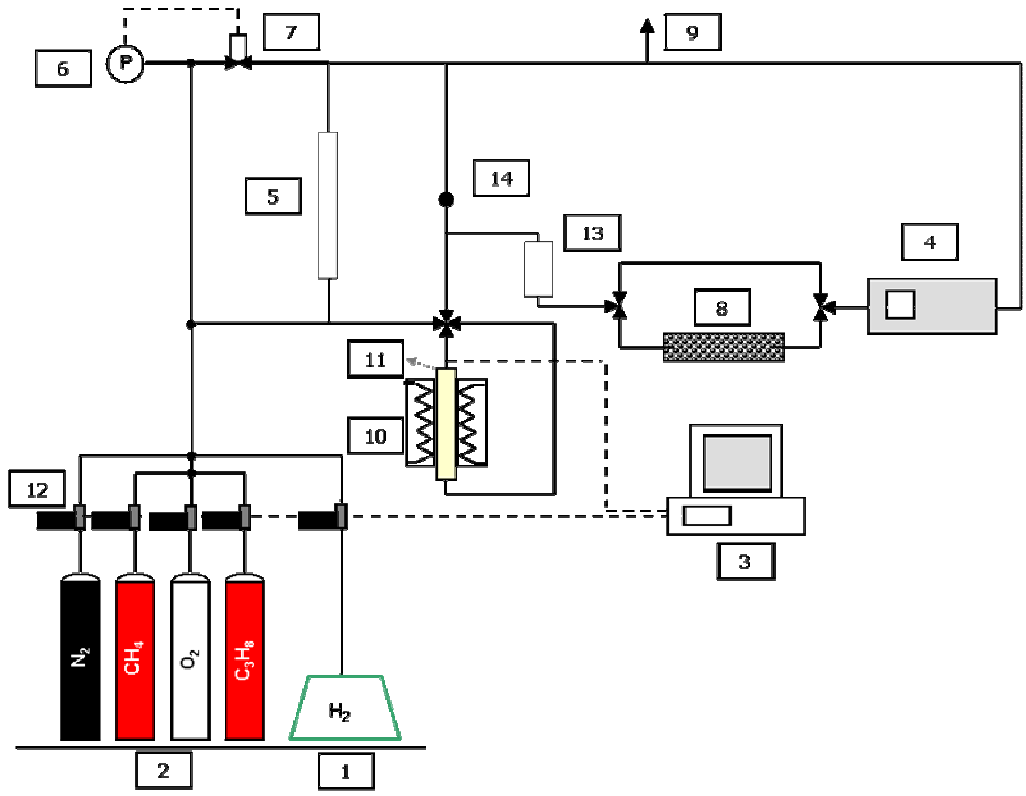

Legend:

1. ***H_2 Generator***
2. ***Gas cylinders***
3. ***Computer provided with a data acquisition board***
4. ***Analyzer or Gas Chromatograph***
5. ***Bubble flow meter***
6. ***Pressure transductor***

7. Electro valve
8. $CaCl_2$ trap
9. Venting
10. Heating elements
11. Reactor
12. Mass flow controller
13. Ice bath condenser
14. Needle valve
--- Data lines and electrical signals

Figure 3.11 *A description of the experimental apparatus for auto-thermal combyustion tests*

3.2.3 Measurements of electricity generators performances

To quantify power generation, the thermoelectric module is connected in series with a rheostat to simulate the operation of a portable electronic device. A voltmeter and an ammeter are used to measure respectively load voltage and current as a function of load resistance by varying the resistance of the rheostat.

In Figure 3.12 is reported the electric circuit considered in the testing of the generators. In such a figure, thermoelectric modules is represented by the box, the internal resistance of TEs is R_{int}, the load resistance is R_L and the A and V circles are respectively the ammeter and the voltmeter.

The ammeter is connected is series with the thermoelectric and measures the current i flowing through the circuit. The voltmeter is connected in parallel with the thermoelectric and measures the potential difference at its ends, V_{CD}. However, V_{CD} is also equal to the voltage drop at the ends of R_L, V_{CE}. According to the equation Eq. III.1, the power developed, P_{EL}, is obtained by the product of the measured values of the voltage and the current.

Moreover, in the electrical circuit shown in Figure 3.12 V_{AB} is the electrical potential developed by the thermoelectric module or Seebeck voltage. By applying Ohm's law on the whole circuit is possible to calculate the current as a function of V_{AB} and R_{int} (Eq. III.2). As a results, by substituting such an expression of current in Eq. III.1, it is possible to obtain P_{EL} as a function of the Seebeck voltage, of R_{int} and of R_L. Actually, considering the first derivative of P_{EL} as regard R_L it results that P_{EL} shows a maximum in correspondence with $R_L=R_{int}$.

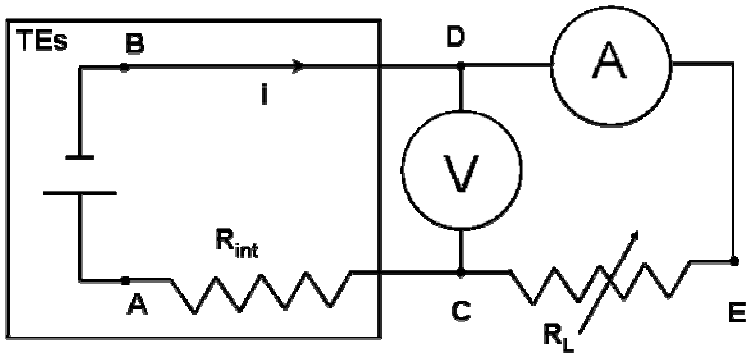

Figure 3.12 *Electrical circuit considered in the perfomances tests of 2pTER and 3pTER generators .*

Seebeck voltage, V_{AB} is obtained multiplying the thermal gradient at which TEs are subjected (T_{HOT}-T_{COLD}) by the apparent Seebeck coefficient, α', exhibited by the module (see Eq. III.3). However, V_{AB} is related to the measured electrical potential through the equation Eq. III.4. Once noted the internal resistance of the module and the number of thermocouples constituting it, by measuring voltage and current as indicated it is possible to evaluate the Seebeck coefficient α of the material constituting TEs (see Eq. III.5).

$$P_{EL} = V_{DC} \cdot i = R_L \cdot i^2 = R_L \cdot \left[\frac{\alpha' \cdot (T_{HOT} - T_{COLD})}{R_L + R_{int}} \right]^2 \qquad \textit{Eq. III.1}$$

$$i = \frac{\alpha' \cdot (T_{HOT} - T_{COLD})}{R_L + R_{int}} \qquad \textit{Eq. III.2}$$

$$\alpha' \cdot (T_{HOT} - T_{COLD}) = V_{AB} \qquad \textit{Eq. III.3}$$

$$\alpha' \cdot (T_{HOT} - T_{COLD}) - R_{int} \cdot i = V_{DC} \qquad \textit{Eq. III.4}$$

$$\alpha = \frac{R_{int} \cdot i + V_{DC}}{(T_{HOT} - T_{COLD}) \cdot n} \qquad \textit{Eq. III.5}$$

V_{DC}	(measured voltage)
i	(measured current)
V_{AB}	(Seebeck voltage)
T_{HOT}	(temperature of the hot junction of thermoelectric)
T_{COLD}	(temperature of the hot junction of thermoelectric)
α'	(apparent Seebeck coefficient)

α	(Seebeck coefficient)
n	(number of thermocouples constituting thermeoelectric)

CHAPTER 4

COMBUSTION TESTS UNDER DILUTED CONDITIONS

Combustion of methane, hydrogen and their mixtures has been carried out in a novel catalytic micro-structured reactors developed in this Ph. D. research activity, as described in the previous chapter, and tested in the SSR.

Supported perovskite based catalysts have been considered and the effect of doping perovskite with a little amount of platinum has been taken into account and, thus, Pt/Al_2O_3 catalyst has been prepared and tested as reference material too.

The effectiveness of the deposition method in transferring the catalytic properties to the platelet shaped substrates has to be preliminarily verified. At this proposal, the activity of the catalytic platelets has been compared with that of the powder constituting the deposed layer. As a consequence, the first paragraph of this chapter is devoted to the results of combustion tests carried out on powder samples in PwQR.

In a structured catalytic reactor, and in particular in a micro-combustor, the proceeding of heterogeneous reaction may be strongly affected by fluid dynamics issues. In particular, flow distribution may be critical because of gas by-passing and channeling as well as the presence of dead volumes in the reactor, resulting in a loss of combustor efficiency. Moreover fuel conversion may be transport limited thus not allowing an efficient use of the catalyst, especially in a fully developed laminar fluid dynamics regime, typical in micro-combustion.

As described in the previous chapter, the SSR reactor design has included specific solution to allow a good flow distribution. In particular SiC carbide foams inserted before and after the plates are determinant in minimizing gas channeling and stagnation phenomena. Furthermore, the high precision adopted in the realization of the catalytic micro reactor allows to suppress any gas path alternative to that through the combustion chamber, actually avoiding gas by-passing.

However, a specific study is needed for the comprehension of eventual transport limitation on fuel conversion. As demonstrated in the following, the proposed micro-structured reactor is an effective tool to carry out such a study because of the total uncoupling of the reactive phenomena with fluid dynamics. In fact, such a reactor gives the possibility to perform combustion tests with varying the characteristic properties of transport maintaining unaltered the catalysis. In the specific,

the height of the combustion chamber is changed by varying the height of the platelet but without modifying the amount of considered catalyst.

The study on CH_4-H_2 combustion has been addressed toward the comprehension of hydrogen effect on methane oxidation rate. Specifically, the chosen operating conditions allow to neglect the thermal effect and to focalize the attention on eventual chemical synergies occurring in the co-combustion.

4.1 Operating conditions

Activity tests have been carried out under isothermal and strongly diluted conditions. In such conditions the power generated by the reaction is not enough to guarantee auto-thermal process and an external power source is needed to carry out the reaction. On the contrary, the amount of heat released by the conversion of fuel is almost negligible with respect to the warming power needed from outside, so that isothermal and controlled conditions could be assured. As already reported in the previous chapter, electric ovens are employed to heat the catalytic combustor until a specific reaction temperature. Specifically, activity tests have been performed at a maximum temperature equal to 800°C.

Unless otherwise noted, as prepared catalysts are pre-treated at 800°C for 3h before being tested.

Hydrogen and methane oxidation tests have been carried out at different flow rates in the range 15-70 slph. Fuel percentage in the mixture was 0.25vol% in the case of methane and 1vol% in the case of hydrogen (in both the cases fuel concentration is below the LFL that is 4 and 5% respectively foe H_2 and CH_4 combustion), thus approximately supplying the same overall heating value of 80 $J \cdot Nl^{-1}$ despite of the fuel. Oxygen content is four times higher than the stoichiometric value required for complete combustion occurrence, corresponding to an equivalence ratio (Φ=0.25).

In Table IV.1. compositions of the fuel mixtures considered for H_2 and CH_4 combustion tests are reported.

Concerning the study of H_2-CH_4 mixtures combustion, experiments have been carried out by varying the H_2/CH_4 ratio at a total flow rate varying between 15÷70 slph (see Table IV.2 for details). As it is reported in Table IV.2, Mix1 up to Mix6 are characterized by a growing content of H_2 while leaving the overall calorific value of the fuel constant (80 $J \cdot Nl^{-1}$). The molar H_2 fraction in the H_2-CH_4 mixtures varyies from 0% in Mix1 to 91% in Mix6, corresponding to a maximum energetic substitution equal to 75% of the total power input. Mix7 and Mix8 are methane free mixtures and are characterized by a lower overall heating, respectively equal to 33 and 45 $J \cdot Nl^{-1}$. Hydrogen and methane are fed in very diluted conditions, below the LFL of the considered

mixtures. Moreover, oxygen concentration is maintained constant and equal to 2vol%, resulting in excess with respect to fuel oxidation stoichiometry. In Mix7 and Mix8 hydrogen concentration is the same as that respectively present in Mix3 and Mix4; methane free mixtures are tested in order to have a reference of hydrogen combustion occurring at the same partial pressure as in H_2-CH_4 mixtures.

Table IV.1 *Operating conditions considered in the case of H_2 and CH_4 combustion tests*

	H_2 combustion, %	**CH_4 combustion, %**
H_2	1.00	0
CH_4	0	0.25
O_2	2.00	2.00
N_2	97.00	97.75
Total Flow Rate = 15÷70 slph		

Table IV.2 *Hydrogen substitution and operating conditions considered in H_2-CH_4 mixtures combustion tests.*

	Molar composition			**H_2 in H_2-CH_4, %**	
	CH_4, %	*H_2, %*	*H_2/CH_4 Ratio*	*Molar*	*Energetic*
Mix 1	0.25	0	0	0	0
Mix 2	0.21	0.21	1.0	50	23
Mix 3	0.17	0.34	2.0	67	38
Mix 4	0.14	0.46	3.3	77	50
Mix 5	0.11	0.55	5.0	83	60
Mix 6	0.07	0.68	10.0	91	75
Mix 7	0	0.34	-	100	100
Mix 8	0	0.46	-	100	100
Total Flow Rate = 15÷70 slph					

4.2 Methane combustion tests on powder catalysts

Catalytic combustion tests of methane have been carried out in PwQR packed bed reactor on PwLM sample. As already reported, PwLM is a $LaMnO_3$/La-Al_2O_3 based catalyst characterized by a perovskite loading equal to 20wt% with respect to the total weight; moreover, it is constituted by the particles forming the catalytic layer deposed on the platelets.

A total flow rate equal to 40 slph and 0.2 g of catalyst have been employed in the activity tests. Considering a particle size distribution ranging between 200 and 400 μm, it resulted in a catalytic bed height approximately equal to 0.6 cm.

A packed bed reactor is a system of proven effectiveness in measuring the kinetic constant of an heterogeneous reaction. For such a reactor, in fact, it is possible to establish operating conditions such as to neglect any fluids dynamics and transport influence on the proceeding of the catalytic reaction.

An high enough catalytic bed is needed to neglect flow instability due to the entrance effects. Actually, the height of the bed considered in this study is reported to be large enough to avoid such an instability.

On the basis of the previous assumptions, the catalytic bed reactor employed in the present investigation could be considered as a plug flow reactor, provided that axial dispersion is shown to be negligible. This assumption is validated by previous assumptions together to the evaluation of the characteristic Peclet number (Pe_r) of the reactor. Pe_r is calculated starting from the evaluation of Pe_p, characteristic of the flow around the single particle.

On the basis of the previously reported operating conditions adopted in the combustion tests and geometric properties of the PwQR reactor it is possible to determine the following parameters:

m_{cat}	(total weight of the catalysts)	0.2g
Q_{TOT}	(total flow rate)	$2.7 \cdot 10^{-5} m^3 \cdot s^{-1}$
$\tau_C = \frac{m_{cat}}{Q_{TOT}}$	(contact time)	$7407.4 g_{cat} \cdot s \cdot m^{-3}$
$<d_P>$	(average particle size)	$3 \cdot 10^{-4} m$
ε	(catalytic bed empty fraction)	0.36
L	(catalytic bed length)	0.0060m
u_L	(average gas velocity in the catalytic bed)	$1.5 m \cdot s^{-1}$
A	(annular section of the quartz reactor)	$5 \cdot 10^{-5} m^2$
ρ_{app}	(apparent density of the catalyst)	$1.8 g \cdot cm^{-3}$

Gas velocity and total flow rate are calculated assuming the minimum temperature taken into account in the experiments (450°C).

Below the properties of reactive mixture assumed to be air are reported considering the same temperature reference.

μ	(air viscosity)	$3.6 \cdot 10^{-5}$ Pa·s
ρ	(air density)	0.47 Kg·m^{-3}
D_{CH4}	(diffusivity of CH_4 in air, Perry and Green, 1997)	$1.0 \cdot 10^{-4}$ m^2·s^{-1}

It is possible to calculate a Reynolds number (Re) and a Schmidt number equal to:

$$Re = \frac{< d_P > \cdot u_L \cdot \rho}{\mu} \cong 6$$

$$Sc = \frac{\mu}{\rho \cdot D_{CH4}} \cong 0.8$$

Based on these parameters it is possible to evaluate Pe_p (Levenspiel, 1962):

$$Pe_p = \frac{< d_P > \cdot u_L}{D} \cong 2$$

Finally, Pe_r evaluation follows

$$Pe_r = \frac{u_L \cdot L}{D} = \frac{Pe_P \cdot L}{< d_P >} \cong 40$$

Such a Pe_r value is high enough to validate the hypothesis of plug flow reactor for the catalytic bed considered in the activity tests.

According to the reported assumptions, the PwQR packed bed reactor is well represented by the equation Eq. IV.1, that is a mass balance on the fuel (methane) under the hypothesis of plug flow reactor. Methane oxidation reaction in fact, may be assumed as a single irreversible reactive step, A→B where the kinetics are described by a simple power rate law thus considering unitary the reaction order with respect to the methane and zero to the oxygen. Concerning CH_4 reaction order, the first order assumption is in agreement with many studies reported in literature performed on Pt and perovskite based catalysts (Arai et al. 1986, Cimino et al. 2000). As regards the reaction order

of the oxygen it is reported that is slightly higher than zero (Arai et al. 1986, Cimino et al., 2000). However, the oxygen excess considered in the reaction tests allows to neglect the effect on the reaction rate of the variation of the O_2 concentration respect to that of CH_4. After all, the reported assumptions on the reaction order are reasonably valid especially when the aim is a preliminary evaluation of the kinetic constant.

$$\frac{dc}{dt} = -r_{app} = -k \cdot c = -k_0 \cdot e^{-\frac{E}{R \cdot T}} \cdot c \qquad \textbf{Eq. IV.1}$$

$$\ln k = \ln k_0 - \frac{E}{R \cdot T} = \ln\left[-\frac{\ln(1-x)}{\tau_C}\right] \qquad \textbf{Eq. IV.2}$$

c	(methane concentration)	$mol \cdot m^{-3}$
c_0	(initial methane concentration)	$mol \cdot m^{-3}$
k	(apparent kinetic constant for unit of catalyst amount)	$m^3 \cdot s^{-1} \cdot g_{cat}^{-1}$
r_{app}	(apparent reaction rate)	$mol \cdot m^{-3} \cdot s^{-1}$
k_0	(pre-exponential factor)	$m^3 \cdot s^{-1} \cdot g_{cat}^{-1}$
E	(apparent activation energy)	$cal \cdot mol^{-1}$
x	(fuel conversion)	mol/mol

Among the reported parameters, r_{app} is the apparent reaction rate of the process, generally derived on the basis of laboratory experiments. Such a parameter depends on transport effects and it is equivalent to the intrinsic reaction rate only in a pure kinetic controlled regime. The combined effect on the effective reaction rate of interphase and interparticle diffusion is reduced in a catalyst efficiency, η_C, given by the ratio between the apparent and the intrinsic reaction rate (Ertl et al., 1997).

$$\eta_C = \eta_{pore} \cdot \eta_{ext} = \frac{r_{app}}{r_b} \qquad \textbf{Eq. IV.3}$$

$$\eta_{pore} = \frac{r_{app}}{r_s} \qquad \textbf{Eq. IV.4}$$

$$\eta_{ext} = \frac{r_s}{r_b} \qquad \textbf{Eq. IV.5}$$

In the equations Eq. IV.3 and IV.5, r_b is the reaction rate that is obtained if the reactant concentration on the catalyst corresponds to that in the bulk. Nevertheless, a concentration drop occurs because of the resistance to mass transport in the gas phase and in the catalyst pores. In a kinetic controlled regime transport rate is much higher compared to that of the intrinsic reaction and the catalyst efficiency my be assumed unitary.

The equation Eq. IV.1 is solved taking into account the initial condition on methane concentration, $c(t=0)=c_0$; the solution is represented by the equation Eq. IV.2 that is the Arrhenius plot and provides the kinetic constant estimated from the experimental measurements as a function of the fuel conversion (and hence, of the experimental conditions adopted). From equation Eq. IV.2 it follows the characteristic time of the packed bed reactor, the contact time, defined as the amount of catalyst divided by the total flow rate. Its unit is not properly a time, but it can be possible to have the residence time (in the contact with catalysts) by multiplying it for an apparent packed bed density.

In Figure 4.1 the results of methane combustion tests performed on PwLM are reported while in Table IV.3 some extrapolated experimental data are resumed.

In Figure 4.1a, the fuel conversion is reported as a function of the temperature measured inside the catalytic bed. The threshold temperature of PwLM catalyst for CH_4 oxidation, defined as the temperature at which 10% of fuel is converted, lies at about 565°C; fuel conversion is 95% at 750°C, while it is expected to be 100% at 800°C. In the investigated conditions, the presence of CO as by-product of CH_4 oxidation is not detected being methane completely converted to CO_2. In Figure 4.1 b the kinetic constant of methane combustion over PwLM catalyst is shown in terms of the Arrhenius plot; in Table IV.3 the values of the activation energy and the pre-exponential factor as well as the kinetic constant at 800°C are resumed. It is worth mentioning that the detected activation energy (31.8 kcal·mol^{-1}) is rather high respect to the typical values, comprised between 23 e 26 Kcal/mol, reported in the case of methane combustion on non supported perovskite (Cimino et al., 2000, Seiyama, 1992, Kirchnerova et al., 2002). This experimental evidence points out that γ-Al_2O_3 support affects the kinetic mechanism of methane combustion on perovskite probably because of an alteration in the morphology of the active phase due to the interactions occurring between manganese and alumina (Choudhary et al., 2002, Cimino et al., 2000, Arnone et al., 1998).

Nevertheless, a different behaviour is observed by testing, under the same operating conditions, LM(10, 20, 30) constituted by the same $LaMnO_3$/La-γ-Al_2O_3 active phase as PwLM but not representative of the platelet catalyst (in such a case supported perovskites prepared by impregnating stabilized γ-Al_2O_3 is not further mixed to Boehmite and nitric acid but directly calcined, see Chapter 2 for details). In particular, the activation energy shown by LM(10, 20, 30)

samples is significantly lower than that measured for PwLM (see Table IV. 3) and it is in agreement with that reported in literature for both supported and unsupported perovskites (Cimino et al., 2000, Seiyama, 1992, Arnone et al., 1998, Choudhary et al., 2002). As a result, catalytic properties of perovskites are altered in the case of PwLM catalyst. Based on this evidence, it is possible to conclude that eventual interactions occurring between manganese and alumina in $LaMnO_3$/La-γ-Al_2O_3 are exalted by structuring the catalyst.

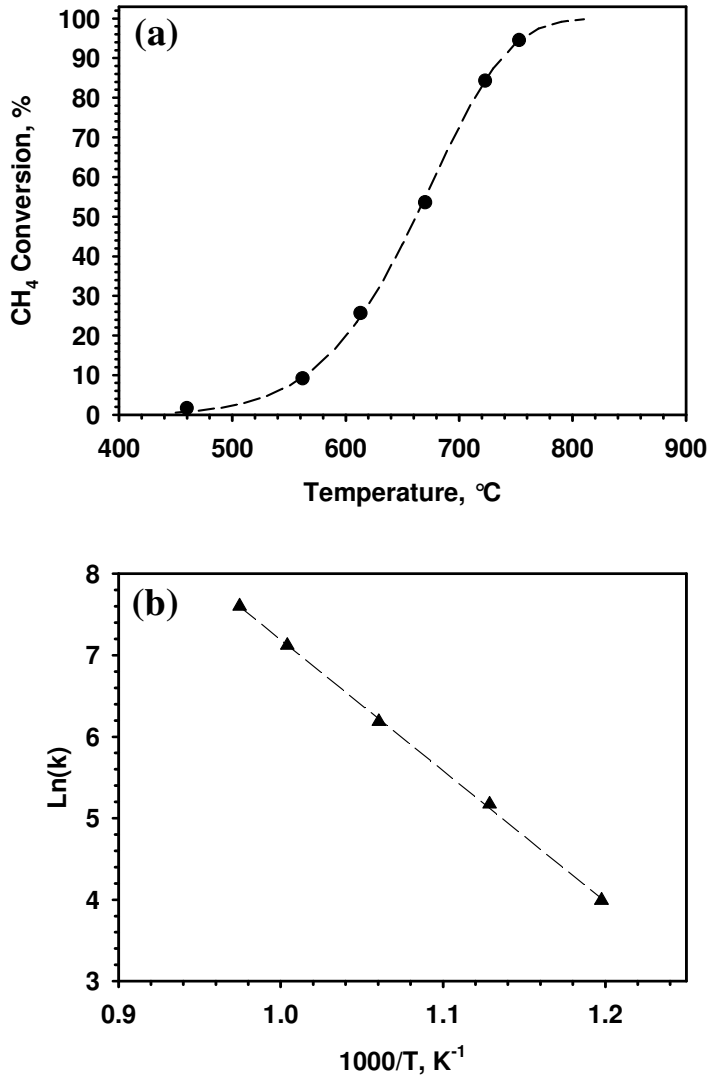

Figure 4.1 *CH_4 combustion test performed on PwLM catalyst (contact time τ_c = 18 g·s·Nl^{-1}). (a) Fuel conversion as a function of the temperature measured in the catalytic bed. (b) Arrhenius plot.*

In table IV.3 it is also pointed out that the kinetic constant evaluated at 800°C shown by LM(10, 20, 30) samples is unchanged and it is significantly lower that that measured for PwLM. This result is due to the different ageing treatments performed on the catalysts. Specifically a more severe

treatment is considered in the case of LM(10, 20, 30) samples that are exposed to 900°C for three hours.

Table IV.3 *CH_4 combustion test performed on PwLM and LM(10, 20, 30)catalyst. Resume of some extrapolated experimental data.*

Catalyst Code	Contact time $g_{cat}\cdot s\cdot Nl^{-1}$	E $Kcal\cdot mol^{-1}$	k_0 $Nl\cdot s^{-1}\cdot g_{cat}^{-1}$	$T_{10\%}$ °C	K(800°C) $mmol\cdot s^{-1}\cdot g_{cat}^{-1}$
PwLM	18.00	31.8	$3.48\cdot10^{6}$	565	12
LM10	18.00	26.4	$1.4\cdot10^{5}$	574	6
LM20	18.00	23.6	$3.2\cdot10^{4}$	550	6
LM30	18.00	23.0	$2.3\cdot10^{4}$	550	5

Once the apparent kinetic constant has been derived experimentally for PwLM sample, it is possible to evaluate the catalyst efficiency thus estimating the transport effects. In particular, η_C is calculated following the treatment reported in Eartl et al, 1997. Based on this method catalyst efficiency is evaluated from Weisez and mass transfer Biot modules, respectively ψ and Bi,m in the equations Eq. IV.6 and IV.7. The former is defined as the ratio of the effective pseudohomogeneous reaction rate, r_{app}, versus the maximum effective rate of diffusion at the external pellet surface, thus including the effect of pore diffusion on the reaction rate. Physically, the Weisz modulus can be looked at as the ratio of the time constants of diffusion and reaction. The effective diffusivity, D_{eff}, is derived from molecular diffusivity of methane in air, D_{CH4}, by multiplying and dividing it respectively by the porosity and tortuosity factors of the catalyst particles. Specifically, ε_P=0.6 and τ=3 are assumed.

Concerning Bi,m, it is interpreted as the ratio of internal to external transport resistance (interparticle diffusion versus interphase diffusion) thus including the effect of film diffusion on the reaction rate. Diffusion velocity, K_D, is evaluated from j_D that is estimated through the correlation, $j_D=0.91\cdot Re^{-0.51}$ (Perry and Green, 1997).

$$\Psi = \frac{k\cdot\rho_{app}\cdot(1-\varepsilon)\cdot<d_P>^2}{4\cdot D_{eff}} \qquad \textit{Eq. IV.6}$$

$$Bi,m = \frac{K_D\cdot<d_P>}{2\cdot D_{eff}} \qquad \textit{Eq. IV.7}$$

$D_{eff} = \frac{D_{CH_4} \cdot \varepsilon_P}{\tau}$ (effective diffusivity)

ε_P=0.6 (porosity factor of particle)

τ=3 (tortuosity factor of the particle)

K_D (diffusion velocity)

$j_D = \frac{K_D}{u_L} \cdot (Sc)^{2/3}$ (Colburn factor for mass transfer)

In Table IV.4 the values of η_C, ψ and Bi,m are reported as a function of the temperature. These modules are calculated assuming a particle diameters, $<d_P>=3\cdot10^{-4}$m, characteristic of PwLM catalyst. Moreover, in order to understand the effect of such a parameter on catalysts efficiency, a $<d_P>=1\cdot10^{-4}$ m is considered too.

Considering the higher particle diameter, at T=700°C an unitary catalyst efficiency is calculated thus pointing out a kinetic controlled regime. By increasing the temperature a decrease in the catalyst efficiency is observed. In particular, η_C is 0.95 and 0.7 at 725°C and 800°C respectively. Such a trend of η_C is expected because the reaction rate increases exponentially with the temperature while transport parameters are roughly unchanged. Interphase diffusion velocity is higher than interparticle one even if the same order of magnitude is calculated (see Bi,m values in Table IV.4).

In the range of investigated temperature (450÷750°C) PwLM catalyst efficiency is sufficiently high to neglect any transport effect on the reaction rate. On the contrary, beyond T=750°C the mass transfer become determinant and a mixed kinetic and transport controlled regime occurs.

However, in the case of a lower particle diameter, $<d_P>=1\cdot10^{-4}$m, an unitary efficiency is calculated in a wider range of temperature and in particular η_C=1 results at 800°C. Actually, a decrease in $<d_P>$ involves an increase in the mass transfer rate compared to that of the chemical reaction.

It is worth mentioning that $<d_P>=1\cdot10^{-4}$m is approximately the thickness of the catalytic layer deposed on a substrate. As a consequence, a kinetic controlled regime is expected in the case of oxidation test on catalytic platelets assuming that reaction rate is maintained the same as that of unstructured catalyst.

Table IV.4 *Combustion test on PwLM: η_C, ψ and Bi,m are reported as a function of the temperature*

Temperature, °C	$\langle d_P \rangle = 3 \cdot 10^{-4}$ m			$\langle d_P \rangle = 1 \cdot 10^{-4}$ m		
	η_C	ψ	*Bi,m*	η_C	ψ	*Bi,m*
700	1	0.18	4.46	1	0.02	2.60
725	0.95	0.26	4.43	1	0.03	2.58
750	0.85	0.37	4.39	1	0.04	2.56
775	0.80	0.51	4.35	1	0.06	2.54
800	0.70	0.70	4.32	1	0.08	2.52

4.3 Combustion tests on platelets catalysts

Catalytic combustion tests of methane, hydrogen and mixture between them have been carried out in SSR reactor on catalytic platelets. For such a peculiar system, a preliminary study is needed to understand any eventual limitations to fuel conversion due to fluid dynamics and transport issues. Before presenting the results of an experimental campaign, a mathematical description of the SSR reactor is also reported with the aim to understand and assess the main phenomena involved in the micro combustor operation.

As already reported, in SSR structured reactor gas flows in the channel, tangentially with respect to the catalytic surface. In order to have a good contact between the reactants and the catalyst, the Peclet number, defined as the ratio between the residence and the diffusion time, needs to be much higher than unity. Moreover, in order to avoid a transport limited regime the diffusion time has to be much lower that the reaction time.

Reactor geometry, gas properties, combustion test operating conditions, parameters and non dimensional groups employed are reported below.

Geometrical reactor properties:

W	(platelet width)	0.015 m
L	(reactor length)	0.0300 m
δ	(combustion chamber height)	0.0010 m
$\delta_H = 4 \cdot \frac{CrossSection}{WetPerimeter} = 4 \cdot \frac{W \cdot \delta}{2 \cdot (W + \delta)}$	(equivalent diameter)	0.0019 m
δ_W	(washcoat thickness)	$5 \cdot 10^{-5}$ m

Considered operating conditions (reference temperature is equal to 800°C):

$Q_{TOT}=4.0\cdot10^{-5}$ $Nm^3\cdot s^{-1}$
$u_L=2.7$ $m\cdot s^{-1}$

Gas properties values (reference temperature is equal to 800°C):

$\rho=0.32$ $Kg\cdot m^{-3}$
$\mu=4.3\cdot10^{-5}$ $Pa\cdot s$
$D_{CH4}=1.9\cdot10^{-4}$ $m^2\cdot s^{-1}$

Parameters and variables:

k_b	(intrinsic kinetic constant for unit of catalyst amount)	$m^3\cdot s^{-1}\cdot g_{cat}^{-1}$
k_b'	(intrinsic kinetic constant for unit of catalytic surface)	$m\cdot s^{-1}$
$\tau_R = \frac{L}{u_L}$	(residence time)	s
c_S	(fuel concentration in the solid phase)	$mol\cdot m^{-3}$

Non dimensional groups:

Re	(Reynolds number)	$\rho\cdot v\cdot\delta_H/\mu$
Sc	(Schmidt number)	$\mu/(\rho\cdot D_{CH4})$
Sh	(Sherwood number)	$K_D\cdot\delta_H/D_{CH4}$
Pe	(Peclet number)	$(L/u_L)/(\delta_H/K_D)$

Gas flows through the SiC foams and enters the combustion chamber with a Re number varying in the range of 35÷40. At the entrance section the velocity profile is flat and a certain reactor length is required to allows the developing of the laminar regime, as represented in Figure 4.2. The hydrodynamic entrance length L_{ent}, under the hypothesis of isothermal and incompressible flow, is given by the equation Eq. IV. 8 (Hayes and Kolaczkowski, 1997) and is equal to 2.4 mm. Considering that the reactor is 30mm long, more than 90% of the total combustor length is characterized by a fully developed laminar flow. On the basis of this estimation, the flow is considered laminar along the whole channel.

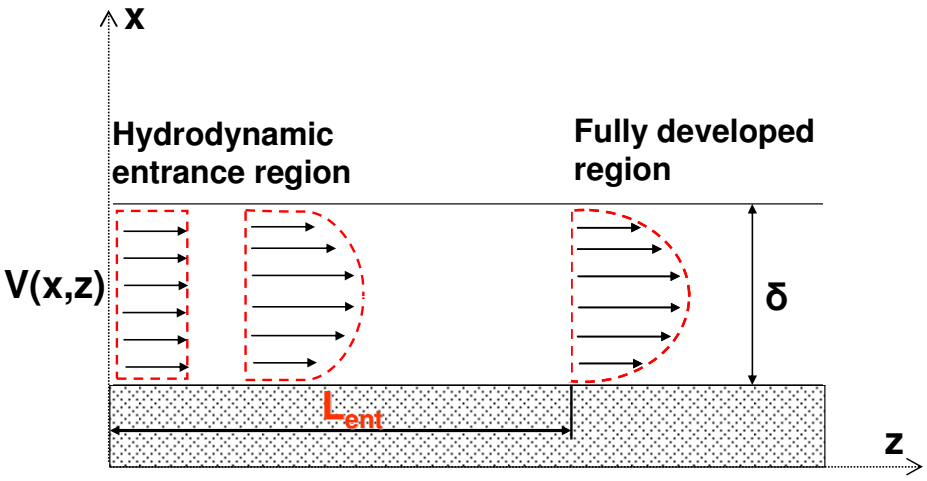

Figure 4.2 *Velocity profile development in the entrance of SSR micro-structured reactor.*

$$L_{ent} = 0.035 \cdot \delta_H \cdot Re \qquad \textit{Eq. IV. 8}$$

In the conditions of fully developed laminar regime, it is possible to evaluate a Sh number approximately equal to 4 (Bird et al., 1979). This value of Sh number together with the values of diffusivity and equivalent diameter previously reported supply a diffusion velocity $K_D = 0.41$ m·s^{-1}. Once evaluated the diffusion velocity, it is possible to calculate the Peclet number. In the specific, a Pe ≈ 30 is estimated, a value enough high to allow considering the reactants diffusion on the catalytic substrate satisfactorily efficient to avoid gas exiting from the reactor without contacting the catalyst.

The reactor behaviour can be hence described through a one dimensional model and more specifically through an heterogeneous model (Hayes and Kolaczkowski, 1997). According to this model, no transverse concentration gradient occurs in the gas phase. Species concentration shows a discontinuity at the gas-solid interface thus providing the driving force for the reactants transport on the catalyst. Separate mole balance is written for the solid which is coupled with gas phase equations. Reactants diffusion from the gas bulk to the catalytic surface is described through K_D (that is a diffusion velocity in the gas phase). This is coherent with the hypothesis of one dimensional model not including the solution of species mass balance on the transverse direction.

The equations Eq. IV.9-11 represent the mass balance in the gas phase. Basically, considering the elemental reactor volume represented by the red broken line in Figure 4.3, the difference between the incoming and outcoming moles must be equal to the moles transported to the catalyst

surface. In Eq. IV. 9 the mass balance is reported in terms of differential equation with the corresponding boundary condition.

[Moles in]- [Moles out]- [Moles transported to catalyst surface]=0 ***Eq. IV. 9***

$$Q\cdot[c(z)-c(z+dz)]-K_D\cdot(c-c_S)\cdot W\cdot dz=0 \qquad \textit{Eq. IV. 10}$$

$$\begin{cases} Q\cdot\dfrac{dc}{dz}-K_D\cdot W\cdot(c-c_S)=0 \\ c(z=0)=c_0 \end{cases} \qquad \textit{Eq. IV. 11}$$

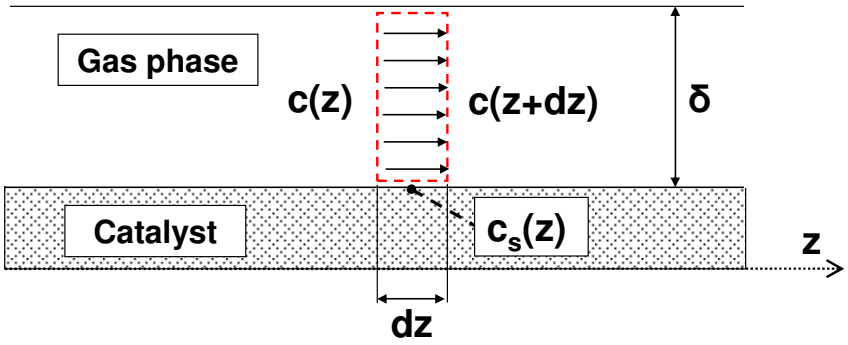

Figure 4.3 SSR*: approximations of the heterogeneous model. No transverse profile of concentration in the gas phase. The gas solid interface is a discontinuity.*

The equations Eq. IV.12-14 represent the mass balance in the solid phase. Basically, considering an elemental catalytic surface, it is assumed that the moles transported to the catalyst surface react following a first order reaction rate. In Eq. IV. 14 the value of the fuel concentration on the catalytic surface, c_S, is calculated as a function of the fuel concentration in the gas phase, c.

[Moles reacted on the catalyst]- [Moles transported to catalyst surface]=0 ***Eq. IV. 12***

$$k_b'\cdot c_S(z)\cdot W\cdot dz - K_D\cdot(c-c_S)\cdot W\cdot dz=0 \qquad \textit{Eq. IV. 13}$$

$$c_S=\frac{K_D\cdot c}{K_D+k_b'} \qquad \textit{Eq. IV. 14}$$

Substituting the equation Eq.IV.14 into the Eq. IV.11, it is possible to obtain a differential equation with the gas phase concentration, c, as the only unknown. The Eq. IV.15 represents the solution of the differential problem and provides the fuel conversion at the exit of the reactor.

$$x = 1 - \exp\left(- \frac{K_D \cdot k_b^{'}}{K_D + k_b^{'}} \cdot \frac{W \cdot L}{Q} \right) \qquad \textbf{\textit{Eq. IV. 15}}$$

Assuming $K_D >> k_b^{'}$, that is what happens under a kinetic regime, the solution of the mass balance equation is given by Eq. IV.16, which has been given in terms of $k_b^{'}$. By multiplying and dividing the exponential term by both the thickness and the apparent density of the catalytic layer, it is possible to obtain the solution in terms of k_b. It is worth mentioning that fuel conversion, in the case of a kinetic regime, does not depend on the geometry of the reactor and particularly on the height of the combustion chamber, but should depend only on the intrinsic activity of the catalyst and contact time $\tau_C = m_{cat}/Q$.

$$x = 1 - \exp\left(- k_b^{'} \cdot \frac{W \cdot L}{Q} \right) = 1 - \exp\left(- \frac{k_b^{'}}{\delta_W \cdot \rho_{app}} \cdot \frac{m_{cat}}{Q} \right) = 1 - \exp\left(- k_b \cdot \frac{m_{cat}}{Q} \right) \qquad \textbf{\textit{Eq. IV. 16}}$$

On the other hand, looking at the case characterized by $K_D << k_b^{'}$, that is the transport-limited regime, the solution of the mass balance equation is given by Eq. IV.17. Multiplying and dividing the exponential term by the height of the combustion chamber it is possible to obtain the solution in terms of the residence time. Moreover, expressing K_D as a function of the Sh number, it follows the dependence of fuel conversion on the height of the combustion chamber.

$$x = 1 - \exp\left(- K_D \cdot \frac{W \cdot L}{Q} \right) = 1 - \exp\left(- \frac{Sh \cdot D_{CH4}}{\delta} \cdot \frac{W \cdot L}{Q} \right) = 1 - \exp\left(- \frac{Sh \cdot D_{CH4}}{\delta^2} \cdot \tau_R \right) \qquad \textbf{\textit{Eq. IV. 17}}$$

The reported analysis reveals that fuel conversion depends on the height of the combustion chamber only in a transport limited or mixed, kinetic and transport limited, regimes. In the case of a pure kinetic regime no dependence of the fuel conversion on the channel height should be detected.

Consequently, the experimental proof of the absence of any transport restriction on fuel conversion in the isothermal tests of CH_4 oxidation has been performed by measuring fuel conversion on a fixed catalytic substrate with varying the height of the combustion chamber and maintaining the same flow rate. In particular, reaction tests are performed at 40 slph increasing the

channel gap from 1 to 4 mm. F2LM catalytic platelet has been considered for such an analysis, which is 2mm thick, so providing, as reported in Table II.3, a combustion chamber 4 mm high. In order to change the height of the channel some wedges are used in order to increase the platelet thickness until a value of 5 mm. It follows an unchanged contact time, equal to 1.26 $g_{cat}\cdot s\cdot Nl^{-1}$ and a residence time varying between 11 and 45 ms (evaluated at 800°C). CH_4 conversion is reported as a function of the temperature detected along the reactor. At least three thermocouples, equally spaced on the reactor length, have been employed in the combustion tests. With varying the position of the thermocouple, variation in the measured temperature is always ±1°C. Actually, the strong diluted conditions adopted guarantee an isothermic profile along the reactor despite of the developed combustion heat. The temperature shown in the presented results is measured at the entrance of the catalyst. The results, presented in Figure 4.4, show that methane conversion is not affected by the height of the combustion chamber. This experimental data points out the absence of transport limitation on fuel conversion, the latter resulting unchanged because of the unchanged contact time.

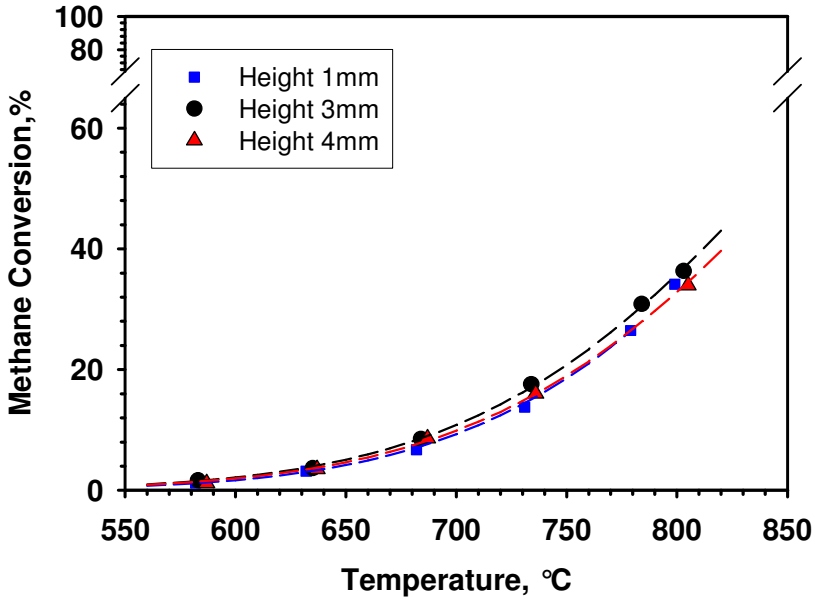

Figure 4.4 *Methane combustion tests on Fe2LM in SSR. Fuel conversion at* τ_C*=1.26* $g_{cat}\cdot s\cdot Nl^{-1}$ *with varying the combustion chamber height (δ): δ=4mm (red triangles); δ=3mm (black circles); δ=1mm (blue squares).*

4.3.1 Stability of the catalytic layer

The deposition of a well anchored catalytic layer on a substrate is a critical issue. In a combustion environment, in fact, the integrity of the deposed film is strongly affected by thermal stresses particularly due to temperature overshoot.

In particular, high temperature operation involves a worsening in catalyst performances mainly due to chemical and physical deactivation phenomena (sintering, solid-solid interactions; McCarty et al., 1999, Zwinkels et al., 1999, Cimino et al., 2001). At this proposal, activity has been detected after several ageing cycles of the sample. In the specific, catalytic substrates have been tested for methane combustion just prepared and after being treated in air at 800°C for 30h at most. In Figure 4.5 methane conversion on A5LM-2 catalytic platelet is reported as a function of the temperature, with varying the ageing treatment duration. A slight de-activation of the catalyst is observed in the first 12h of treatment, as it is expected. Specifically, at 785°C CH_4 conversion decreases from 43%, measured for the "just prepared" catalyst, to 37%, measured for the 12h aged catalyst, corresponding to a decrease of about 14%. After longer treatment the decreasing in fuel conversion is no more significant; for example, a further 18h ageing treatment performed on the 12h treated catalyst involves a methane conversion decrease of only 5%.

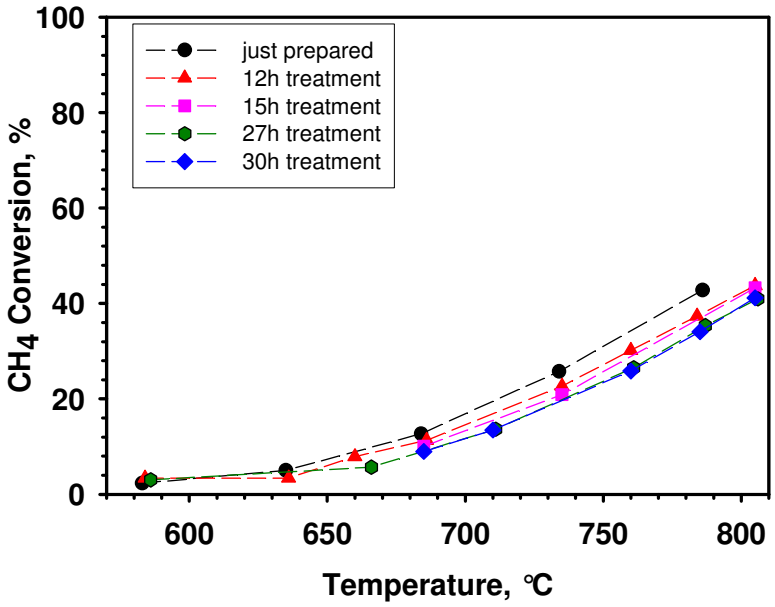

Figure 4.5 *Methane combustion tests on A5LM-2 in SSR. Fuel conversion at* τ_C*=1.62* g_{cat}*·s·Nl*$^{-1}$ *with varying the duration of ageing treatment: catalyst just prepare (black circles); treatment 12h long (red triangles); treatment 15h long (pink squares); treatment 27h long (green hexagons); treatment 30h long (blue rhombs).*

It follows that a 12h treatment is long enough to obtain a catalytic system working in stable conditions.

Moreover, a worsening in catalyst performances may occur even in consequence of a bad anchoring of the catalytic film in the substrate. At this proposal, the catalytic substrates have been

subjected to mechanical stresses at room temperature in an ultrasonic bath showing a weight loss lower than 5wt% as regards the layer weight after a 30min long treatment. Moreover, the catalytic system didn't show a weight loss after the described ageing cycles thus attesting the good anchoring of the deposed film in consequence of both mechanical and thermal stresses.

On the basis of these results, each prepared catalytic platelet has been tested after being pre-treated in air at 800°C for 12h.

In the case of A5LM-2, under stable working conditions of the catalyst, a methane conversion equal to 44% is detected at 805°C, the maximum investigated temperature. Moreover, $T_{10\%}$, the temperature at which 10% of fuel is converted, is equal to 680°C. Kinetic parameters are resumed in Table IV.5 and will be discussed in the following paragraph.

4.3.2 Repeatability of the preparation method

Other preliminary experiments are carried out in order to verify the repeatability of the preparation method. Activity tests are performed on catalysts provided with the same formulation and prepared with the same procedure. In the specific, two identical FeCralloy catalytic plates, F5LM and F5LM-2, and alumina plates, A5LM and A5LM-2, are prepared and tested for methane combustion at the same conditions. In Figure 4.6 the Arrhenius plots related to the tested catalyst are reported while in Table IV.5 the main results are resumed. The Arrhenius plots are evaluated assuming a first order reaction for methane combustion.

Table IV.5 *Repeatability of the preparation method: CH_4 combustion on F5LM, F5LM-2, A5LM and A5LM-2. Deviation in the kinetic parameters.*

	Alumina substrates			**FeCralloy substrates**		
	A5LM	*A5LM-2*	***Deviation, %***	*F5LM*	*F5LM-2*	***Deviation, %***
E, Kcal·mol^{-1}	32.6	29.2	**10**	26.2	25.5	**3**
k(800°C), mmol·g_{cat}^{-1}·s^{-1}	17.0	14.0	**16**	18.0	19.0	**5**

The preparation method shows a good repeatability in the case of FeCralloy substrates. In fact, the deviation in the activation energy and in the kinetic constant measured for F5LM and F5LM-2 is respectively 3 and 5%.

A worsening in the repeatability of the preparation method is observed for the alumina substrates. Considering A5LM and A5LM-2 catalysts deviations of about 10% and 16% are observed respectively in the values of activation energy and in the values of the kinetic constant.

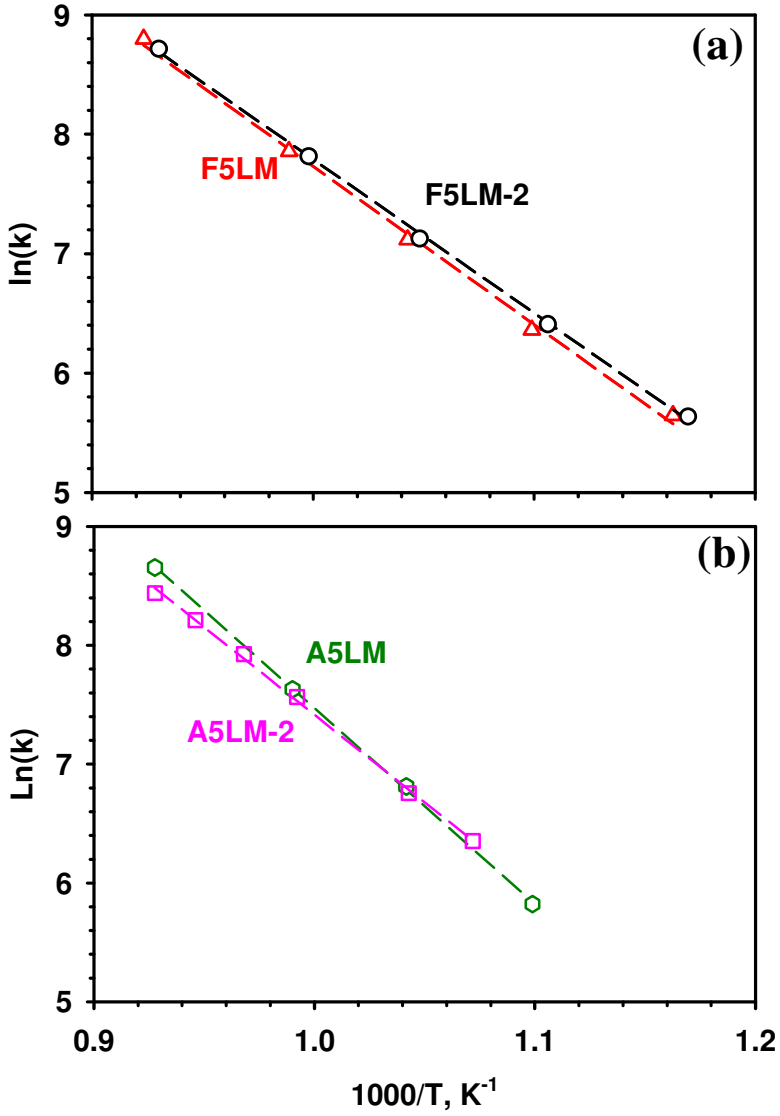

Figure 4.6 *Repeatability of the preparation method. (a) CH_4 combustion tests on F5LM and F5LM-2 in SSR. Arrhenius plot related to F5LM-2, τ_C=1.65 $g_{cat}\cdot s\cdot Nl^{-1}$ (black circles); F5LM, τ_C=1.44 $g_{cat}\cdot s\cdot Nl^{-1}$ (red triangles). (b) CH_4 combustion tests on A5LM and A5LM-2 in SSR. Arrhenius plot related to A5LM-2, τ_C=1.62 $g_{cat}\cdot s\cdot Nl^{-1}$ (pink squares); A5LM, τ_C=1.71 $g_{cat}\cdot s\cdot Nl^{-1}$ (green hexagons).*

4.3.3 Effect of the substrate on the catalytic activity

Combustion tests of CH_4 have been carried out supporting $LaMnO_3/Al_2O_3$ based catalyst on different platelets. Moreover, the substrate activity is measured by testing the platelets lacking in the active phase. The experiments have been performed considering a 1mm high combustion chamber and at a total flow rate equal to 40 slph. F5LM, F2LM, A5LM and A5 platelets have been tested. Considering the amount of catalyst deposed on each substrate, the catalysts supply a different

contact time, as it specified in Table IV.6. In the case of FeCralloy catalytic platelets, F5LM is 5 mm thick (see Table II.3) and provides a combustion chamber 1mm high. On the contrary, F2LM is 2mm thick (see Table II.3) and in order to obtain the same combustion chamber height a 3mm thick wedge is used.

Methane conversion as a function of the temperature and Arrhenius plots are reported for the different tested substrates respectively in Figure 4.7a and 4.7b. Moreover, the most meaningful results are resumed in Table IV.6.

Concerning the combustion tests performed on F2LM and A5LM catalysts, CH4 conversion detected at the maximum temperature is respectively 34 and 53%. Moreover, $T_{10\%}$ is higher in the case of the former catalyst (see Table IV.6); specifically it is 710°C and 680°C respectively for FeCralloy and alumina catalytic substrates. This outcome is expected because of the lower contact time resulting in the combustion test on F2LM sample compared to that supplied by A5LM. Looking at the Arrhenius plot reported in Figure 4.7b, approximately the same activation energy is obtained for the two catalysts (it is 31.3 and 32.6 $Kcal \cdot mol^{-1}$ respectively for F2LM and A5LM) while a slightly higher kinetic constant is calculated for A5LM (see Table IV.6).

Concerning F5LM catalytic platelet, CH_4 conversion detected at the maximum temperature is 52% while $T_{10\%}$ is 660°C. Furthermore, at low temperature F5LM shows an higher catalytic activity if compared to that of A5LM and F2LM; this result is pointed out by the significantly lower activation energy measured for the former sample (approximately 26.2 $Kcal \cdot mol^{-1}$). However, at high temperature F5LM activity is in line with that of A5LM and F2LM. This result is highlighted by approximately the same kinetic constant calculated at 800°C for F5LM and A5LM (see Table IV.6). It is worth mentioning the difference of activity between F5LM and F2LM. These samples are characterized by the same FeCralloy substrate that is 5mm thick in the former case and 2mm in the latter. The difference in activity is probably due to the different amount of γ-alumina taken out on the surface of the substrate following up FeCralloy pre-treatment before proceeding to the catalyst deposition (see Chapter 2). Actually, an higher thickness may result in a bigger amount of alumina on the substrate surface and, as consequence, in an higher activity of the further deposed catalytic layer.

In Figure 4.7a the performances of A5, catalyst free α-alumina substrate, are reported. Maximum CH_4 conversion is around 5%, much lower than that provided by the catalytic platelets: the substrate as well as the reactive paths in the gas phase don't play a role in the methane conversion under the investigated conditions.

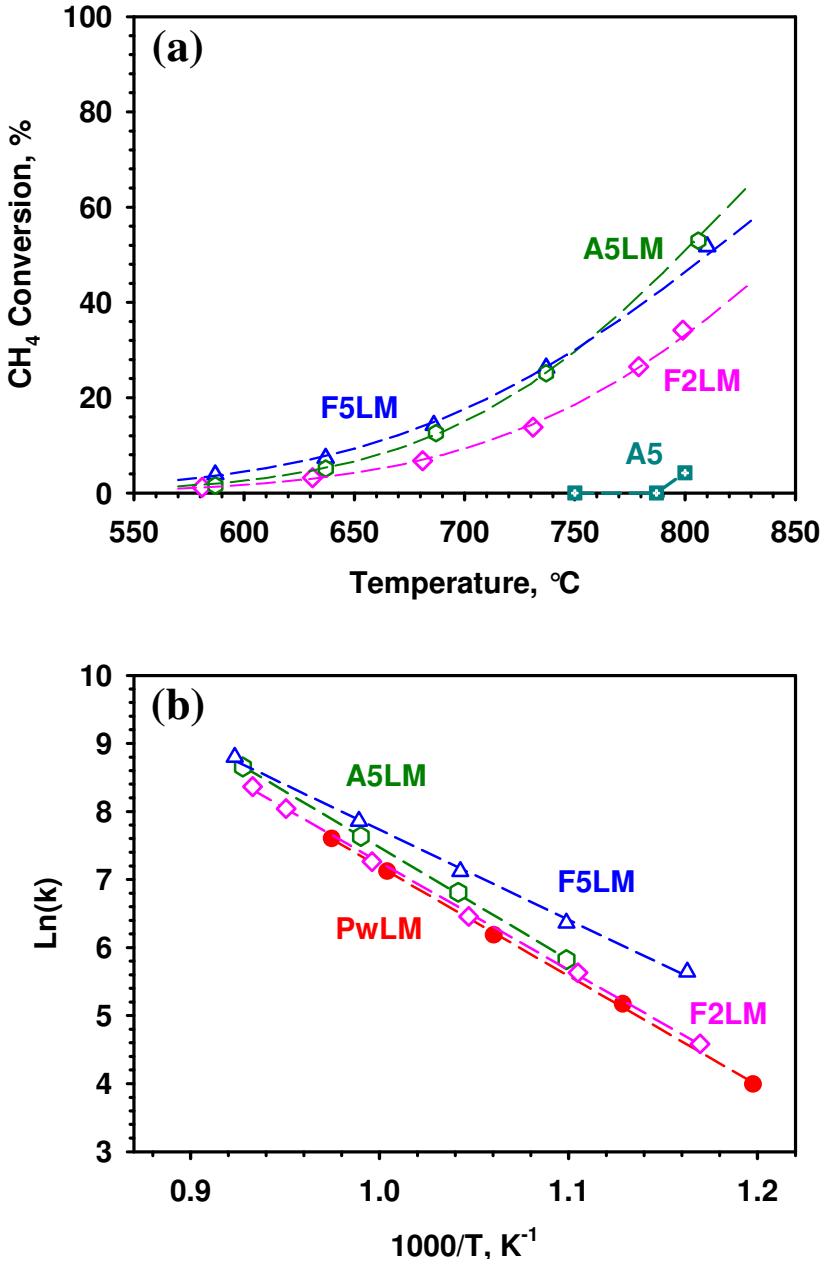

Figure 4.7 *Effect of the substrate on the perovskite catalytic activity in CH_4 combustion. (a) CH_4 conversion as a function of the temperature on F5LM (blue open triangles), F2LM (pink open rhombs), A5LM (green open hexagons), and A5 (cyan squares) ;(b)Arrhenius plot related to tests on F5LM (blue open triangles), F2LM (pink open rhombs), A5LM (green open hexagons), PwLM (red closed circles).*

Table IV.6 *Effect of the substrate on the perovskite catalytic activity in CH_4 combustion. Resume of some extrapolated experimental data.*

Catalyst code	τ_C $g_{cat}\cdot s\cdot Nl^{-1}$	$T_{10\%}$ °C	E $Kcal\cdot mol^{-1}$	K_0 $Nl\cdot s^{-1}\cdot g_{cat}^{-1}$	k(800°C) $mmol\cdot s^{-1}\cdot g_{cat}^{-1}$
F5LM	1.44	660	26.2	$3.6\cdot10^5$	18.0
F2LM	1.26	710	31.3	$2.9\cdot10^6$	13.0
A5LM	1.71	680	32.6	$7.0\cdot10^6$	17.0
A5	0	-	-	-	-
PwLM	18.00	565	31.8	$3.5\cdot10^6$	12.0

In Figure 4.7b and in Table IV.6 the activity of the catalytic plates is compared with that of the catalytic layer tested in the form of powder, PwLM.

The higher contact time provided by the powder catalyst compared to that of the platelets, allows a significantly lower $T_{10\%}$ in the former case. In the specific, $T_{10\%}$ is 565°C for PwLM and is comprised between 650 and 700°C for the structured catalysts (see Table IV.6).

Comparing the performances of PwLM with those of A5LM, it results a lower kinetic constant evaluated at 800°C in the case of the powder catalyst while approximately the same activation energy is detected (see Table IV.6). On the basis of these results, the characteristic feature of the kinetics of the methane oxidation on perovskite-based catalysts seem to be unchanging by passing from a powder to a structured material, as it is attested by the same measured energy barrier. On the contrary, by deposing the catalyst on a substrate a better active phase dispersion is achieved thus allowing an increase in the number of the active sites available for the reaction to occur, as it is attested by the reported increase in the pre-exponential factor of the kinetic constant (k_0 in Table IV.6).

Comparing the performances of PwLM with those of FeCralloy catalytic substrates, the previous considerations are still valid. Nevertheless, the increase in perovskite activity by structuring the catalyst is observed only in the case of F5LM while it is not significant for F2LM. Actually, as already discussed, an improving of the catalyst dispersion is obtained considering F5LM because of the amount of the "taken out" γ-alumina greater and greater with increasing the thickness of the substrate.

4.3.4 Reaction order

An evaluation of the reaction order of methane and hydrogen is presented in this paragraph. The reaction order is obtained by measuring conversion as a function of the initial concentration of the fuel at a fixed temperature and equivalence ratio. The oxygen is in large excess with respect to the fuel total oxidation stoichiometric; in such a way O_2 concentration is almost constant through the reactor thus not influencing the reaction rate.

The conversion measurements are fitted by the kinetic law represented by the equation Eq. IV. 19. The latter is obtaining by assuming a reaction rate depending on a power law equation as regards the fuel concentration (see the equation Eq. IV.18) and a reactor working under isothermal plug flow conditions. In Eq. IV.19 the fuel conversion (x) is reported as a function of the reaction order (α), the kinetic constant (k), the contact time (τ_C) and the initial fuel concentration (c_0), the first two constituting the fitting parameters while the other the input parameters.

$$r_{app} = \rho_{app} \cdot k \cdot c^{\alpha} \qquad \textbf{Eq. IV. 18}$$

$$x = 1 - \left[1 - c_0^{\alpha-1} \cdot (1-\alpha) \cdot k \cdot \tau_C\right]^{\frac{1}{1-\alpha}} \qquad \textbf{Eq. IV. 19}$$

The reaction order of methane total oxidation is evaluated in the case of $LaMnO_3/Al_2O_3$ based catalyst. In Figure 4.8 it is reported CH_4 conversion on A5LM-2 as a function of the initial fuel concentration, the latter being comprised between $4.0 \cdot 10^{-5}$ and $2.0 \cdot 10^{-4}$ M. Experiments are carried out at two temperatures, 785°C and 685°C and at an equivalence ratio Φ = 0.2. The conversion measurements are fitted by means of the previously specified regression law (Eq. IV.19); the resulted fitting parameters are reported in Table IV.7. Methane conversion decreases with increasing the initial fuel concentration, this behaviour being due to a less than linear dependence of the reaction kinetics on CH_4 concentration. The methane reaction order is estimated, in fact, at approximately 0.8 at 685°C and 0.9 at 785°C. These values are very close to the reaction order equal to 0.84 reported by Cimino et al. (2000) for CH_4 oxidation on the same $LaMnO_3/Al_2O_3$ based catalyst. These results are also useful to weigh the error made by consider a first order dependence for methane combustion on perovskite; actually, such an assumption could be considered acceptable, depending on the context and the precision requested. Moreover, as already reported, a first order rate dependence on methane has been also claimed even in the case of Pt based catalysts (Arai et al. 1986), so that it follows that in the present study a first order as regard the fuel has been assumed for the methane combustion independently on the catalyst.

The reaction order of hydrogen oxidation is evaluated in the case of Pt-$LaMnO_3/Al_2O_3$ based catalyst. In Figure 4.9 H_2 conversion on A5Pt1LM is reported as a function of the initial fuel concentration and the contact time, respectively variable in the ranges of $5 \cdot 10^{-5} < c_0 < 4 \cdot 10^{-4}$ M and $1.65 < \tau_C < 2.88$ $g_{cat} \cdot s \cdot Nl^{-1}$. Experiments are carried out at 147°C and at an equivalence ratio Φ = 0.24. The fitting parameters obtained from the regression are reported in Table IV.7. As it has been observed in the case of methane combustion, hydrogen conversion decreases with increasing the initial fuel concentration, resulting in a less than linear dependence of the reaction kinetics on H_2 concentration. In the specific, the measured hydrogen reaction order is approximately 0.73. On the basis of this result, the assumption of a first reaction order as regards fuel concentration for H_2 combustion on Pt-$LaMnO_3/\gamma$-Al_2O_3 is a reasonable hypothesis too, especially considering that the aim of this study is a rough evaluation of the activity shown by different catalysts in order to compare their performances. A first order rate dependence has been considered in the present study even in the case of H_2 combustion on Pt/γ-Al_2O_3 catalyst, assuming that the presence of perovskite does not involve a significant change in the mechanism of hydrogen combustion on platinum. Moreover, a first order kinetics is kept even on unpromoted perovskite catalysts: in such a case, in fact, a reaction order of 0.8÷1 is reported in literature (Cimino et al., 2003)

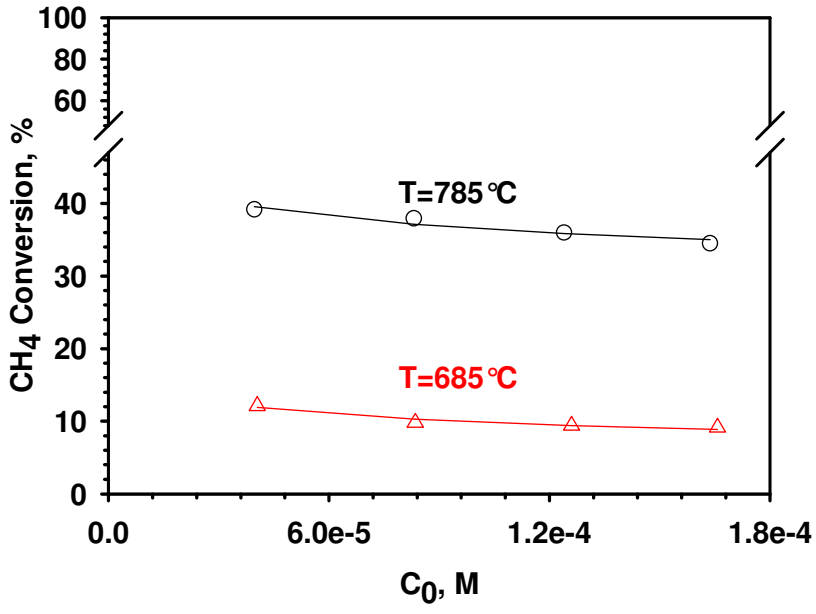

Figure 4.8 *Methane combustion on A5LM-2 catalyst in SSR. Fuel conversion at τ_C=1.62 $g_{cat} \cdot s \cdot Nl^{-1}$ and Φ=0.2 as a function of initial fuel concentration with varying the temperature. T=685°C (red triangles); T=785°C (black circles).*

Table IV.7 *Kinetic constants and fuel reaction order resulting from the regression. Methane combustion on A5LM-2 catalyst in SSR at τ_C=1.62 $g_{cat}\cdot s\cdot Nl^{-1}$. Hydrogen combustion on A5Pt1LM catalyst in SSR at 1.65 <τ_C< 2.88 $g_{cat}\cdot s\cdot Nl^{-1}$: kinetic constant and H_2 reaction order resulting from the regression.*

Temperature, °C	α	k, $l^{\alpha}\cdot mol^{1-\alpha}\cdot s^{-1}\cdot g_{cat}^{-1}$
CH_4 Combustion		
685	0.78	$8\cdot10^{-3}$
785	0.89	0.102
H_2 Combustion		
147	0.73	1.66

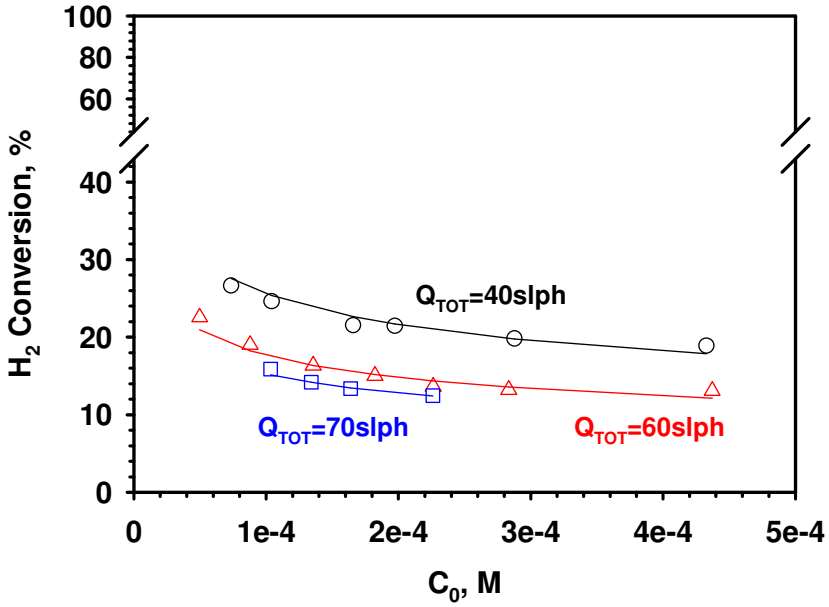

Figure 4.9 *Hydrogen combustion on A5Pt1LM catalyst in SSR. Fuel conversion measured at 147°C and Φ=0.24 as a function of initial fuel concentration with varying the flow rate. Total flow rate equal to 40slph and τ_C=2.88 $g_{cat}\cdot s\cdot Nl^{-1}$ (black circles); total flow rate equal to 60slph and τ_C=1.92 $g_{cat}\cdot s\cdot Nl^{-1}$ (red triangles); total flow rate equal to 70slph and τ_C=1.65 $g_{cat}\cdot s\cdot Nl^{-1}$ (blue squares).*

4.3.5 Combustion of CH_4: effect of the active phase

Different γ-alumina supported active phases are tested in the methane combustion. In particular, perovskite, platinum and the phase constituted by their mixture are taken into consideration with the

aim of accurately studying the effect of the presence of platinum in the perovskite structure on the measured combustion rate. At this proposal, the activity of F5LM is compared with that of F5Pt1LM and F5Pt1, tested under the same operating conditions. Combustion tests have been carried out considering a fuel mixture total flow rate of 40slph and with a combustion chamber 1mm high. The results are reported in Figure 4.10a and b respectively in terms of fuel conversion and selectivity to CO as a function of the temperature; in Figure 4.11 the Arrhenius plot corresponding to the tested samples are reported while in Table IV.8 the most meaningful results are resumed.

Comparing F5LM and F5Pt1LM performances, it is clearly shown that adding platinum to the perovskite structure is not effective in enhancing catalytic performances. On the contrary, the Pt doped perovskite gives rise to a worsening in the unpromoted phase activity. This is made evident considering the lower $T_{10\%}$ shown by F5LM if compared to that provided by F5Pt1LM despite of the lower contact time presented by the former catalyst (see Figure 4.10a and Table IV.8). Also, perovskite catalyst presents an higher kinetic constant due to the lower activation energy and the higher pre-exponential factor (see Figure 4.11 and Table IV.8). The worsening in $LaMnO_3$ activity because of Pt doping may be due to the decrease in the catalyst specific surface caused by the co-presence of the noble metal and perovskite in the γ-alumina pores (see Chapter 2). The observed results are in line with data reported by Giebeler et al. (2007) in a recent study on methane oxidation on Pt, Pd, Rh promoted $LaMnO_3$ catalysts. In particular, the insignificant role of noble metals in enhancing perovskite activity was traced back to the particular morphology of the mixed phase catalyst in which Pt, Pd and Rh were incorporated in $LaMnO_3$ lattice rather than forming another phase on the catalyst surface.

Moreover, the ineffectiveness of adding Pt to $LaMnO_3$ in enhancing catalytic performances is expected because of the lower activity of the noble metal in methane combustion if compared with that of the perovskite. Actually, F5Pt1 is characterized by the highest $T_{10\%}$ ($T_{10\%}$ = 720°C where it is 660°C for F5LM and 675 for F5Pt1LM). Moreover the kinetic constant calculated at 800°C is approximately the half of that observed for the perovskite based catalysts (see Table IV.8).

Finally, the following scale of activity is observed in methane combustion: $LaMnO_3$ > Pt-$LaMnO_3$ > Pt.

In Figure 4.10b it is shown the selectivity to CO measured for the different catalyst. Generally speaking, at 800°C the selectivity to CO is maximum 5%, corresponding to a maximum carbon monoxide production equal to 70ppm. However, it is shown that F5Pt1 catalyst guarantees a lower selectivity to CO if compared to that provided by F5LM. Moreover, F5Pt1LM shows a selectivity to CO intermediate between the values obtained in the case of F5LM and F5Pt1 catalysts. These

results indicate that, considering CO oxidation reaction, platinum based catalysts present an higher activity than perovskite; consequently, promoting $LaMnO_3$ structure with a few amount of Pt is in this case a practicable road to enhance the catalytic performances, as it is also reported by Giebeler et al. (2007). However, the lower selectivity to CO shown by F5Pt1 if compared to that of F5Pt1LM, characterized by the same amount of platinum, indicates that Pt exhibits lower activity when dispersed on the perovskite matrix rather than only on γ-alumina. This may be due to different dispersion or migration of Pt inside the perovskite structure, effectively reducing the amount of noble metal available for reaction.

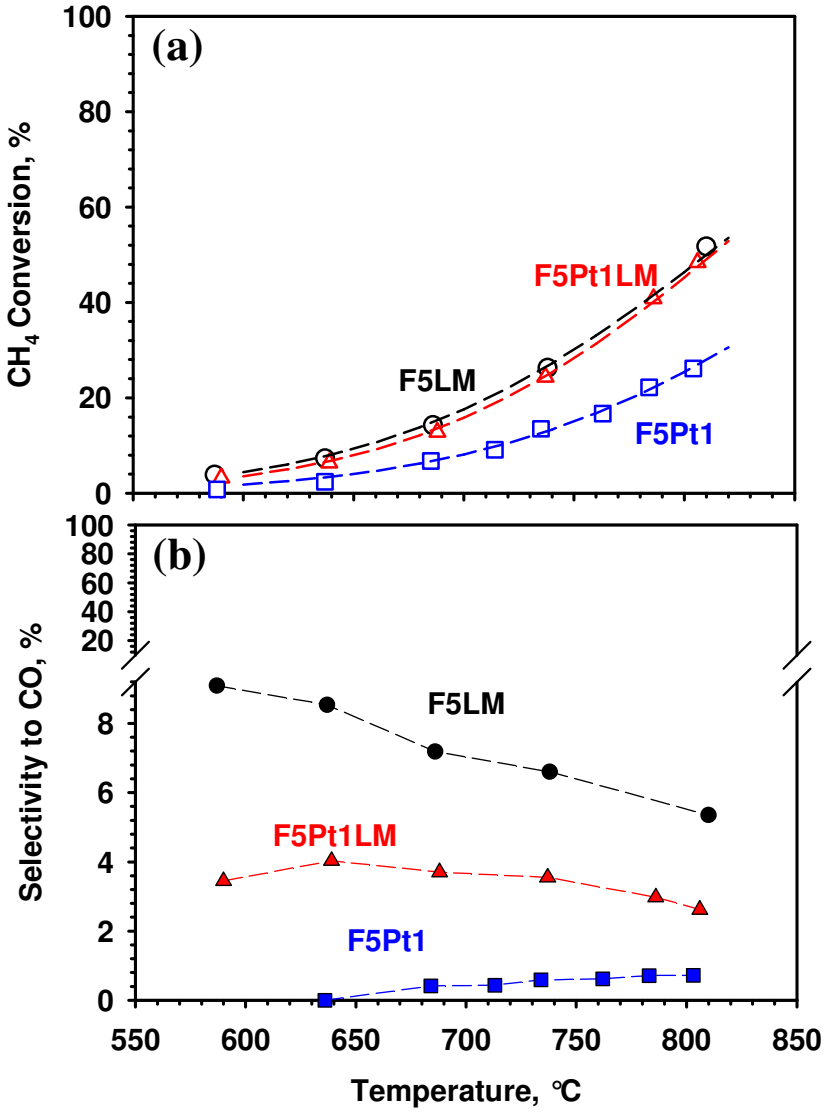

Figure 4.10 *Methane combustion on different active phase. (a) Fuel conversion as a function of the temperature; (b) Selectivity to CO. F5LM, τ_C=1.44 $g_{cat}\cdot s\cdot Nl^{-1}$ (black circles); F5Pt1LM, τ_C=1.53 $g_{cat}\cdot s\cdot Nl^{-1}$ (red triangles);F5Pt1, τ_C=1.49 $g_{cat}\cdot s\cdot Nl^{-1}$ (blue squares).*

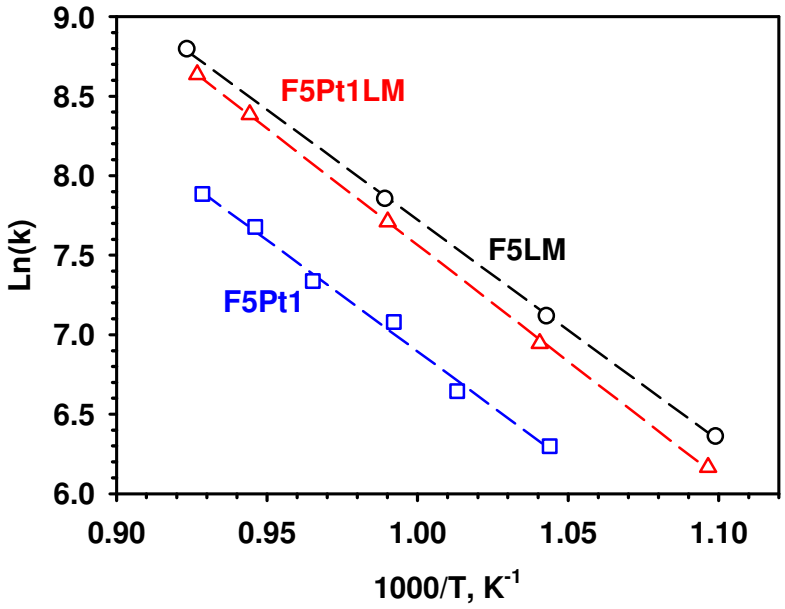

Figure 4.11 *Methane combustion on different active phase. Arrhenius plot corresponding to F5LM, τ_C=1.44 $g_{cat}\cdot s\cdot Nl^{-1}$ (black circles); F5Pt1LM, τ_C=1.53 $g_{cat}\cdot s\cdot Nl^{-1}$ (red triangles);F5Pt1, τ_C=1.49 $g_{cat}\cdot s\cdot Nl^{-1}$ (blue squares).*

Table IV.8 *Effect of the active phase on CH_4 combustion. Resume of some extrapolated experimental data.*

Catalyst code	τ_C $g_{cat}\cdot s\cdot Nl^{-1}$	$T_{10\%}$ °C	E $Kcal\cdot mol^{-1}$	k_0 $Nl\cdot s^{-1}\cdot g_{cat}^{-1}$	k(800°C) $mmol\cdot s^{-1}\cdot g_{cat}^{-1}$
F5LM	1.44	660	26.2	$3.6\cdot10^5$	18.0
F5Pt1LM	1.53	675	29.0	$1.1\cdot10^6$	15.0
F5Pt1	1.49	720	27.7	$3.3\cdot10^5$	8.0

4.3.6 Combustion of H_2: effect of the active phase

As in the case of methane combustion, perovskite, platinum and the phase constituted by their mixture are tested in hydrogen combustion with the aim to understand the interactions between the noble metal and $LaMnO_3$ perovskite and the correlations to catalytic activity.

At this proposal, A5LM and F5LM are tested and the resulting activity is compared with that of F5Pt1LM and F5Pt1. Combustion tests have been carried out considering a fuel mixture total flow rate of 40slph and with a combustion chamber 1mm high. Hydrogen combustion tests on perovskite

are shown in Figure 4.12. Moreover, in that figure the catalytic performances of A5, representative of the activity of the α-alumina substrate, are shown. In Figure 4.13 the activity of Pt based catalyst is presented, while in Table IV.9 the most meaningful results are resumed.

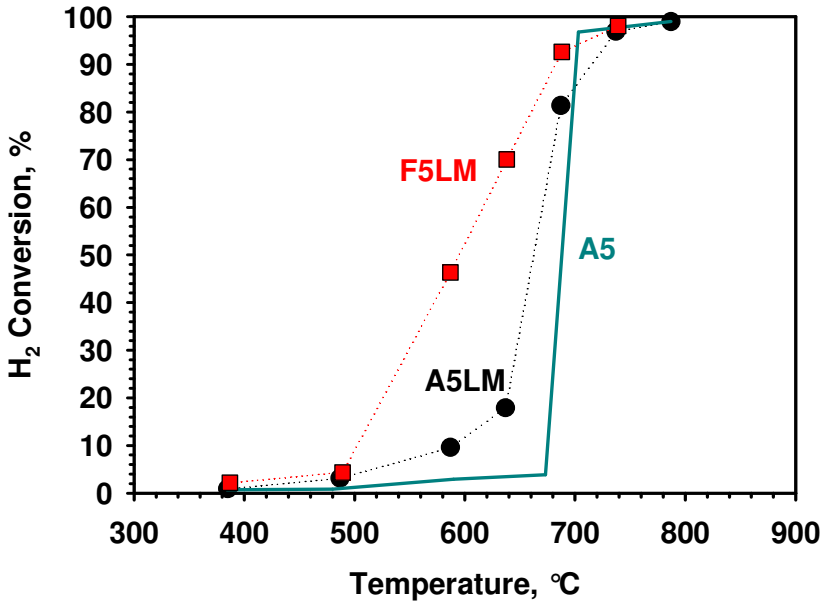

Figure 4.12 *Hydrogen combustion tests on perovskite and on "catalyst free" α-alumina substrate. F5LM, τ_C=1.44 $g_{cat}\cdot s\cdot Nl^{-1}$ (red squares); A5LM, τ_C=1.71 $g_{cat}\cdot s\cdot Nl^{-1}$ (black circles); A5 (cyan line).*

The results reported in Figure 4.12 show that perovskite is characterized by a very low activity in hydrogen oxidation, as it is evident by considering the high values of $T_{10\%}$ found. Considering A5LM, in fact, $T_{10\%}$ is equal to about 600°C; moreover, based on the available data, it is not easy to derive $T_{10\%}$ in the case of F5LM but it is evident that 500°C<$T_{10\%}$<600°C is found. Such a surprisingly high $T_{10\%}$ is in agreement with other studies reported in literature (Cimino et al., 2003). In fact, employing published kinetics data, under the PFR hypothesis a $T_{10\%}$=500°C is obtained assuming the same contact time as that considered in A5LM experiments. In Figure 4.12 is also evident that a total fuel conversion is observed only at about 740°C in the case of both F5LM and A5LM. Nevertheless, at the specified temperature hydrogen is totally converted even without a catalyst on the α-alumina substrate, A5. In the case of the catalyst free substrate, in fact, at a temperature comprised between 670 and 700°C a steep increase in hydrogen conversion from 0 to 100% is observed. Such a temperature level, in fact, is high enough to the occurrence of gas phase combustion via radical reactions. Moreover, the presence of a substrate may play an significant role in the activation of the reactive paths in the gas phase by promoting the radical formation. This

result reveals that in the case of H_2 oxidation on perovskite, it is not possible to neglect the contribute of combustion in the homogeneous reactions, the latter being determinant in completing the conversion of the fuel. Such a phenomenon, not ascribed to the presence of a catalyst, is not a classical flame combustion. Actually, the strong reactants dilution determines a slow flameless process, known in literature as "mild combustion" (Schefer et al., 2002, Dagaut e Nicolle, 2005, Sabia et al., 2007, Derudi et al., 2007).

In the case of A5LM, as already observed for A5, a steep increase in fuel conversion from 18 to 81% is observed at a temperature comprised between 637 and 687 °C. At a temperature lower than 637°C H_2 is converted only thanks to the presence of catalyst; on the contrary, above this temperature fuel is mainly converted in the gas phase. For A5LM and A5 temperature at which a jump in conversion is observed is roughly the same. The threshold temperature at which gas phase reactive paths occur is very different considering F5LM where perovskite is deposed on FeCralloy substrate. In this case a jump in fuel conversion from 4 to 46% is observed at a temperature comprised between 489 and 587°C. The specified range of temperature is strongly lower than that observed in the case α-alumina substrates are considered thus revealing a more relevant role of FeCralloy in promoting the radical formation. Notwithstanding in F5LM combustion in the gas phase starts at a lower temperature, total H_2 conversion is observed at the same temperature level observed in the case of A5 and A5LM. This behaviour is ascribed to the typical slowness of combustion in "mild" conditions.

Promoting perovskite with a little amount of platinum is very effective in enhancing the catalytic activity in hydrogen combustion. $T_{10\%}$ measured in the case of F5Pt1LM, in fact, is 95°C, more than 5 times lower if compared to that measured for F5LM (see Table IV.9). The much higher activity of platinum promoted perovskite compared to the unpromoted sample inhibits eventual combustion paths occurring in the gas phase.

From the comparison of the catalytic performances of F5Pt1LM and F5Pt1 (reported in Figure 4.13 and in Table IV.9), it results that Pt/γ-Al_2O_3 shows a higher activity. This is made clear by comparing the value of $T_{10\%}$ measured in the case of F5Pt1LM and F51Pt, respectively equal to 95°C and 65°C (see Table IV.9). Moreover, Pt/γ-Al_2O_3 provides a lower activation energy and an higher kinetic constant calculated at 200°C (see Table IV.9). The lower activity shown by F5Pt1LM if compared to that of F5Pt1, despite of the same amount of noble metal present on the two different catalysts, as already described may be due to the different dispersion or migration of Pt inside the perovskite structure determining a decrease in the amount of noble metal available for the reaction. Moreover, such a result may be further explained by considering the lower specific surface area exhibited by F5Pt1LM compared to that of F5Pt1 (see Chapter 2).

Finally, the following scale of activity is observed in hydrogen combustion: Pt > Pt-$LaMnO_3$> $LaMnO_3$, namely exactly the reverse one compared with methane oxidation.

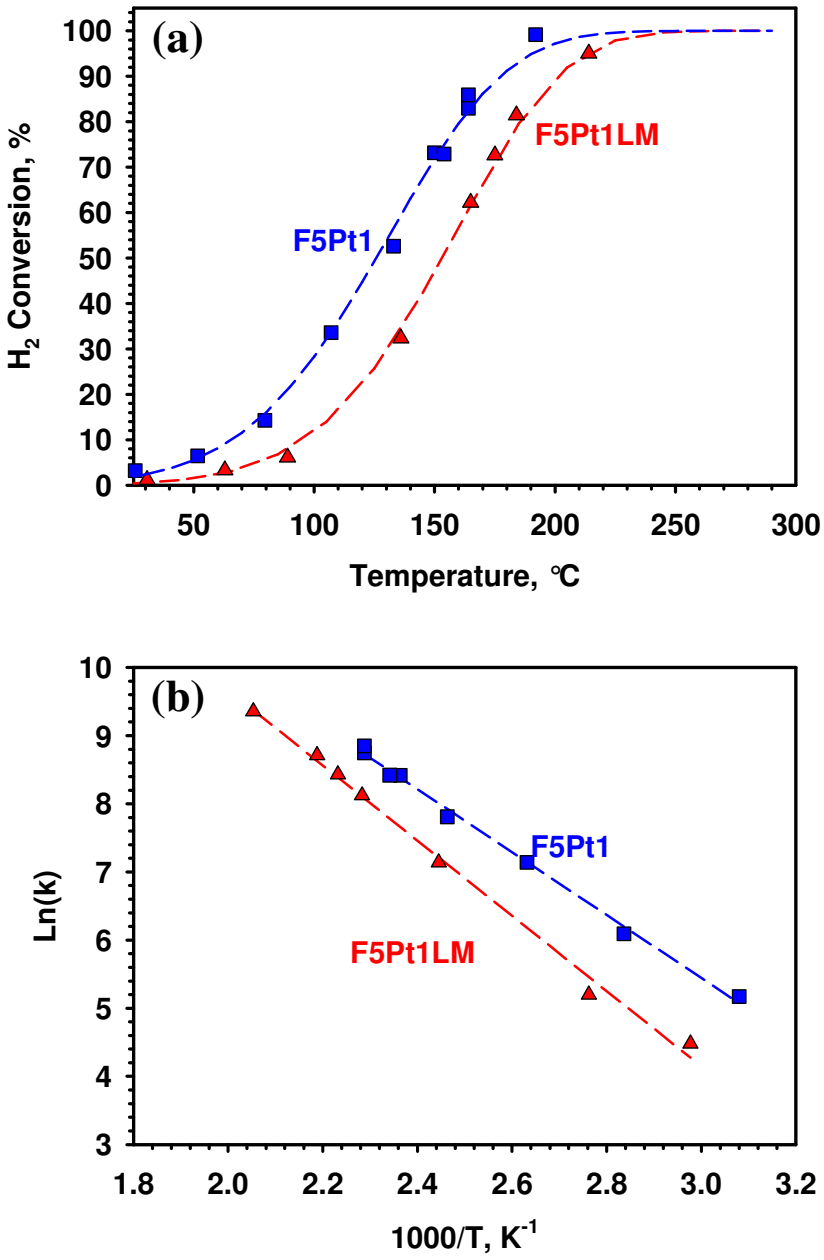

Figure 4.13 *Hydrogen combustion on different active phase. (a) Fuel conversion as a function of temperature; (b) Arrhenius plot. F5Pt1LM,* τ_C*=1.53* g_{cat}*·s·Nl*$^{-1}$ *(red triangles); F5Pt1,* τ_C*=1.49* g_{cat}*·s·Nl*$^{-1}$ *(blue squares).*

Table IV.9 *Effect of the active phase on H_2 combustion. Resume of some extrapolated experimental data.*

Catalyst code	τ_C $g_{cat}\cdot s\cdot Nl^{-1}$	$T_{10\%}$ °C	E $Kcal\cdot mol^{-1}$	k_0 $Nl\cdot s^{-1}\cdot g_{cat}^{-1}$	k(200°C) $mmol\cdot s^{-1}\cdot g_{cat}^{-1}$
F5LM	1.44	500	-	-	-
F5Pt1LM	1.53	95	10.9	$2.7\cdot10^5$	60.0
F5Pt1	1.49	65	9.1	$6.6\cdot10^4$	100.0

4.3.7 Combustion of H_2-CH_4 mixtures

The study on the combustion of methane and hydrogen mixtures has been carried out in SSR reactor on structured catalysts constituted by γ-alumina supported perovskite deposed on FeCralloy and α-alumina platelets. Different operating conditions have been considered; in particular, different fuel mixtures and flow rates (as already reported in Table IV.2) as well as different combustion chamber heights have been taken into account. By varying simultaneously the flow rate and the channel height but maintaining the catalyst amount, it is possible to change the process contact time (τ_C) without affecting the residence time (τ_R); vice versa, by varying the combustion chamber height but maintaining the same flow rate and catalyst amount it is possible to perform experiments at different τ_R but at the same τ_C.

In Figure 4.14 combustion experiments performed on F2LM catalyst in a 4 mm high combustion chamber and at total flow rate equal to 40slph are presented. Specifically, conversion of hydrogen and methane as well as the selectivity to carbon monoxide of converted CH_4 are shown as functions of the temperature in the case of Mix1, Mix2, Mix3, Mix4, Mix7 and Mix8.

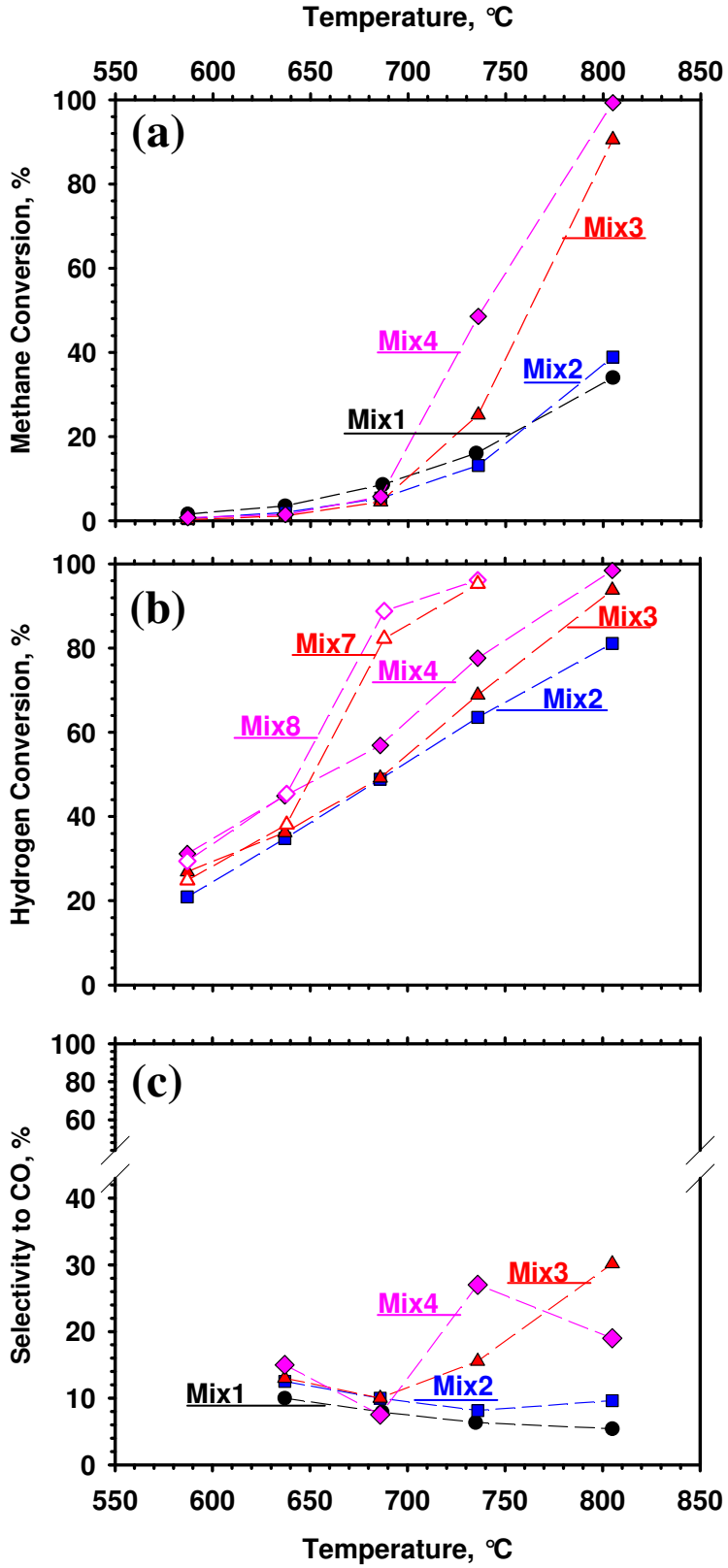

Figure 4.14 *H_2-CH_4 mixtures combustion on F2LM at τ_C=1.26 $g_{cat}\cdot s\cdot Nl^{-1}$ and at τ_C=162 ms (evaluated at STP). (a) H_2 conversion as a function of temperature; (b) CH_4 conversion as a function of temperature; (c) Selectivity to CO as a function of temperature. Mix1 (closed black circles); Mix2 (closed blue squares); Mix3 (closed red triangles); Mix4 (closed pink rhombs); Mix7 (open red triangles); Mix8 (open pink rhombs).*

Concerning methane conversion (Figure 4.14a), in the case of hydrogen free mixture (Mix1), as already reported in Figure 4.4, 40% of fuel is converted at the maximum investigated temperature (T_{MAX}). In Mix2, where 50vol% of methane is substituted with hydrogen (H_2/CH_4=1), hydrocarbon conversion does not vary significantly (see Figure 4.14a). In the specific, up to a temperature of about 750°C CH_4 conversion measured in the case of Mix2 is approximately the same as that detected in Mix1, despite of the lower inlet methane concentration This is expected because of the first order of the oxidation reaction as regards CH_4 concentration. At the maximum investigated temperature, on the contrary, an higher fuel conversion is observed in the case of Mix2. This circumstance recurs and it is more pronounced further increasing the H_2/CH_4 ratio in the fuel mixture. In the specific, considering Mix3 (H_2/CH_4=2) up to a temperature of about 700°C methane conversion is very close to that detected in the case of Mix1 and Mix2 (see Figure 4.14a). Beyond this temperature in Mix3 CH_4 conversion starts to increase more significantly till to reach at T_{MAX} a value of about 90%, much higher than that detected in the case of Mix1 and Mix2 (see Figure 4.14a). The enhanced system performances in converting CH_4 is ascribed to a thermally activated promoting effect due to the co-feeding of hydrogen. Such an effect, is accentuated with further increasing H_2 content in the fuel mixtures. In the specific, considering Mix4 (H_2/CH_4=2) beyond 700°C methane conversion experiences a steep increase, similarly to the case of Mix3. However, higher is the amount of hydrogen in the fuel mixture, higher is CH_4 conversion. In confirming with that, in Figure 4.14a it is shown that at about 740°C fuel converted in Mix4 is about 50% while it is only 25% in Mix3. Moreover, differently from combustion tests on Mix3, a total methane conversion is detected at T_{MAX} when a H_2/CH_4=3.3 is considered.

In Figure 4.14b it is reported hydrogen conversion measured in the case of H_2-CH_4 mixtures (Mix2, Mix3, Mix4) as well as in methane free mixtures, Mix7 and Mix8, under the operating conditions specified at the beginning of this paragraph (F2LM catalyst and 4mm high combustion chamber). As already described in the paragraph 4.3.6 (Figure 4.12), hydrogen combustion on perovskite is very slow and a very high temperature is needed to totally convert the fuel. Moreover, it has been shown as the thermal level required to efficiently burn H_2 on that catalyst is high enough to activate reactive paths in the gas phase. Such a flameless combustion, occurring in “mild” conditions, strongly enhances hydrogen combustion rate completing its conversion. These assumptions are confirmed analyzing H_2 conversion measured in the case of Mix7 and Mix8 (CH_4 free fuel mixtures). These mixtures are characterized by a much lower fuel partial pressure if compared with 1vol% of hydrogen considered in the combustion tests reported in the paragraph 4.3.6 (compare values reported in Table IV.1 and Table IV.2); moreover, the latter experiments were performed on F5LM and A5LM catalysts in a 1mm high combustion chamber. Analyzing the

results reported in Figure 4.14b, in both Mix 7 and Mix8 fuel conversion is very low up to a temperature of 640°C; beyond this temperature a steep increase in the converted hydrogen (from 45% to 89% in the case of Mix8 and from 38% to 82% in the case of Mix7) is observed till a total fuel conversion is obtained at 740°C. This temperature is very close to that reported in the paragraph 4.3.6 in the case of A5LM and F5LM catalysts, despite of the pronounced differences in the adopted operating conditions. Concerning the temperature at which the "jump" in hydrogen conversion is observed in the case of Mix7 and Mix8 on F2LM, it is consistent with that reported in Figure 4.12 in the case of A5LM. Despite of the same material of the substrate, this temperature, instead, is much higher than that obtained for F5LM. Actually, this catalytic substrate, thicker than F2LM (the thickness is respectively 5mm and 2mm), has already shown an higher catalytic activity in methane combustion (see Figure 4.7) and, at the same way, may show higher performances in H_2 combustion. Nevertheless, fuel partial pressure strongly affects the combustion rate in the gas phase thus rendering not much meaningful a comparison between the results presented in this section and that reported in the paragraph 4.3.6. Moreover, further confirming the latter assumption, later in this paragraph it will be shown as the combustion chamber height too plays an important role on the reactive paths in the gas phase. The effect of the inlet hydrogen partial pressure on the fuel conversion is reported in Figure 4.14b where combustion tests of Mix7 and Mix8 are compared. Despite of the very low difference in H_2 inlet concentration, respectively 0.34 and 0.46vol%, a significant higher fuel conversion is observed in the case of Mix8.

A different behaviour is observed in the hydrogen combustion when H_2-CH_4 fuel mixtures are considered. Comparing H_2 conversion in the case of Mix8 and Mix4, characterized by the same H_2 partial pressure, a significantly lower fuel conversion is detected in the case methane is present in the fuel mixture (Mix4). In particular, the conversion is the same up to 640°C while beyond this temperature the "jump" in fuel conversion observed in the case of Mix8 doesn't occur in the CH_4-H_2 mixture resulting in a lower converted fuel in the latter case. In further confirming of that, Mix4 shows a total hydrogen conversion at about 800°C where, under the same investigated conditions, it was observed at 740°C in Mix8. The same conclusions are drawn by comparing hydrogen conversion in the case of Mix7 and Mix3, characterized by a lower H_2 content. It is worth noting that, as already observed in the case of methane free fuel, even in the CH_4-H_2 mixture H_2 conversion increases with increasing the fuel inlet partial pressure. In the case of Mix2, characterized by the lowest hydrogen content, the maximum investigated temperature is not enough to guarantee a total H_2 conversion. In this case it is about 80% where both in Mix3 and Mix4 it was 100% .

On the basis of these results, it is clear that hydrogen shows a promoting effect on methane combustion rate. Such an effect is thermally activated and it is more and more significant with increasing the degree of methane substitution with hydrogen. At the same time, the presence of methane in the fuel mixture is unfavourable to hydrogen combustion and, specifically, inhibits the H_2 conversion in the gas phase. A reasonable explanation of such a phenomenon is ascribed to the occurrence of reactive paths in the gas phase between methane and radicals involved in hydrogen combustion mechanism. Based on this assumption, the observed promoting effect occurs because H_2 constitutes a source of radicals that favours CH_4 combustion in the gas phase at relatively low temperature. Moreover, a part of these radicals, involved in methane consumption reactions, is no more available to sustain hydrogen combustion thus giving an explanation to the inhibiting effect of methane on H_2 oxidation in CH_4-H_2 fuel mixtures (compare H_2 conversion measurements obtained in Mix7 and Mix3 as well as in Mix8 and Mix4 reported in Figure 4.14b).

The reported assumptions are supported by several studies in literature on "mild" combustion of CH_4-H_2 mixtures. (Schefer et al., 2002, Dagaut e Nicolle, 2005, Sabia et al., 2007, Derudi et al., 2007). As it is known, $OH^{\cdot}$ radicals play the most relevant role in the light-off of methane combustion in the gas phase: these radicals, in fact, chemically activate the hydrocarbon molecules abstracting from them $H^{\cdot}$ radicals, thus producing $CH_3^{\cdot}$ radicals (r IV.1). As it is shown by Dagaut and Nicolle (2005), without co-burning hydrogen, $OH^{\cdot}$ radicals are mainly produced by the breaking of oxygen molecules through the reaction r IV.2. Because of the great chemical stability of oxygen, r IV.2 requires high temperature to occur and, specifically, at least 900°C is needed. By adding hydrogen to the methane fuel mixture a changing in the $OH^{\cdot}$ formation mechanism occurs: in particular, by increasing the hydrogen content in the fuel, hydroxyl radicals are produced more and more significantly through r IV.3 and, specifically, from $HO_2^{\cdot}$, an intermediate product of low temperature H_2 combustion. Practically speaking, hydrogen presence in the fuel improves system performances in converting methane because determines an increase in the production of hydroxyl radicals at a temperature relatively low thus allowing hydrocarbon combustion in the gas phase at an unexpectedly low thermal level.

$$CH_4 + OH^{\cdot} \Leftrightarrow CH_3^{\cdot} + H_2O \qquad \text{r IV.1}$$

$$O_2 + H^{\cdot} \Leftrightarrow OH^{\cdot} + O^{\cdot} \qquad \text{r IV.2}$$

$$H^{\cdot} + HO_2^{\cdot} \Leftrightarrow OH^{\cdot\cdot} + OH^{\cdot} \qquad \text{r IV.3}$$

An experimental verification of the occurrence of methane combustion in the gas phase is reported in Figure 4.14c, where selectivity to carbon monoxide is reported in the case of Mix1,

Mix2, Mix3 and Mix4. In the case of hydrogen free fuel mixture (Mix1), selectivity to CO decreases monotonically with the temperature. In the specific, at the maximum investigated temperature CO selectivity is about 5%, corresponding to a carbon monoxide production of approximately 50ppm. By adding to the fuel mixture an hydrogen content high enough to allow methane total conversion a different behavior is observed. In particular, considering Mix3, characterized by an H_2/CH_4 ratio equal to 2, selectivity to CO is very close to that measured for Mix1 up to a temperature of 700°C. On the contrary, beyond this temperature and in correspondence with the "jump" observed in methane conversion (see Figure 4.14a) CO selectivity strongly increases in the case of Mix3 till to reach much higher values than those detected for Mix1. In particular, Mix3 exhibits at T_{MAX} a selectivity of 30%, corresponding to a carbon monoxide production of approximately 490ppm. Similar considerations are valid in the case of combustion experiments of Mix4. In particular it is worth noting that, in correspondence of methane conversion "jump", selectivity to CO measured for Mix4 is higher than that of Mix3. On the contrary this trend is inverted at T_{MAX}. The enhanced production of carbon monoxide in correspondence with the increase in methane conversion in H_2-CH_4 fuel shows that hydrocarbon reacts in the gas phase. Actually, hydrocarbon catalytic combustion proceeds assuring a quite total selectivity to CO_2. On the contrary, under the investigated conditions, carbon monoxide is a typical product of homogeneous combustion because the temperature is too low to allow the further oxidation of CO to CO_2.

The promoting effect of hydrogen on methane combustion has been studied with varying the temperature and the H_2/CH_4 ratio. Nevertheless, it may be interesting to understand the role of the residence time, τ_R, on the system performances in converting the H_2-CH_4 fuel mixtures. Actually, τ_R is the characteristic time of the reactions occurring in the gas phase and, as consequence, by changing it the hydrogen promoted reactivity of methane in the homogeneous phase may be affected too. In Figure 4.15 methane conversion is reported as a function of the H_2/CH_4 ratio with varying τ_R. In order to study the effect of the residence time on the combustion rate specifically in the gas phase, the experiments are carried out maintaining unchanged the characteristic time of the catalysis (contact time, τ_C). In particular, the experiments are performed on F2LM at a total flow rate of 40slph resulting in a τ_C=1.26 $g_{cat}\cdot s\cdot Nl^{-1}$. Moreover, the temperature is maintained constant and, specifically, T=800°C. Such a temperature is higher than the thermal threshold required to activate the reactive paths involving methane consumption in the gas phase. The residence time is changed by varying the height of the combustion chamber: in the specific, 1, 3 and 4 mm high combustion chambers have been considered, corresponding to residence times respectively equal to 11, 34 and 45 ms (evaluated at 800°C).

In Figure 4.15 methane conversion follows two different trends with varying τ_R depending on H_2/CH_4 ratio. At a H_2/CH_4 ratio less than one, fuel conversion doesn't depend significantly on the residence time. This happens because $H_2/CH_4 \leq 1$ (Mix1 and Mix2) is not high enough to allow a reactivity of CH_4 reactivity in the gas phase and fuel is converted exclusively on the catalyst. Moreover, at fixed catalyst formulation methane conversion doesn't change with τ_R because the unchanged contact time, as it has been already discussed in the paragraph 4.3 and specifically shown in Figure 4.4.

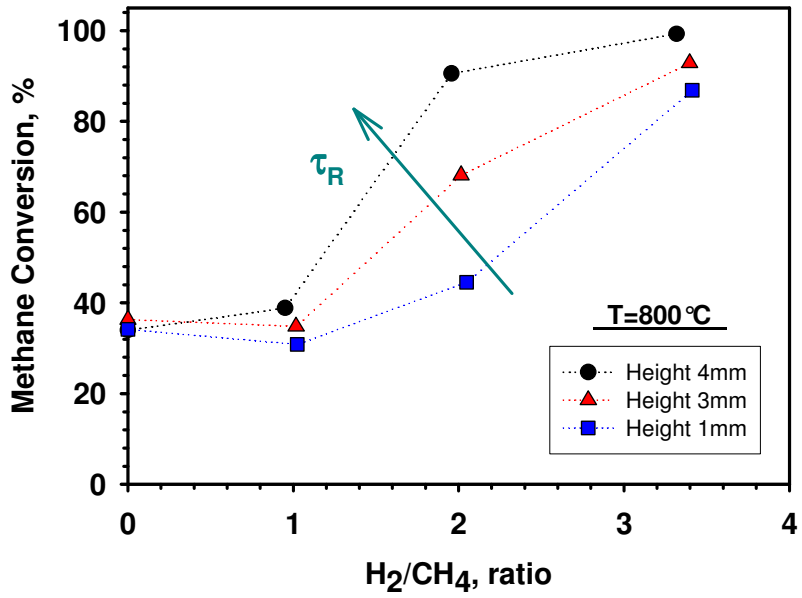

Figure 4.15 *H_2-CH_4 mixtures combustion on F2LM at τ_C=1.26 $g_{cat}\cdot s\cdot Nl^{-1}$. CH_4 conversion as a function H_2/CH_4 ratio at 800°C with varying the residence time (evaluated at 800°C). τ_R=45ms (closed black circles); τ_R=34ms (closed red triangles); τ_R=11ms (closed blue squares).*

By increasing the H_2/CH_4 ratio in the fuel mixture (Mix3 and Mix4), as it has already reported, a steep increase in methane conversion is observed; moreover the amount of converted fuel increases with the residence time. By comparing this result with those obtained previously at $H_2/CH_4 \leq 1$ it is clear as a changing in the conversion regime occurs at H_2/CH_4=1: specifically while at $H_2/CH_4 \leq 1$ methane is catalytically converted, at higher ratios the dependence of CH_4 conversion on τ_R shows that the combustion takes place in the gas phase. Specifically, at a H_2/CH_4 ratio equal to 2 (Mix3) it is shown as the methane conversion is 45, 68 and 90% in the case of a τ_R respectively equal to 11, 34 and 45ms. As it is expected, an increase in methane conversion is observed further increasing the

H_2/CH_4 ratio, but the same dependence on τ_R is maintained. In particular, in the case of Mix4 fuel conversion is 87, 93 and 100% respectively at τ_R equal to 11, 34 and 45ms.

Under the investigated conditions, CH_4-H_2 fuel mixtures burn in the gas phase despite of the presence of an active catalyst. On the basis of this result, it is needed to examine in depth the role of the catalyst. First of all, it is worth noting that the catalyst plays a relevant role on the selectivity of the converted methane: in particular, the detected CO selectivity in the CH_4-H_2 (see Figure 4.14c) is much lower than that which is expected in a "pure" homogeneous combustion. Based on this consideration, the catalyst, even if not involved in the reaction of methane consumption, is certainly determinant in oxidizing CO to CO_2 improving combustion efficiency. However this may be not the only role of the catalyst and in order to better understand the possible synergy between the homogeneous and the heterogeneous some specific experiments have been performed. Specifically, CH_4-H_2 combustion tests have been carried out on F2LM at a fixed residence time with varying the contact time. As already specified, this is possible by changing simultaneously the total flow rate and the combustion chamber height. In Figure 4.16 CH_4 conversion is shown as a function of the H_2/CH_4 ratio with varying the contact time; the residence time and the temperature are maintained constant and are respectively 34 ms and 800°C.

At low H_2/CH_4 ratio($H_2/CH_4 \leq 1$), where only catalytic reaction occurs, fuel conversion increases by increasing the contact time, as it is expected. In particular, in the case of H_2/CH_4=1 (Mix2) CH_4 conversion is 77 and 35% respectively at τ_C=3.84 and 1.26 $g_{cat} \cdot s \cdot Nl^{-1}$.

By increasing the H_2/CH_4 ratio (H_2/CH_4>1), homogeneous reaction paths are expected; in these conditions, methane conversion still increases by increasing the contact time, despite of the same residence time. For example, in the case of H_2/CH_4=2 (Mix3) CH_4 conversion is 92 and 68% respectively at τ_C=3.84 and 1.26 $gcat \cdot s \cdot Nl^{-1}$. Moreover, higher is the contact time and lower is the ratio H_2/CH_4 at which methane is totally converted. As a result, an increase in the contact time shows a positive role on the H_2 assisted methane combustion in the gas phase, revealing a certain synergy between heterogeneous and homogeneous reaction. In particular, the catalyst, partially converting methane on its surface, reduces the amount of the hydrocarbon in the gas phase thus increasing the effective H_2/CH_4 ratio. This results in a lower and lower H_2 amount necessary to burn efficiently CH_4-H_2 fuel with increase the contact time.

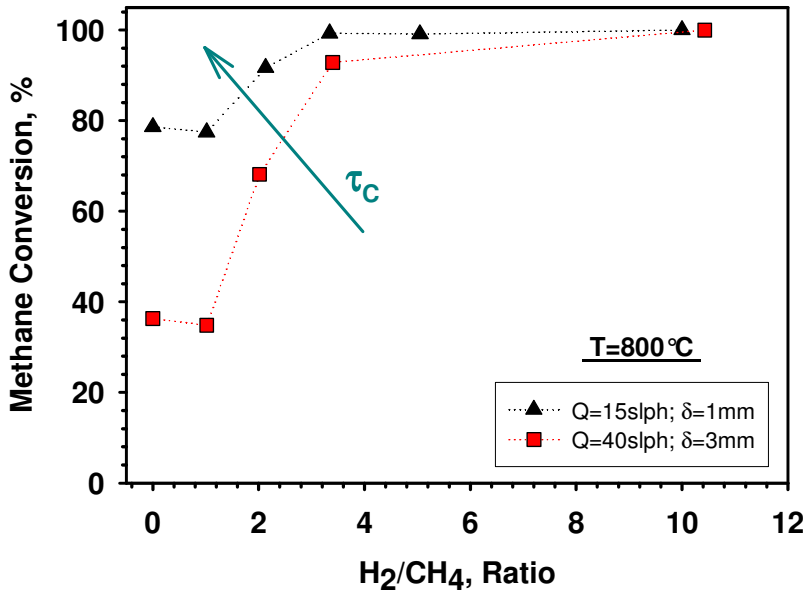

Figure 4.16 *H_2-CH_4 mixtures combustion on F2LM at τ_R=34 ms (evaluated at 800°C). CH_4 conversion as a function H_2/CH_4 ratio at 800°C with varying the contact time. τ_C=3.84 gcat·s·Nl^{-1} (black triangles); τ_C=1.26 gcat·s·Nl^{-1} (red circles).*

CHAPTER 5

AUTOTHERMAL COMBUSTION OF CH_4 AND H_2-CH_4 MIXTURES

In this chapter an experimental study on the catalytic combustion of hydrogen, methane and their mixtures under autothermal conditions is presented.

γ-Alumina supported Pt-$LaMnO_3$ catalyst has been taken into account. Among the different active phases considered in this study, this choice results optimal in the case of H_2-CH_4 mixtures combustion, since, as previously reported, such a catalyst is constituted by the combination of the most active phases for both methane (i.e., perovskite) and for hydrogen (i.e., platinum) oxidations.

Under autothermal conditions, the heat generated by the reaction should be high enough to guarantee the self-sustainability of the combustion process. As a consequence of ignition, total fuel conversion involves a steep rise of the system temperature that is sustained by the release of the heat of combustion despite of the relatively cold incoming gas. In the actual experimental conditions, however, the steady state temperature measurements result in lower values with respect to the adiabatic temperature of combustion, due to the unavoidable heat losses that are also expected in a pronouncedly not adiabatic system like a microcombustor. In addition, as already discussed in the first chapter, autothermal combustion is stable in a narrow operating window because of the occurrence of two quenching modes, extinction and blowout, associated to a drop in temperature and conversion (Ronney, 2003, Norton and Vlachos, 2004, Kaisare et al., 2008) due to different causes. In the extinction mode, stability is lost due to a too large heat loss (towards surroundings) compared to the thermal power provided via combustion. In the blowout mode, quenching occurs because of a too large flow rate, resulting in incomplete fuel conversion for both insufficient residence time and a considerable shift of the reaction front downstream, due to insufficient cold feed gas pre-heating.

The main pursued object is to study the ignition behaviour and the stable combustion limits of H_2, CH_4 and H_2-CH_4 fueled monolithic microcombustor. In particular, light-off temperature and quenching conditions are measured with varying inlet fuel compositions and total flow rate. Differently from isothermal H_2-CH_4 combustion tests (discussed in the previous chapter), focused to the comprehension of the eventual promoting effect of hydrogen on the chemistry of methane combustion, autothermal tests proposed in this section allow to understand the role of H_2 in

thermally assisting CH_4 combustion. Actually, the great reactivity of hydrogen on Pt based catalysts (see paragraph 4.3.6) allows its ignition roughly at room temperature. The thermal power developed by H_2 combustion could bring about a rise in the catalyst temperature thus lowering the ignition temperature of a CH_4-H_2 mixtures in comparison with that of CH_4 only. Aside the specified effect on ignition behaviour, hydrogen may play a role in enlarging the operating window of methane self-sustained combustion by keeping away extinction and blowout instability modes.

5.1 Operating conditions

Combustion tests have been carried out in MQR reactor on C1PtLM900 catalyst (see 2.1.5 and 3.1.3 paragraphs for details).

In order to achieve autothermal conditions, a sufficient thermal power needs to be developed through combustion. As a consequence, an high overall heating value fuel is required, differently from isothermal tests where a strong reactant dilution was taken into account. In Table V.1 the specifics of the considered fuel mixtures are reported.

Table V.1 *Composition of fuel mixtures in the case of CH_4, H_2 and CH_4-H_2 combustion tests under autothermal conditions.*

	Fuel			
	CH_4		**CH_4- H_2**	**H_2**
	Mix1	*Mix2*	*Mix3*	*Mix4*
H_2, %	-	-	2.1	2.1
CH_4, %	2.8	3.8	2.2	-
O_2, %	10.0	10.0	10.0	10
N_2, %	87.2	86.2	85.7	87.9
Equivalence ratio, Φ	0.56	0.76	0.54	0.1
Heating value, $KJ \cdot Nl^{-1}$	0.9	1.2	0.9	0.2
Thermal Power, W	10-35	13-47	10-35	2-8
Q_{TOT}=40÷140slph				

For safety issues, fuel composition is always below the LFL of each considered fuel. In particular, concerning methane combustion, fuel composition is under 5%vol and it is 2.8% and

3.8%vol respectively for Mix1 and Mix2. Moreover, O_2 content was kept at 10% vol. for the same reason.

The specified compositions supply an overall heating value that is 0.9 and 1.2 $kJ \cdot Nl^{-1}$, respectively in the case of Mix1 and Mix2. A CH_4-H_2 mixture, Mix3, is prepared with the same overall heating value of Mix1. Specifically, an H_2/CH_4 ratio of 0.95 is taken into account corresponding to a substitution of methane with hydrogen of 49% as regards the molar content while it is 22% considering the energetic content of H_2 with respect to the overall heating value of the mixture. Methane and hydrogen concentrations in Mix3 are respectively of 2.2 and 2.1%vol. Such a fuel percentage is below the mixture LFL that is equal to 4.5%vol. Concerning Mix4, it is a $H_2/O_2/N_2$ mixture prepared with the same hydrogen content as Mix3 and by replacing CH_4 with N_2. Such a fuel is characterized by an overall heating value of 0.2 $kJ \cdot Nl^{-}1$ (of course lower than that of Mix3) and is considered as a reference of the thermal power supplied by hydrogen in CH_4-H_2 combustion. Finally, as regards the oxygen content, it is 10%vol in all the investigated fuel mixtures. Such a O_2 concentration is in excess with respect the total combustion stoichiometry but not higher than MOC value. The considered compositions result in different equivalence ratio, as it is reported in Table V.1.

In Table V.1 it is also reported the range of the investigated gas flow rate, Q_{TOT}; specifically, Q_{TOT} is ranging from 40 and 140slph corresponding to an input power that varyies in the range of 2÷50W.

The experiments provide for the ignition of the fuel mixture by means of the reactor pre-heating; in particular, the minimum ignition temperature (MIT) is here defined as the gas temperature at which light off occurs at the minimum pre-heating. Once obtained fuel ignition, the external pre-heating is progressively decreased and stable combustion is observed until system is quenched at a specific temperature, QT, corresponding to minimum value external pre-heating of entrance gas temperature that allows stable combustion.

MIT and QT are measured according to a specific experimental procedure. In particular, the system is heated in inert atmosphere up to a specific furnace set-point temperature. Then the fuel mixture is fed to the reactor and temperature profile inside the catalyst as well as fuel conversion are continuously measured. Temperature set point of the external electric furnace is increased with a step of 5°C till fuel ignites and MIT is found (through the measurements of thermocouples inserted in the monolith, and not evaluating the actual furnace temperature). After fuel mixture ignition, steady states of combustion are measured by decreasing furnace set-point temperature until to reach the quenching point at QT.

MIT and QT (as well as $T_{pre\text{-}heating}$ reported in the following graphs) of a specific fuel mixture, fixed the total flow rate, represent gas temperatures obtained if the same flow rate of an inert N_2-O_2 (10vol% in oxygen) mixture is preheated inside the reactor at a furnace temperature set-point corresponding respectively to combustion ignition and quenching. The reactor is placed in a zone of the furnace where it is possible to neglect any border effect on heating: consequently an isothermal profile in the reactor should be expected in the case an inert mixture is heated at a specified furnace set point. Even so, the detected temperature increases along the catalytic reactor length because of the heat transferred by convection and a maximum temperature difference of about 20°C is detected between inlet and outlet of the monolithic reactor. Based on this, the choice of MIT and QT is not univocally determined. However, as regards the ignition phenomena the temperature considered is the highest one (i.e. the exit temperature); on the contrary as regards the quenching it is the lowest one (i.e. the entrance temperature).

Combustion performances are compared for the various operating conditions studied herein in terms of MIT and QT measured values. In particular, the latter is a very good metric of combustor stability. In the following graphs, the quenching point is indicated with vertical arrows.

The catalyst has been pre-treated in a combustion environment up to 1000°C for approximately 6h. Such a treatment allows to stabilize the catalyst properties. Actually, a good reproducibility is found for each single experiment, repeated some time after many days of tests; this is proved by no relevant change in the measured values of MIT and QT after the catalyst was used for several hours (approximately 120 h).

Finally, it is worth mentioning that no carbon monoxide is detected in all the performed combustion tests as it is typical in Pt based catalyst (see Chapter 4).

5.2 Ignition and limits of stable operation in CH_4 combustion

In Figure 5.1 it is reported the transient of the ignition at MIT measured in the case of combustion of Mix1 at a total flow rate of 80slph: CH_4 concentration and conversion (respectively Figure 5.1 a and b) as well as thermal profile inside the monolith (Figure 5.1c) are reported as functions of time. Concerning Figure 5.1c, T_1, T_2 and T_3 are respectively the temperatures measured at the inlet, the centre and the exit of the reactor.

In the graphs shown it is possible to distinguish more regions, Zone 1, 2, 3 and 4.

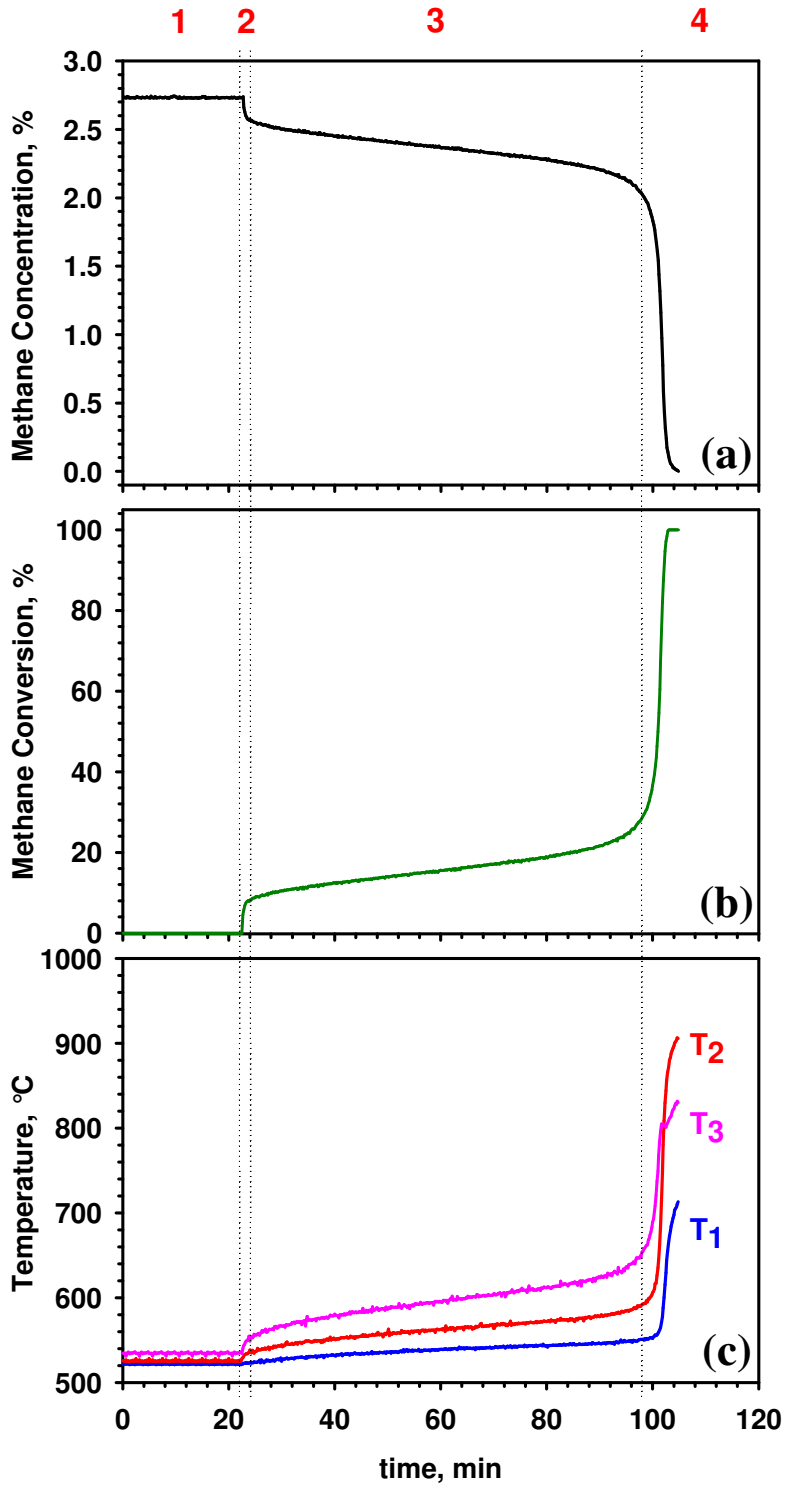

Figure 5.1 *CH_4 combustion on C1PtLM900 in MQR at Q_{TOT}=80slph; Ignition transient of Mix1 at MIT=534°C. Section 1: Evaluation of MIT: thermal profile for an O_2-N_2 mixture. Sections 2, 3, 4: CH_4 is sent to the reactor: fuel light-off. (a) CH_4 concentration (black line). (b) CH_4 conversion (green line). (c) thermal profile inside the monolith: T_1 (blue line), T_2 (red line), T_3 (pink line).*

Zone 1 is characterized by an almost constant temperature profile: it represents the minimum pre-heating condition which gives place to the ignition of methane combustion. Consequently, by analyzing the zone 1 thermal profile, it can be derided the MIT value. As already discussed, the detected temperature increases along the catalytic reactor length because of the heat produced by methane conversion to carbon dioxide and transferred from the entry to the exit sections of the monolith by convection. In the specific, T_1, T_2 and T_3 assume the values of respectively 522, 525 and 534°C and, based on previous assumption, MIT=534°C.

In Zone 2 Mix1 is sent to the reactor. A methane conversion of about 10%vol is observed (see Figure 5.1b) as detected by the decrease of fuel exit concentration (see Figure 5.1a). Considering the kinetic parameters evaluated in the Chapter 4 and assuming a PFR reactor, the measured conversion is consistent with that expected at a temperature equal to MIT, fixing the contact time, τ_C=49.6 $g_{cat}\cdot s\cdot Nl^{-1}$. Moreover, the insulation of the combustor makes sure that part of the developed thermal power is not lost towards the environment but trapped inside the system. This is made clear by considering the increase in temperature observed on the catalyst (see Figure 5.1c). Specifically, an increase of about 20, 15 and 5°C is measured respectively in the case of T_3, T_2 and T_1.

The increase in the reactor temperature determines an increase in fuel conversion and, consequently, a further increase in the system temperature. The repeating of this cycle brings about the progressive increase with the time in methane conversion and catalyst temperature as it is shown in the Zone 3. Specifically, in this region a rise in the percentage of converted CH_4 up to about 30%vol is observed; moreover, T_1, T_2 and T_3 are respectively 550, 580 and 650°C.

A certain induction time (about 75 min) is needed in the Zone 3 to have combustion "run-away". In the Zone 4, in fact, the temperature level reached by the system is sufficiently high to allow the total conversion of the methane. A steep increase in the fuel converted with a negligible production of carbon monoxide is thus observed. The total selectivity to CO_2 of the process points out that methane is converted on the heterogeneous phase, being CO one main product of homogeneous combustion in this range of operating conditions (Hayes and Kolaczkowski, 1997). Moreover, the available thermal power is totally developed and, as a consequence, system temperature strongly raises. The ignition takes place at the exit of the monolith where the temperature is higher. This is clearly shown in Figure 5.1c where it is shown that a temperature "jump" occurs firstly for T_3 and then for T_2 and T_1. On the basis of the last recorded data (that are not representing the steady state yet), at the end of the fourth zone, T_1, T_2 and T_3 are respectively 700, 920 and 840°C. Differently from the thermal profile measured in Zone 2 and 3, in correspondence with the fuel ignition, maximum temperature shifts from the exit to the centre of the reactor. A temperature wave travelling from the exit to the inlet of the reactor is thus observed pointing out the reaction front

propagation backwards. Such a result is a relevant advancement towards the understanding of microcombustor behaviour; however, a similar ignition behaviour was observed a few years ago by Cimino et al. (2001) who investigated methane autothermal combustion in pronouncedly not adiabatic laboratory reactors.

It is worth noting that the transient of methane ignition at the MIT, from the feeding to the total combustion of the fuel, lasts about 90 min and a still longer evolution is expected to have a steady state (the latter is not reported). Such a quite long induction time is more and more reduced as the preheating temperature is increased with respect to MIT.

In Figure 5.2 the steady state of Mix1 combustion at a total flow rate of 80slph is reported, as function of the decreased pre-heat temperature. In the specific, it has been reported methane conversion (Figure 5.2a) and temperature measurements inside the monolithic reactor (Figure 5.2b).

As already discussed, at the specified flow rate Mix1 ignition occurs at a MIT=534°C. However, once ignited, the catalytic combustion of methane still remains effective with reducing the pre-heating temperature. Examining Figure 5.2a and, specifically, the low conversion branch (open red circles), before the ignition most of CH_4 stays unconverted at a pre-heating temperature lower than MIT (a fuel conversion less than 10%vol is detected). By progressively heating up the system from such an unlighted state, fuel conversion slightly increases till it jumps in correspondence with MIT (pointed out in the graph by a red upward arrow). By subsequently decreasing the pre-heating temperature from such an ignited state, fuel conversion does not retrace the curve exhibited during the heating up process and, in particular, does not drop thus constituting an high conversion branch (closed black circles in Figure 5.2a). It is so revealed the existence of two stable steady states at the same pre-heating temperature. Such a behaviour is typical of highly exothermic reactions (Levenspiel, 1962, Hayes and Kolaczkowski, 1997) for which a multiplicity of steady states may result from energy and mole balance equations for any given set of inlet conditions to reactor. Examining the high conversion branch shown in Figure 5.2a, the percentage of converted methane decreases with decreasing the pre-heating temperature. In particular, methane conversion is higher than 96% at a $T_{pre\text{-}heating}$>367°C; then it starts to decrease more significantly till to reach a value of 93% in correspondence with the quenching point (at a pre-heating temperature so named QT). Further decreasing the temperature beyond this value, the fuel conversion suddenly drops going back to the low conversion branch and the combustion process quenches. The minimum pre-heating temperature at which stable combustion is observed, i.e. the critical temperature QT, represents the thermal limit of combustion operation; under the specified conditions of Mix1 and 80 slph QT is equal to 333°C, significantly lower than MIT. Such a discrepancy points out the hysteresis of about 200°C exhibited by the cooling/heating curve.

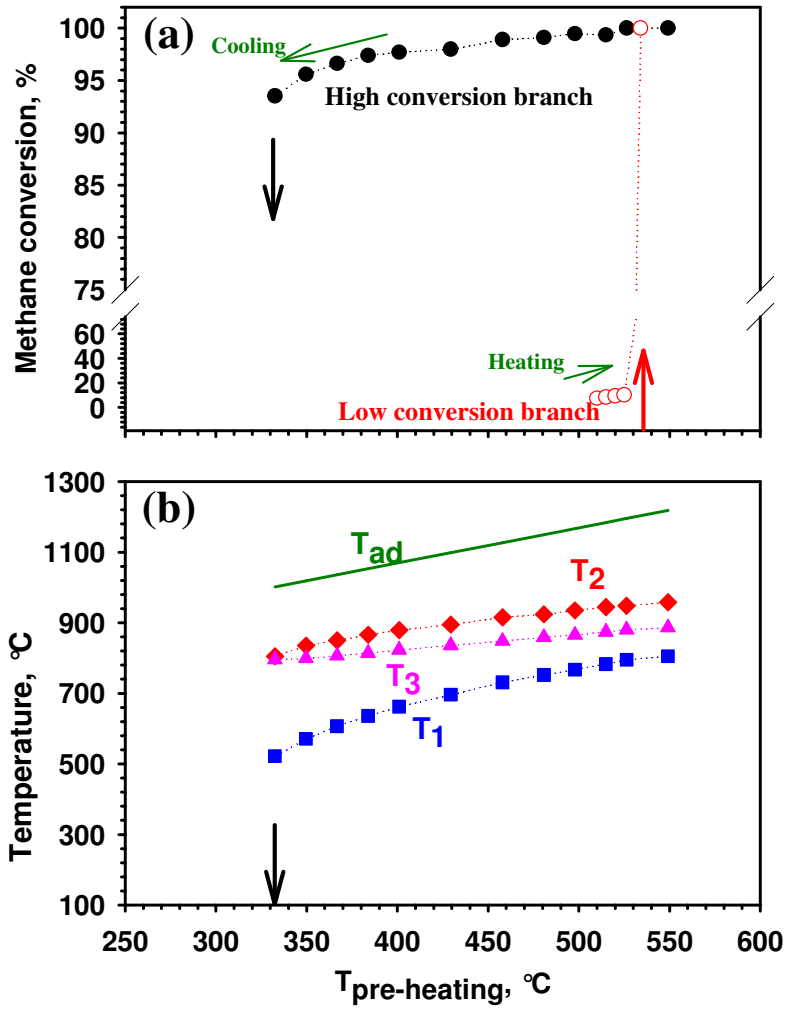

Figure 5.2 *Stability limits of CH_4 combustion on C1PtLM900 in MQR; QT for Mix1 at Q_{TOT}=80slph as a function of $T_{pre\text{-}heating}$. (a) CH_4 conversion: high (black closed circles) and low (red open circles) conversion branches. (b) Temperature in the high conversion branch (T_1, blue squares, T_2, red rhombs, T_3, pink triangles) and theoretical adiabatic temperature (Tad, green line).*

A multiplicity of stable steady states curves for any given pre-heating temperature is expected even in terms of temperature measured inside the reactor. Similarly to the case of conversion, in fact, by heating up the system starting from unlighted conditions a transition to high temperature ignited state occurs at MIT, while on the contrary, by cooling down the system starting from ignited conditions, the transition to low temperature quenched state occurs at QT. Nevertheless, in Figure 5.2b only the high temperature branch is reported. In that figure T_1, T_2 and T_3 as well as adiabatic temperature of the fuel mixture, T_{ad}, are reported. The latter is ranged between 1220 and 1000°C (depending on the preheating temperature) under the investigated condition and it is always higher than the measured combustion temperatures, T_1, T_2 and T_3. This result points out the intrinsic non-

adiabaticity of such a kind of micro-structured system, that is a typical feature of practical micro-combustors. Considering the maximum investigated pre-heating temperature of approximately 550°C, T_1, T_2 and T_3 are respectively, 805, 958 and 886°C, highlighting that a maximum temperature is set in proximity of the centre of the reactor, as it has been already shown in Figure 5.1. Based on this result, the reaction front, consistently with the maximum temperature position, stabilizes at the center of the monolith; moreover, the second half of the reactor is a post-combustion zone, where the detected temperature decreases because of the heat losses, while the first half of the reactor provides for the gas pre-heating, above all through the axial heat flux from the combustion zone. By decreasing the pre-heating temperature a general decrease in the temperature level is observed as a consequence of the lower adiabatic temperature. However, a different decreasing slop is observed for the three measured temperatures. Concerning the entrance temperature, its drop with $T_{pre\text{-}heating}$ is consistent with T_{ad} decrease: this assumption is made clear considering that T_1 and T_{ad} decrease slopes are approximately the same, at least till methane is totally converted (see Figure 5.1). In particular, in consequence of a decrease in pre-heating of about 200°C T_1 decreases of about 280°C. On the contrary, in correspondence with the same decrease in pre-heating T_2 and T_3 decrease is significantly lower and specifically of 153 and 90°C respectively. It follows that the observed phenomena are strongly non linear: actually they are ruled by the heat losses that under these conditions are controlled by radiative heat transfer depending on T^4. The weaker variability of the exit thermal level points out that by decreasing the pre-heating temperature T_2 and T_3 tend to overlap till they are approximately the same at $T_{pre\text{-}heating}$=QT (at a preheating temperature equals to QT, T_2 and T_3 are respectively 805 and 796°C). Actually, by decreasing the temperature of the incoming gas (i.e, $T_{pre\text{-}heating}$ in Figure 5.2) in order to reach the same thermal threshold to sustain the combustion process a longer and longer pre-heating length is needed in the reactor. As a consequence, a reaction front drift downstream is observed while the post-combustion zone becomes shorter resulting in a decrease in its active surface. However, the increase in the pre-heating length observed with decreasing the temperature of the incoming gas brings about a lower and lower contact time of the reactants with the high temperature reactor zone, as it is shown by the drop in fuel conversion (see Figure 5.2a).

In Figure 5.3 it is reported the transient behaviour of the system during the quenching of Mix1 combustion at a flow rate of 80slph for a pre-heating temperature of 328°C, a value lower than QT. In particular, temperature and methane conversion measurements are reported as a function of time respectively in Figure 5.3a and b. At t=0 T_1, T_2 and T_3 are respectively 524, 807 and 797°C while fuel conversion is 93%. Still, after 10min these values are practically unchanged. Nevertheless, after this segment, T_1 and T_2 start simultaneously to decrease while T_3 slightly increases till to exceed T_2

at t=15min. A temperature wave is thus observed travelling from the inlet to the exit of the reactor. Such a behaviour is connected to combustion quenching phenomena in the presence of important heat losses and it is due to the insufficient gas preheat or insufficient contact time at the necessary high temperature zone and results in the reaction front shift downstream and its subsequent exit from the reactor. After 45 min T_1, T_2 and T_3 are respectively 425, 626 and 816°C. At that instant T_3 reaches a maximum after which it quickly decreases. At t=55 min the system is, in fact, totally quenched. Concerning methane conversion it follows the same T_3 trend: in particular, the percentage of converted fuel is practically unchanged compared to that revealed at t=0 (it is actually more than 90%) till T_3 drop (t>45min). After that instant, in agreement with T_3 behaviour, methane conversion strongly decreases and at t=55min fuel is practically unconverted.

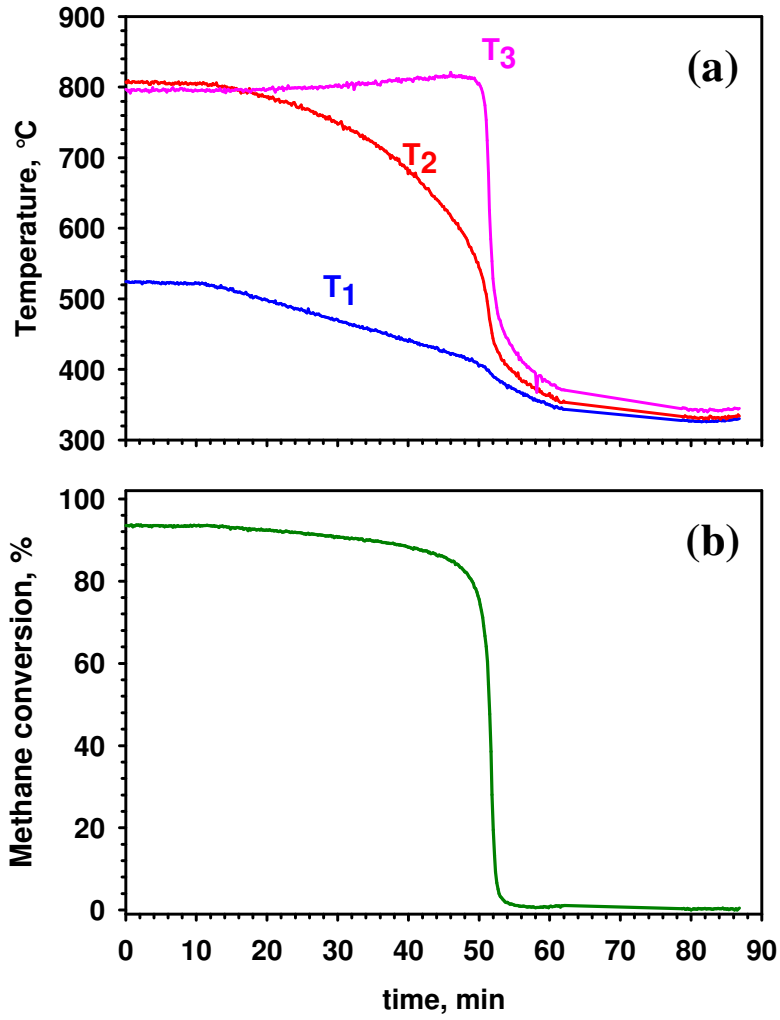

Figure 5.3 *CH_4 combustion on C1PtLM900 in MQR. Quenching transient of Mix1 at Q_{TOT}=80slph and $T_{pre\text{-}heating}$=328°C. (a) CH_4 conversion (green line). (b) Temperature measurements (T_1, blue line, T_2, red line, T_3, pink line).*

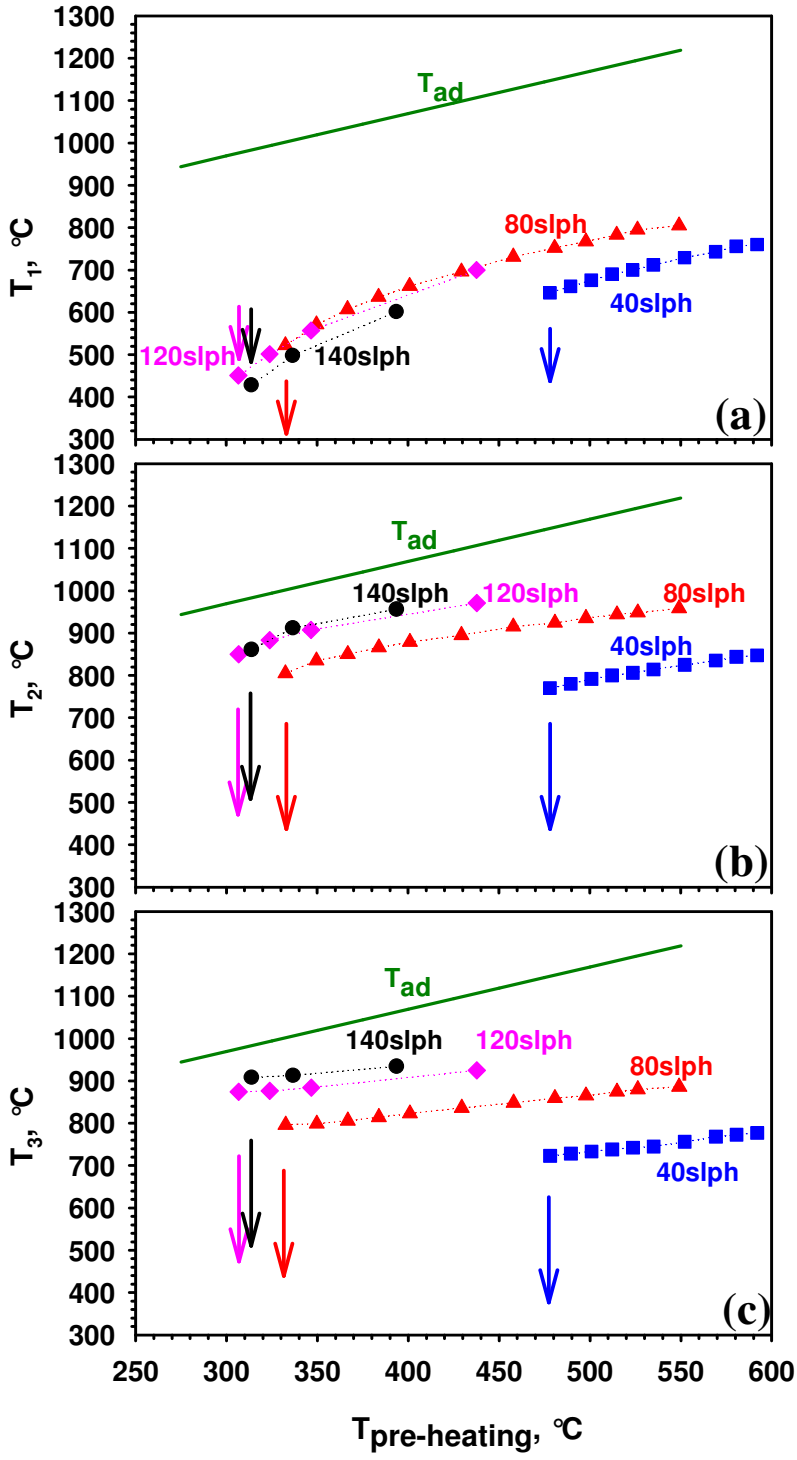

Figure 5.4 *Stability limit of methane combustion on C1PtLM900 in MQR; QT for Mix1 with varying the flow rate. Temperature measured in the high conversion branch. (a) T_1; (b) T_2; (c) T_3 as a function of the pre-heating temperature. Total flow rate of 40slph (blue squares), 80slph (red triangles), 120slph (pink rhombs), 140slph (black circles); adiabatic temperature (Tad, green line).*

The behaviour observed and described in Figg. 5.1-5.3 presents some relevant difference in dependence of the flow rate adopted. Actually, maintaining the same chemical composition (Mix1), the thermal power of the mixture entering the micro-reactor depends on the flow rate (and is proportional to it), hence all thermal effects can be severely affected. In Figure 5.4 and Figure 5.5 the high conversion branch of Mix1 combustion is shown respectively in terms of measured temperature and CH_4 conversion, as a function of the pre-heating temperature, at different values of the flow rate. The reported arrows point out the quenching temperature observed and the window of stable combustion at the different operating conditions. It is shown as the quenching temperature progressively decreases with increasing flow rate from 40 to 120slph, thus extending the limits of stable combustion. On the contrary, it starts to decrease further increasing the gas flow from 120 to 140slph. Specifically, QT is 478, 333, 306°C at Q_{TOT} respectively equals to 40, 80, 120slph while it is 314°C at Q_{TOT}=140slph. Increasing the flow rate a different behaviour is observed in the detected temperature in dependence on the particular reactor section (see Figure 5.4).

Concerning the entrance temperature, T_1, it increases by increasing the flow rate from 40 to 80slph; on the contrary, it is practically unchanged varying the gas flow from 80 to 140slph. Considering the temperature measured at the centre of the reactor, T_2, it increases in a larger flow rate range in comparison with T_1 case; particularly, T_2 progressively increases by increasing flow rate up to 120slph while it does not vary any more further increasing the flow rate up to 140slph. Finally, concerning T_3, reactor exit temperature, it increases in all the investigated flow rate range.

By increasing the flow rate a dual effect is expected on combustion stability. In particular, considering the same fuel composition, the power developed by the combustion linearly increases with total flow rate. At the steady state and for a non adiabatic reactors (like a microcombustor) the power released via combustion is equal to the sum of the power lost through the reactor walls and in the exhausted gases. To balance the increase in the combustion power this sum has necessarily to increase linearly with the total flow rate. However, the heat losses through the reactor walls don't depend on the total flow rate and the sensible heat of exhausted only linearly. Consequently, in order to get over the higher power released via combustion at higher flow rates the system has to reach higher temperatures. In such a way, in fact, by increasing the total flow rate the power lost in the exhausted gases increases more than linearly; moreover, the heat lost through the walls increases too in consequence of the increase in the heat transfer driving force. As a result, an increase in the flow rate determines an increase in the system adiabaticity level because heat losses are a fraction less and less important of the thermal power increase developed by methane combustion. Nevertheless, an increase in the flow rate brings about a decrease in the contact time

and, as a consequence, a possible worsening of fuel conversion, if contact time becomes insufficient. These considerations suggest a tradeoff behaviour regarding the total flow rate. Specifically, in a range of low gas velocity, such as to guarantee a sufficient contact time, an enhancement of combustion stability is expected by increasing flow rate. An increase in the system adiabaticity, in fact, is effective in preventing extinction, as it has been already shown in the first chapter (Kaisare and Vlachos, 2007, Kaisare et al., 2008). Nevertheless, in a range of gas velocity not more compatible with the total fuel conversion, an increase in flow rate is detrimental for combustion stability causing blowout (Kaisare and Vlachos, 2007, Kaisare and al., 2008).

Based on these considerations, the expansion of combustion operation limits (i.e., the decrease in QT) observed by increasing the flow rate from 40 to 120slph is consistent with an enhanced system adiabaticity. Assuming T_3 as the temperature of the exhausted gas, from experimental data one can calculate the power lost in the exhausted gas and comparing it to the total power generated it is possible to evaluate the heat lost through the reactor walls. At a $T_{pre\text{-}heating}\approx500°C$, for example, considering a Q_{TOT}=40slph the power released via combustion is about 10W and the sensible power of exiting gases is about 3.5W. As a result, the power lost trough the reactor walls is approximately 6W that correspond to a 65% of the total power confirming the pronounced thermal dissipation in a microcombustor. By increasing the total flow rate and specifically at Q_{TOT}=80slph but maintaining the same $T_{pre\text{-}heating}\approx500°C$, the power released via combustion is about 20W, the sensible power of exiting gases is about 11W; the power lost trough the reactor walls is thus about 9W that correspond to a 45% of the total power confirming the enhanced adiabaticity of the system. Further increasing the total flow rate from Q_{TOT}=80slph to Q_{TOT}=120slph, at $T_{pre\text{-}heating}\approx345°C$ the percentage of heat lost through the reactor walls still decreases from 28 to 17%. As a result, under these conditions loss in combustion stability observed at a pre-heating temperature lower than QT is ascribed to the low power input compared to heat losses through the reactor wall. This particular instability mode occurs at nearly complete fuel conversion and is described as extinction (Kaisare and al., 2008). By analyzing the thermal profiles reported in Figure 5.4, for Q_{TOT}=40÷120slps a maximum temperature is detected in correspondence with the centre of the reactor. Such a maximum increases by increasing the flow rate confirming the enhanced adiabaticity of the system. Moreover, as it is shown in Figure 5.5, the increase in the flow rate in the specified range brings about an increase in the fuel conversion despite of the decrease in the contact time, due to the faster catalytic combustion kinetics consequent to the increased temperature. Furthermore, the dynamics of quenching via extinction is pointed out in Figure 5.3 at Q_{TOT}=80slph. In that graph it is shown that fuel conversion does not significantly decrease despite of the decrease in gas residence time in the high temperature zone due to the temperature wave travelling downstream cooling the entrance and the centre of the

reactor. On the contrary, its drop occurs inevitably when reaction front is pushed outside the reactor, pointed out by the drop in T_3. Such a behaviour confirms that combustion stability in those range of flow rate is not limited by fuel conversion but it only depends on the heat losses.

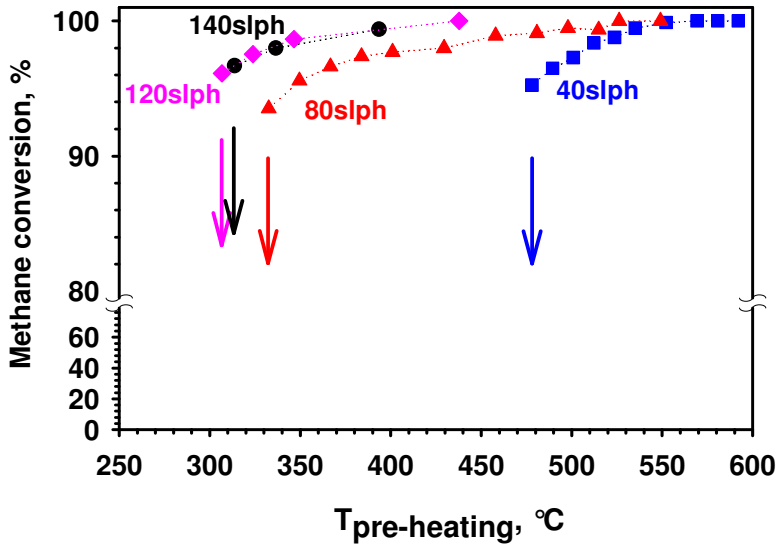

Figure 5.5 *Stability limit of methane combustion on C1PtLM900 in MQR; QT for Mix1 with varying the flow rate. CH_4 conversion measured in the high conversion branch. Total flow rate of 40slph (blue squares), 80slph (red triangles), 120slph (pink rhombs), 140slph (black circles).*

Nevertheless, the worsening in stability observed by further increasing flow rate from 120 to 140slph points out a changing in the combustion quenching mode from extinction to blowout. Under these conditions, the increase in the gas velocity brings about a decrease in the residence time in the high temperature zone, due to the drift of the heat wave downstream. Actually, differently from what already found at lower flow rates, a shift in the position of the maximum temperature from the centre to the exit of the monolith is observed at $T_{pre\text{-}heating}$=336°C. Specifically, at the quenching temperature, T_3 is equal to 908°C, significantly higher than T_1 and T_2, respectively equal to 428, 861°C. Convection, hence, at a so large flow-rate plays a major role. In addition, an increased flow velocity reduces gas pre-heating, which is critical for light-off. The result is ignition further away from the entrance. In confirming with that, at the same pre-heating temperature and close to the quenching point, entrance temperature detected at Q_{TOT}=140slph is about 50°C less than that obtained in the case of Q_{TOT}=120slph. Concerning T_2, only a little discrepancy is observed in the case of the two different flow rates. On the contrary, the exit of the reactor is about 50°C warmer at Q_{TOT}=140slph, thus evidencing a reaction front closer to the exit when an higher flow rate is considered.

5.3 Effect of the fuel concentration on CH_4 combustion stability

On the basis of the above discussed results, there is a maximum beyond which a further increase in the total flow rate does not involve any improvement in combustion stability because of the unavoidable combustion blowout. On the contrary, increasing the equivalence ratio of the fuel mixture is a more effective tool to expand autothermal combustion operation involving an increase in the input power without affecting gas velocity and, as a consequence, gas residence time and fuel conversion.

In Figure 5.6 the high conversion branch of Mix2 combustion is shown in terms of T_2 (Figure 5.6a) and CH_4 conversion (Figure 5.6b) measurements as a function of the pre-heating temperature and with varying the flow rate. The reported arrows point out observed QT and the window of stable combustion at the different operating conditions. A comparison between QTs values of Mix1 and Mix2 combustion is reported in Figure 5.7 as a function of the flow rate. Moreover, in Figure 5.8 thermal profiles detected in the case of Mix1 and Mix2 are compared at the same pre-heating and total flow rate.

Quenching temperature monotonically decreases with increasing flow rate from 40 to 120slph, thus extending the limits of stable combustion. Specifically, QT is 387, 251, 161, 58, 55°C at a Q_{TOT} respectively equal to 40, 60, 80, 100 and 120slph, showing that stable combustion is sustained practically with no external pre-heating at the last two flow rates. It is worth noting that when external preheating is too low it is technically difficult to control set-point temperature of the oven; as a result, critical temperature measurements are not reliable at the highest flow rate. However, the critical temperature detected in the case of Mix2 are strongly lower than those obtained in the case of Mix1 combustion (see Figure 5.7). As a result, a strong increase in combustion stability is observed increasing the equivalence ratio of the fuel mixture. Considering an higher Φ, in fact, combustion extinction is kept away because of the increased thermal power compared to the heat losses (Kaisare et al., 2008). This is clearly shown in Figure 5.8 in which thermal profiles measured in Mix1 and Mix2 combustion are reported in the case of Q_{TOT}=40slph and $T_{pre\text{-}heating}$=478°C. At the specified flow rate, such a preheating level corresponds to the critical temperature of Mix1, while the enhanced stability at an higher Φ is consistent with the increase in the thermal level observed inside the combustor. In particular, T_1, T_2 and T_3 values increase respectively from 646, 770, 723°C detected in the case of Mix1 combustion to 749, 867, 775°C corresponding to Mix2 combustion. As a result, temperature increase is more significant at the inlet section of the reactor suggesting a reaction front closer to the entrance in the case of combustion under richer conditions. Mix2 combustion provides a maximum temperature at the centre of the reactor (i.e., T_2) under all the

range of Q_{TOT} and $T_{pre\text{-}heating}$ investigated. In particular, as it is shown in Figure 5.6a, the differences between T_2 and $T_{pre\text{-}heating}$ monotonically increases with flow rate approaching the system to adiabatic conditions.

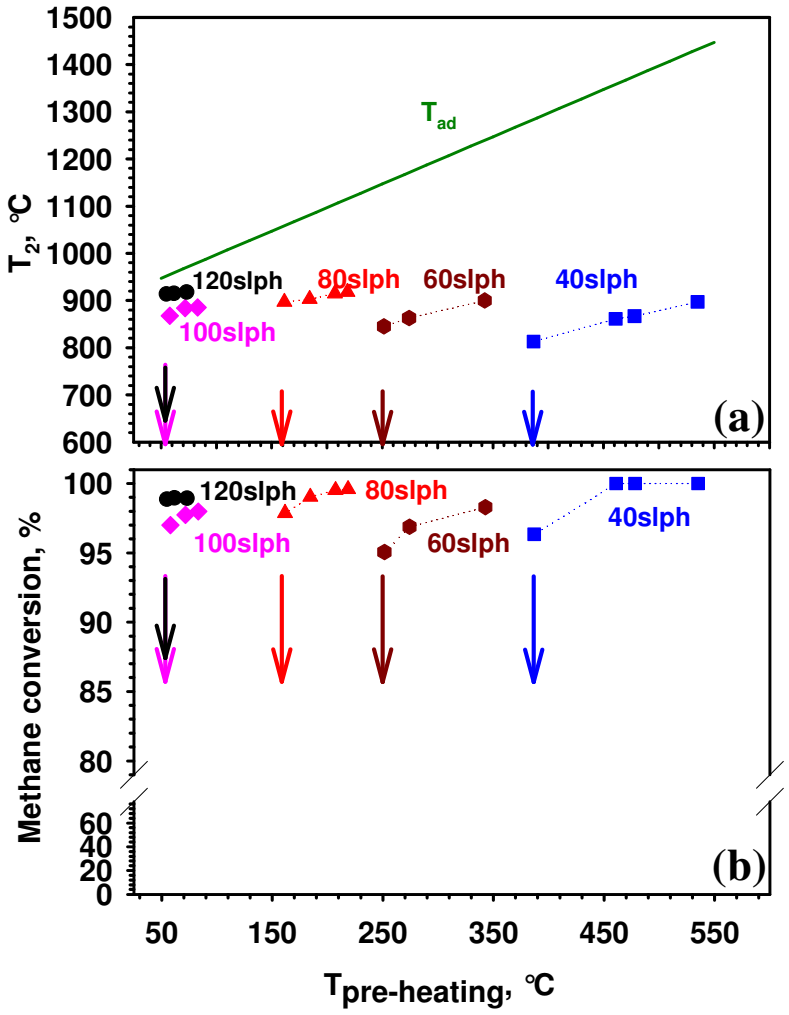

Figure 5.6 *Stability limit of methane combustion on C1PtLM900 in MQR; QT for Mix2 with varying the flow rate. Temperature and conversion measured in the high conversion branch. (a) T_2, (b) conversion as a function of the pre-heating temperature. Total flow rate of 40slph (blue squares), 80slph (red triangles), 120slph (pink rhombs), 140slph (black circles); adiabatic temperature (Tad, green line).*

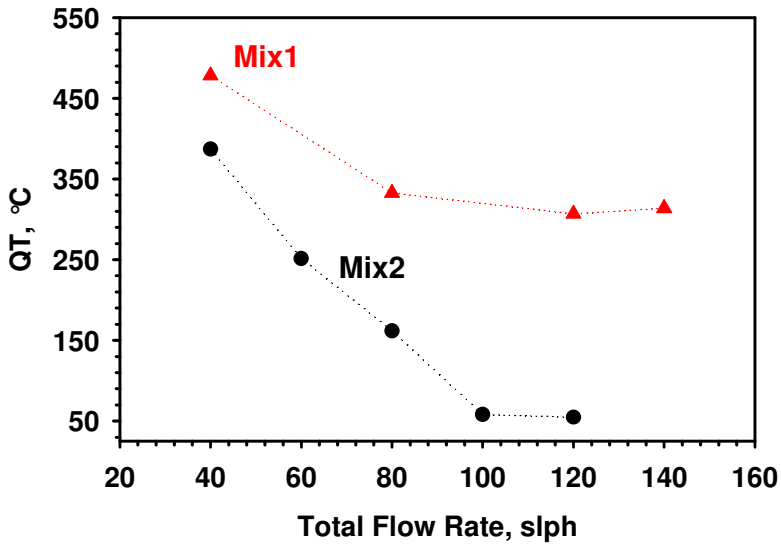

Figure 5.7 *Stability limit of methane combustion on C1PtLM900 in MQR; QT for Mix1 (red triangles) and Mix2 (black circles) with varying the flow rate.*

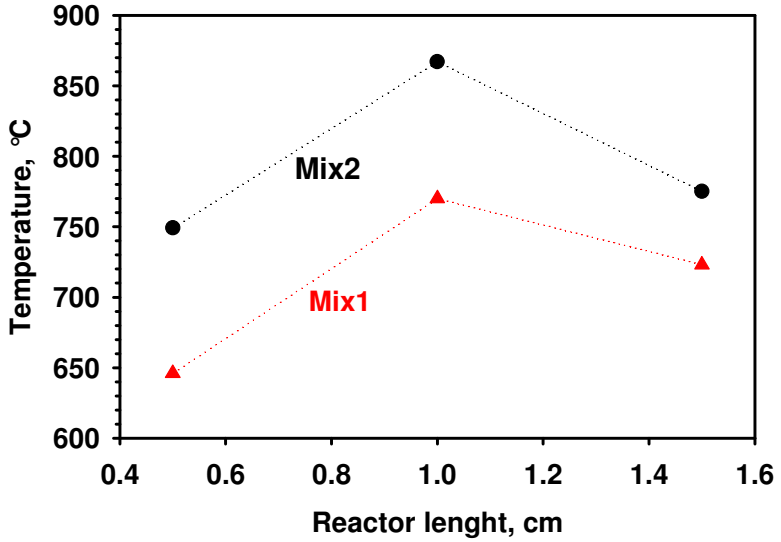

Figure 5.8 *Methane combustion on C1PtLM900 in MQR at $T_{pre\text{-}heating}$=478°C and total flow rate of 40slph. Thermal profile in the case of Mix1(red triangles) and Mix2 (black circles) combustion with varying the flow rate.*

Moreover, the same behaviour is observed for methane conversion (see Figure 5.6b): in particular considering a Q_{TOT}=120slph, a total fuel conversion is measured supplying a significantly lower external preheating (about 50°C) compared to that needed to sustain Mix1 combustion ($T_{pre\text{-}}$

$_{heating}$≈307°C). As a result, a strong improvement of overall combustion efficiency is achieved by increasing the equivalence ratio of the fuel mixture.

However, by analyzing the trend of Mix2 quenching temperature with Q_{TOT} (see Figure 5.7), its decrease shows a tendency to level off at the highest investigated flow rates. Such a behaviour may suggest a transition from an extinction to a blowout quenching regime further increasing the flow rate from Q_{TOT}=120slph. If so, it is confirmed that methane combustion is quenched via blowout at roughly the same flow rate independently on the fuel mixture equivalence ratio.

5.4 Ignition and limits of stable operation in H_2-CH_4 combustion

In Figure 5.9 the ignition transient of Mix3 at MIT is reported. The experiment has been carried out at the same flow rate, Q_{TOT}=80slph, considered in the Mix1 ignition test. In particular, thermal profile inside the monolith (Figure 5.9a) as well as CH_4 and H_2 conversion measurements (Figure 5.9b) are reported as a function of time.

As it was shown for the experiment of Mix1 light-off (see Figure 5.1), in Figure 5.9 it is possible to distinguish four regions, Zone 1, 2, 3 and 4.

Zone 1 shows the MIT by reporting the thermal profile corresponding to the minimum pre-heating of the N_2-O_2 mixture (see Figure 5.9a). MIT is the highest temperature detected along the catalytic reactor length and, specifically, it is 451°C. Such a value is approximately 80°C lower than that obtained in the case of Mix1 combustion. As a result, by substituting part of CH_4 with H_2, maintaining the same input power to the reactor, enhances the fuel reactivity.

In Zone 2 Mix3 is sent to the reactor. As it is expected, at a pre-heating temperature equal to 451°C, hydrogen is totally converted; H_2 conversion, in fact, shows a steep increase from 0 to 100% as soon as hydrogen is fed to the reactor (see Figure 5.9b), a result expected on the basis of results obtained in the study of H_2 combustion under diluted and isothermal conditions (see Chapter 4) . On the contrary, the specified preheating temperature is too low to covert significantly methane. Hydrogen combustion involves an increase in the catalyst temperature; specifically, at t=64min (delimiting Zone 2), T_1, T_2 and T_3 are respectively 518, 573 and 565°C. Nevertheless, methane combustion is active at these temperatures. As a consequence, H_2 assists thermally CH_4 combustion and both fuels are converted in parallel; therefore, after 64 minutes CH_4 conversion is approximately 8%. Such a behaviour is very different from that observed in the ignition of Mix1: in that case, in fact, MIT was high enough to start methane combustion and a steep increase in CH_4 conversion was observed in Zone 2 (see Figure 5.1). On the contrary, the catalyst is practically inactive towards methane combustion at 451°C, i.e. at the minimum ignition temperature of Mix3 but in consequence of the thermal rise produced by hydrogen conversion CH_4 is partially converted

to CO_2 (i.e, methane combustion is thermally assisted by hydrogen): consequently, the increase in CH_4 conversion observed in Zone 2 in the case of Mix3 ignition is slower than that corresponding to Mix1 .

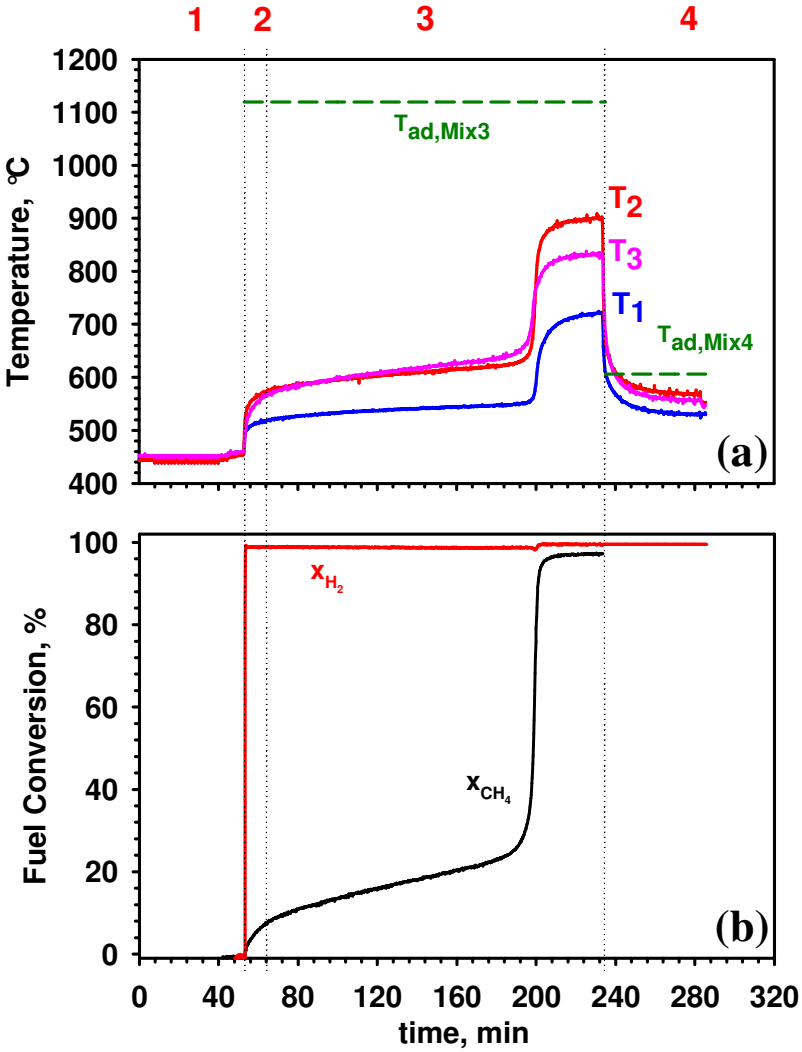

Figure 5.9 *CH_4-H_2 and H_2 combustion on C1PtLM900 in MQR at a total flow rate of 80slph (τ_C=49.6 $g_{cat}\cdot s\cdot Nl^{-1}$); Light-off of Mix3 at MIT=450°C. Section 1: No fuel is sent to the reactor: thermal profile for an O_2-N_2 mixture. Section 2: Ignition dynamics of CH_4-H_2 fuel. Section 3: Mix4 combustion (a) CH_4 (black line) and H_2 (red line) conversion measurements. (b) Thermal profile inside the monolith: T_1 (blue line), T_2 (red line), T_3 (pink line). Adiabatic temperature (T_{ad}) of Mix3 (green line) and Mix4 (cyan line).*

Moreover, it is worth noting that in the case of Mix3 ignition, in Zone 2 a maximum temperature is observed at the centre of the reactor. However, as the time passes, T_3 increases faster than T_2 until at t=75min, in the Zone 3, they are practically equal. Such a thermal profile is very different from that measured in Mix1 ignition where, in the same time region, temperature monotonically increases along the reactor length ($T_1<T_2<T_3$, see Figure 5.1). The particular thermal profile

detected in Mix3 ignition may be ascribed to un uncoupled proceeding of H_2 and CH_4 combustion. Specifically, hydrogen is totally burnt and shows a totally developed reaction front that, as it is expected, is placed at the centre of the reactor. On the contrary, in Zone 2 methane combustion proceeds very slowly in the time unit and is responsible for a gradual temperature increase at the exit of the reactor.

As it has been already found in the light-off of Mix1, after a certain induction time, needed to further increase the temperature inside the reactor, combustion "run-away" occurs in Zone 3 and a steep increase in the converted fuel is observed. Moreover, the available power is totally developed and, as a consequence, system temperature strongly raises approaching adiabatic conditions (see Figure 5.9a and b). In particular, approximately 200min are needed to observe a fully developed CH_4 light-off and under ignited conditions, T_1, T_2 and T_3 are respectively 735, 920 and 840°C.

Once Mix3 fuel mixture is ignited, Mix4 is fed to the combustor (see Zone 4 in Figure 5.9). As it is expected, H_2 is still totally converted (see Figure 5.9b). Moreover, in agreement with the lower overall heating value of hydrogen fuel mixture compared to that of Mix3, temperatures strongly decrease (Figure 5.9a). In particular, at the steady state T_1, T_2 and T_3 are respectively 529, 566 and 549°C. Mix4 fuel combustion actually produces the same thermal power developed by hydrogen in Mix3 combustion. As a consequence, the thermal profile resulting in Mix 4 combustion at a preheating temperature equals to Mix3 minimum ignition temperature, represents the effective MIT of methane in CH_4-H_2 mixture and it is consistent with the minimum ignition temperature of methane measured on the same catalyst and at the same flow rate in absence of hydrogen (see Figure 5.1). These results confirm the role of H_2 in thermally assisting CH_4 combustion thus decreasing its MIT. Moreover, temperatures detected in Mix4 combustion, i.e. the temperatures developed by the co-burnt hydrogen at Mix3 MIT, are higher than those found for CH_4 ignition (30°C higher, compare Zone 1 in Figure 5.1 and in Figure 5.9). This result can be explained keeping in mind that, with respect to CH_4 ignition in Mix1, in Mix3 case methane concentrations is lower; being partially substituted with H_2. Actually, because of the first order of methane combustion reaction, the conversion doesn't change with conversion and in the case of the minor equivalence ratio mixture, fixed the reactor temperature, combustion releases a lower power. As result, in order to ignite methane in Mix3 an higher reactor temperature is needed.

Mix4 combustion shows a maximum temperature at the centre of the reactor, as it is expected in a fully developed hydrogen ignition because of the reaction front closeness to the entrance. By comparing thermal profile detected in Mix4 combustion with that shown by Mix3 in the Zone 2, where the same amount of hydrogen is converted but most part methane remains unconverted, it is worth noting that T_2 and T_3 are lower in the first case. This result can be explained considering that

in Zone 2 methane present in Mix3 is partially converted thus determining a temperature rise at the exit of the reactor more significant than that observed in zone 4. On the contrary, the temperatures at the entrance of the catalytic reactor in Zone 4 and Zone 2 are practically the same thus revealing that the thermal level reached in such a reactor zone is ascribed exclusively to hydrogen combustion.

It is worth mentioning that maximum temperature detected in Mix4 combustion is only 40°C less than its adiabatic temperature. Such a difference is significantly lower if compared to those measured in methane combustion (Mix1 and Mix3) showing a greater adiabaticity of hydrogen combustion process. The latter, in fact, is sustained at lower temperatures at which the heat dissipation is very slow because of the decrease in the heat transfer driving force.

In Figure 5.10 Mix1 and Mix3 minimum ignition temperatures are reported as a function of the fuel mixtures total flow rate. In the case of methane combustion, Mix1, MIT is practically independent on the flow rate in the limit of the experimental errors. Consistently with the MIT reported previously in the case of Q_{TOT}=80slph, MIT is around 530°C in all the investigated cases. This result is ascribed to the dual effect of the flow rate on the fuel ignition. From one side by increasing the flow rate contact time decreases and as consequence fuel conversion decreases too. However, by increasing the flow rate the input power increases too thus allowing the development of an higher developed power. According to the experimental results, these two effects are balanced and increasing the flow rate the same preheating temperature is required for ignition despite of the lower fuel conversion.

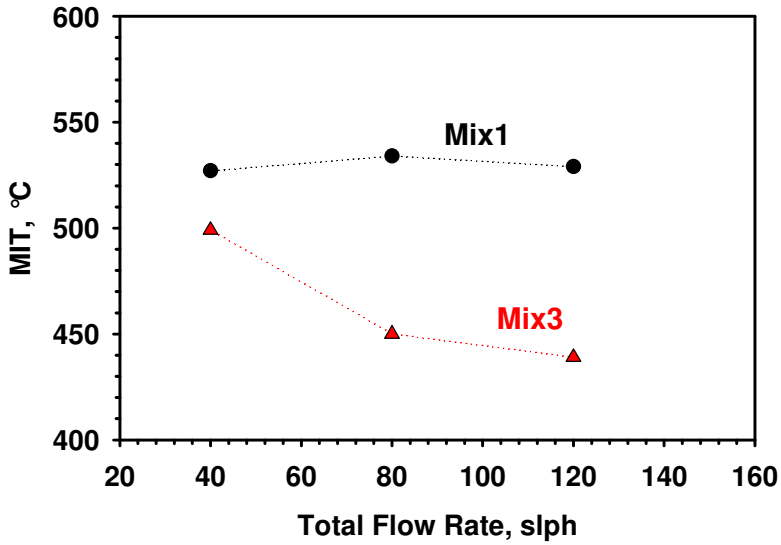

Figure 5.10 *MIT of CH_4 and CH_4-H_2 combustion on C1PtLM900 in MQR as a function of total gas flow rate; MIT for Mix3 (red triangles) and Mix1 (black circles).*

Differently from the case of methane combustion, MIT of CH_4-H_2 fuel strongly depends on the flow rate, as it is shown in Figure 5.10. In the case of Q_{TOT}=80slph, as already discussed, MIT is about 450°C (about 80°C lower than MIT of Mix1 fuel). By decreasing the total flow rate till to Q_{TOT}=40slph an increase in the MIT is observed and particularly MIT=500°C, only 30°C lower than MIT of Mix1 fuel. On the contrary, by increasing the flow rate up to 120slph a decrease in MIT is observed and particularly MIT=440°C, 90°C lower than MIT of Mix1 fuel. These results reveal that the promoting effect of hydrogen on methane ignition is more and more substantial with increasing the gas flow rate. Actually, by increasing the gas flow rate the input chemical potential increases too. Moreover, H_2 combustion is very fast at the investigated temperature (higher than 400°C) and H_2 conversion is practically not affected by the contact time being 100% at every gas flow rate. As a consequence by increasing the flow rate the thermal power released by H_2 increases too and a growing amount of power is available to ignite methane thus determining a decrease in fuel MIT.

Aside the effect on methane ignition temperature, hydrogen may enhance the stability of the hydrocarbon combustion.

In Figure 5.11 the quenching temperature measured in the case of Mix3 combustion is compared to that shown by Mix1 at different flow rates. Based on the obtained results, it is evident that QTs of Mix1 and Mix3 are practically the same independently on the gas flow rate. Eventual differences in Mix1 and Mix3 QTs, in fact, are ascribed to experimental error. As a consequence, hydrogen addiction to methane fuel mixture does not produce a relevant effect on limits of the autothermal combustion operation. This result reveals that combustion quenching is a phenomena ruled by the ratio between the developed power via combustion and the power lost. Independently by the presence of hydrogen, Mix1 and Mix3 are characterized by the same input power and as in both the cases fuel is totally converted the same power is released via combustion. Moreover, Mix1 and Mix3 combustion is performed in the same reactor and assuming that the two fuels determine approximately the same temperatures in the combustor the power lost is also the same. As a consequence, once the system is ignited and fuel is totally converted thus developing a fixed thermal power, quenching limits cannot depend on the nature of the fuel and hydrogen addiction to methane fuel doesn’t produce any promoting effect.

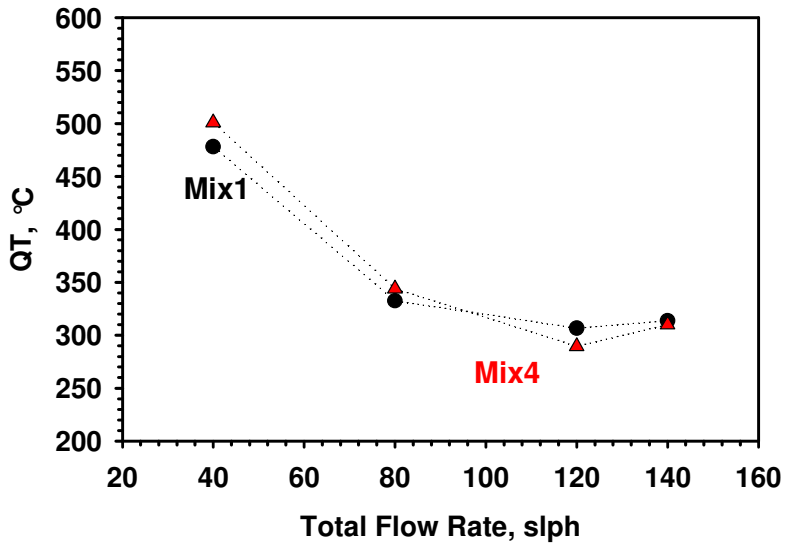

Figure 5.11 *Stability limit of CH_4 and CH_4-H_2 combustion on C1PtLM900 in MQR; QT for Mix1 (red triangles) and Mix3 (green squares) as a function of the flow rate.*

CHAPTER 6

DEVELOPMENT OF MICRO-POWER GENERATORS

Propane fueled catalytic microcombustors are integrated with thermoelectric elements (TEs) thus constituting micro-device for the electricity production.

The range of produced power is typically low (0÷1 Watt) and consistent with the demand of portable devices. This aspect makes the use of any external heating system dramatically heavy on the economy of the process because of an unacceptable decrease in the overall efficiency. However, the development of a efficient combustion system not subjected to an external preheating is not a trivial matter. As already discussed in the Chapters 1 and 5, microcombustion operation is strictly limited due to loss of stability either via extinction or blowout (Ronney, 2003, Norton and Vlachos, 2004, Kaisare and Vlachos, 2007, Kaisare et al., 2008). In confirming with that, the study on autothermal methane combustion in micro-structured reactors shown in the previous chapter has pointed out that a minimum preheating level is needed to sustain the process. Moreover, thermoelectric conversion system abstracts heat from combustion system further reducing the operating window of the device (Federici et al., 2006).

Based on these considerations, a great attention needs to be devoted to the development of an appropriate catalytic combustion system. Such an object is pursued by adopting specific solutions in terms of catalyst and reactor configuration, geometry and wall material such as to have a sufficiently large operating window of autothermal combustion.

As already discussed in the first chapter, an approach to enhance microcombustion stability is based on heat-recovery (Vican et al., 2002, Ronney, 2003, Kaisare and Vlachos, 2007, Kuo and Ronney, 2007, Kim et al., 2007, Ahn et al., 2007, Federici and Vlachos, 2008, Federici et al., 2009). This strategy is carried out in heat recirculation reactors in which the heat of combustion is recovered by means of a variable number of channels devoted to the counter current heat exchange. A n-pass combustor is ideally obtained by folding up a counter current heat recirculation reactor, as it is shown in Figure 6.1. Under adiabatic conditions, no heat is lost through the reactor wall and the power generated via combustion is equivalent to the sensible heat of the exhausted gas. On the contrary, under real conditions part of the combustion heat is transferred to the environment, as it is described by the equation Eq. VI.1, causing combustion quenching via extinction (Ronney, 2003,

Norton and Vlachos, 2004, Kaisare and Vlachos, 2007, Kaisare et al., 2008). An heat-recovery combustion system determines the decrease in the sensible power of the exhausted gas because of the heat transferred. As a consequence, assuming the same generated power, according to Eq. VI.1, the power that is allowed to remove from the system through the reactor wall before combustion quenching (i.e., the critical heat losses) increases thus improving process stability (Federici and Vlachos, 2008).

A thermoelectric system integrated with a combustor acts as a converter of the power lost through the reactor wall into electricity. Actually, TEs are characterized by a certain conversion efficiency, η_{TE} (see Eq. VI.2), that increases by increasing the temperature difference between their hot and cold junctions (see Chapter 1).

An efficient integration of the TEs to the combustor is not a trivial issues. Ideally, the electric power increases by increasing the heat losses of the combustor, consistently with the limits of combustion operation. Based on this consideration, an heat recirculation combustor is particularly suitable for such a kind of application because it involves an increase in the critical heat losses. Moreover, by increasing the number of gas passing till $n \rightarrow +\infty$ it is possible to maximize the transferred power to the TEs; particularly, the latter becomes ideally equal to the combustion power assuming that gas exits from the reactor at room temperature and no power is so lost through the exhausted.

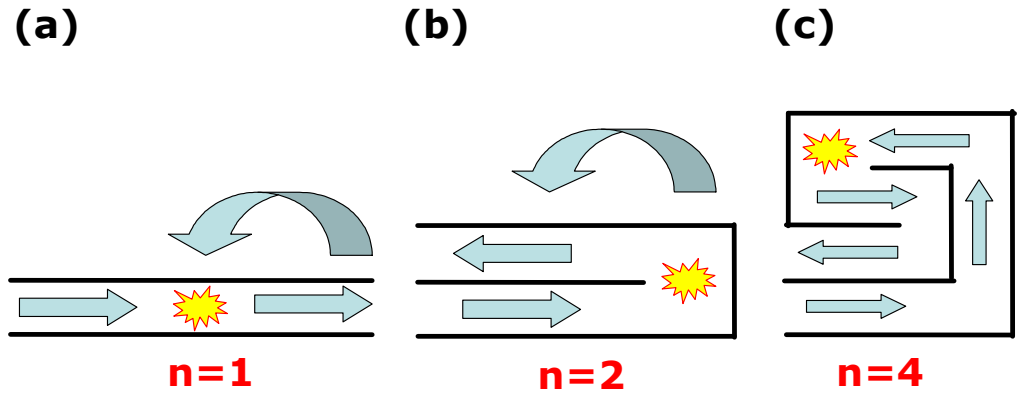

Figure 6.1 *Heat recirculation reactor. (a) 1-pass; (b) 2-pass; (c) 4-pass.*

$$\dot{Q}_{GEN} = \dot{Q}_{SENS} + \dot{Q}_{LOST} \qquad \textit{Eq. VI.1}$$

$$P_{EL} = \eta_{TE} \cdot \dot{Q}_{LOST} \qquad \textit{Eq. VI.2}$$

$\dot{Q}_{GEN}$ (Combustion power)

$\dot{Q}_{SENS}$ (Sensible power of the exhausted gas)

$\dot{Q}_{LOST}$ (Power transferred to the environment through reactor wall)

P_{EL} (Electric power)

η_{TE} (Thermoelectric efficiency)

Nevertheless, electric power does not depend only on the transferred power to TEs but also on the gas temperature. In order to have an adequate value of thermoelectric efficiency, in fact, sufficiently high temperature of the TEs hot junction (but compatible with the maximum working temperature allowed by TEs, see Chapter 1) is needed. Based on this, exhausted gas temperature and consequently the sensible power need to be sufficiently high.

Such a behaviour suggests a tradeoff regarding the number of gas passing in a heat recirculation channel. Particularly, it needs to be balanced in order to allow a sufficient heat flux through TEs (high number of passing is hoped for) but avoid too much lower temperature of the exhausted for the efficient conversion of thermal to electric power (low number of passing is hoped for).

In this study structured catalytic reactors, in the shape of honeycomb monoliths, have been prepared and tested for the autothermal combustion of propane/air mixtures using different catalyst active phases (Pt, $LaMnO_3$, and mixed phases) and monolith porosity (900 and 400 cpsi monoliths). The role of heat-recirculation on the operating window of self-sustained combustion is investigated for a 2-pass quartz reactor; the simpler geometry of such a system compared to that of a swiss-roll reactor (Kuo and Ronney, 2007, Kim et al., 2007, see Chapter 1) enables to obtain fundamental understanding of the effect of the main reactor parameters, the catalyst and the effect of wall conductivity on instability mode (extinction and blowout). In particular, concerning with the latter aspect, no direct experimental validation still exists of an effective improvement of the combustion stability only in the limit of low conductivity materials (Kuo and Ronney, 2007, Kaisare and Vlachos, 2007, Federici and Vlachos 2008, Federici et al., 2009, see Chapter 1 for details), despite the important ramifications for microcombustion.

The main issues involved in the integration of the catalytic combustor with thermoelectric elements (TEs) are successively discussed. In particular, thermal management of the device is studied in order to make as efficient as possible such a coupling. At this proposal, the performances of the generator are evaluated in the case TEs are integrated with both a 2 and 3 pass combustor.

6.1 Operating conditions

R1Pt400, R0.5Pt900, R1Pt900, R0.5PtLM900, R0.5PtLM400 and RLM900 catalysts are tested in HRR and NRR reactors (see 2.1.5 and 3.1.4 paragraphs for details).

As already discussed in the previous chapter, in order to achieve autothermal conditions an high overall heating value fuel is required. In Table VI.1 the specifics of the considered fuel mixtures are reported. In particular, the maximum investigated equivalence ratio is Φ~0.5 and corresponds to a maximum propane concentration not higher than fuel LFL of 2.2%; moreover, such a condition involves an adiabatic temperature rise of ~1250 °C. Flow rates vary from 36 to 150slph; considering the number of channels and the gap height of the tested monoliths, the gas velocity (based on inlet conditions) inside each single channel varies from 1.4 to 5.1 m/s in the case of 400 cpsi and from 0.8 to 2.9 m/s in the case of 900 cpsi monoliths, resulting in a minimum residence time of 10 ms (inlet conditions).

Table VI.1 *Operating conditions adopted in propane/air autothermal combustion tests. Composition, equivalent ratio, heating value, total flow rate and input power of fuel mixture.*

C_3H_8, %	2.2÷0.9
Air, %	99.1÷97.8
Φ	0.54÷0.22
Heating value, KJ·Nl^{-1}	1.9÷0.8
Q_{TOT}	150÷42
Input Power, W	77.1÷8.9

Before a reaction test, each catalyst is reduced for 2 hours at 500 °C in a mixture of hydrogen (99.99%) and helium (99.998%).

After reduction of the catalyst and system cooling in helium, the reacting mixture is fed to the reactor. The combustor is then electrically heated until ignition of the reacting mixture occurs, indicated by a steep increase in the temperature measured at the exit of the catalyst module, whereupon the heat supply is turned off, and the reactor is left running autothermally.

In this study only the high conversion branch will be shown even if an ignition temperature range is provided. In particular, Pt/γ-Al_2O_3 catalysts show the lowest ignition temperature of ~300 °C, whereas for $LaMnO_3$/γ-Al_2O_3 a temperature as high as 550 °C is needed for light-off. The

addition of the same amount of Pt (as in Pt/γ-Al_2O_3) to $LaMnO_3$/γ-Al_2O_3 results in an intermediate ignition temperature of ~450 °C.

Self-sustained (autothermal) combustion was followed by progressively decreasing the equivalence ratio of the fuel mixture while keeping the total flow rate constant, until the process quenched at a critical equivalent ratio Φ_c. Φ_c is a very good metric of reactor stability for various configurations studied herein. In the following graphs, the quenching point, associated with a drop in temperature and conversion, is indicated with vertical arrows.

The catalyst has been pre-treated in a combustion environment up to 850 °C for approximately 6 h. Such a treatment allows stabilization of the catalyst properties. Good reproducibility was found for each single experiment as proved by the lack of any relevant change in the measured values of Φc (within experimental error). This finding is consistent with the lack of volatilization indicated by comparing the Pt loading of fresh and spent catalysts (see discussion above). In addition, no apparent change in activity was observed after the catalyst was used for several hours (approximately 100 h), as well as in testing different catalysts with the same nominal properties (experiments with different monoliths were conducted at least twice).

The temperature inside the central channel of the monoliths is measured via two K thermocouples (0.5 mm thick). Thermocouples are set close to the inlet (0.5 cm from the entrance section of gases) and the outlet (0.5 cm from the exit) of the structured catalyst. The position of thermocouples inside the catalytic reactor is indicated in Figure 3.5 (see chapter 3.0). The thermocouples are inserted inside the monolith in order to ensure that no outside temperatures are obtained due to some uncertainty in exactly positioning the thermocouples. In addition, with the thermocouples being inside the channels, it is avoided temperature measurements that are affected from radiation. The temperatures of the external quartz tube and the exit gas are also measured in order to have a rough idea of the reactor thermal profile. The reactor is insulated with Pyrogel (Aspen Aerogels).

A thermoelectric module is integrated with a catalytic microcombustor according to two different configurations. In particular, 2pTER and 3pTER electricity generators are studied considering R1Pt900 catalyst. In 2pTER a thermoelectric module, properly supported on an aluminum tube, is integrated with HRR; in 3pTER thermoelectric module is directly integrated with a 3-pass combustor whose external wall is constituted by an aluminum tube (see Chapter 3 for details). To ensure a good thermal contact between the elements of the generator, the entire microcombustor/thermoelectric stack is placed under compressive force using a conventional C-clamp (see Chapter 3 for details). The beneficial effect of such a solution on thermoelectric performances was shown by Federici et al. (2006).

As discussed in the Chapters 1 and 3, according to the Seebeck effect a thermoelectric device produces an electrical potential obtained multiplying its Seebeck coefficient by the thermal gradient at which it is subjected. However, a thermoelectric module typically exhibits an internal resistance R_{int}. In the case of HZ-2 (see Chapter 3) a value of R_{int}=4Ω is supplied by Hi-Z Technology, Inc. even if a value of R_{int}=5.3Ω is experimentally measured by Federici et al. (2006). In order to test the performances of thermoelectric it is coupled in series with a resistive device, constituted by a rheostat. The value of the resistance of the load, R_L, is changed perceptually from 0 to 100%. A voltmeter and ammeter are employed to measure respectively the potential difference, ΔV, at the ends of the load and electric current in the circuit, i. Power adsorbed by the load, P_{EL}, is thus derived multiplying i by ΔV; moreover, R_L is obtained too by dividing ΔV by i. The electric power ideally exhibits a maximum in correspondence with R_L=R_{int}=4 Ω; eventual discrepancies are due to the variation of the internal resistance of the device with the thermoelectric working temperature. Still, the measurements of the electrical potential at the ends of the rheostat allows to estimate the Seebeck coefficient of the device (see Chapter 3).

Performance of 2pTER and 3pTER generators are shown in terms of current-voltage characteristic and P_{EL} with varying the total flow rate and the equivalence ratio of the fuel mixtures. Moreover, temperature is measured inside the catalyst and in correspondence with the both the hot and the cold junction of thermoelectric module.

Unless otherwise noted, combustion tests are carried out by considering thermal shields, upstream and downstream of the catalytic monolith.

6.2 Operating limits of self sustained C_3H_8 combustion

6.2.1 Effect of heat recirculation

The effect of heat recirculation on propane combustion stability has been studied for the R1Pt400 catalyst (see Table II.4 for details). Figure 6.2 shows the temperatures near the inlet (T_{C1}) and outlet (T_{C2}) of the catalyst as functions of the equivalence ratio for the NRR for three flow rates (indicated) along with the critical equivalence ratio (arrows).

Due to heat losses, the temperatures are much lower than the adiabatic temperature (~1250 °C at Φ = 0.5 and 1000 °C at Φ = 0.4). It is interesting that on increasing the flow rate, different behavior is observed upstream and downstream of the monolith (ca. T_{C1} and T_{C2}). The temperature near the catalyst exit (T_{C2}), shown in Figure 6.2b, is fairly constant with changing equivalence ratio, and increases with increasing flow rate. The latter behavior is caused by the increased power input to the reactor in comparison to heat losses. The temperature near the inlet of the catalyst (T_{C1}), shown in Figure 6.2a, does not significantly change with flow rate for high equivalence ratios (near Φ ≈

0.5), probably because fuel ignition starts very close to the entrance. Actually, the T_{C1} thermocouple corresponds to the pre-heating zone of the reactor whose temperature is significantly affected by the heat transferred from the catalyst (mainly by radiation at relatively high temperatures).

At lower equivalent ratios ($\Phi < 0.5$) (i.e., approaching the quenching point), T_{C1} decreases with increasing flow rate, probably due to a decrease the residence time which causes a drift of the reaction zone downstream. In addition, a higher flow velocity decreases the length for gas pre-heating, which is necessary for light-off. The result is ignition further away from the entrance. In fact, an inversion in the position of the maximum temperature is observed when varying the flow-rate: at 48 and 78slph, the catalyst entrance is warmer than the exit, whereas at 108slph the opposite is true for all Φs.

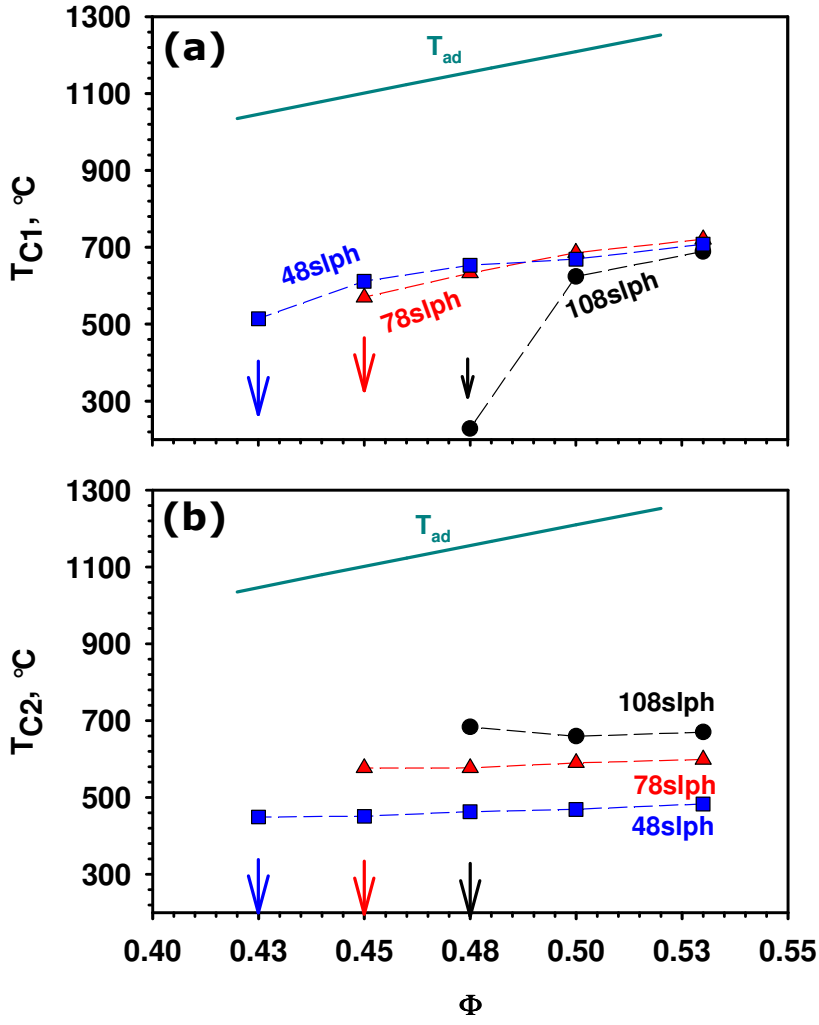

Figure 6.2 *Non-heat recirculation reactor (NRR): temperatures (a) at the inlet of the catalytic monolith (T_{C1}) and (b) at the exit of the catalytic monolith (T_{C2}) and quenching (blowout) points (arrows) at different flow rates (48, 78 and 108 slph) using the R1Pt400 catalyst. Points are experimental data and lines just guide the eye.*

With decreasing equivalence ratio, the temperature at the inlet of the catalyst T_{C1} drops strongly at all flow rates and more so at faster flows (108slph). In contrast, Φ does not significantly affect the exit temperature of the catalyst. The weak variability of T_{C2}, while the entrance zone is getting colder with decreasing Φ, is rationalized with a shift of the hottest catalytic zone downstream in the reactor.

At higher flow rates this phenomenon is significant and steady state exhibits a very cold inlet zone: in particular, for the highest investigated flow rate (108slph), upon decreasing Φ from 0.5 to 0.48, the exit temperature increases, whereas the entrance temperature drops abruptly (from more than 620 to 230 °C). This result reveals also that when a change in a parameter (in this case, Φ) produces a very cold inlet zone, the reactor becomes less stable, as indicated with the high value of Φ_c (0.48 at 108slph).

The critical equivalence ratio varies between 0.43 (for lower flow rates) and 0.48 (for higher flow rates). The overall dependence on (the rather small variation of) flow rate is rather small. What is interesting is that self-sustained combustion becomes narrower with increasing flow rate. One can conclude that in the NRR, an increase in the flow rate decreases combustion stability, despite of the higher power input. This is because of less preheating of the incoming gas with an associated lower contact time of the reactants with the high temperature reactor zone. Based on these considerations, loss in stability in the NRR is caused by incomplete fuel conversion and the system quenches via blowout (Kaisare et al. 2008).

Figure 6.3 reports the results of combustion in the HRR. The data shows that the critical equivalence ratio is significantly lower compared to that of the NRR and lies around 0.30-0.35. The effect of flow-rate on Φ_c is reversed compared to the NRR. In particular, Φ_c appears independent of flow rate at high flow rates and is lower for 108slph than for 48slph. Hence, autothermal operation expands with increasing flow rate.

Temperature measurements in Figure 6.3 reveal, similarly to the NRR, much lower temperatures than adiabatic reactor temperature. However, unlike the NRR, an increase in the flow rate increases both T_{C1} and T_{C2}, probably due to the increased adiabaticity of the reactor under experimental conditions that result in complete propane conversion (see below). Moreover, in the HRR, T_{C1} is higher than T_{C2}, i.e., the maximum temperature of the catalyst is closer to the inlet under all conditions investigated. As explained later, this is a result of heat recirculation that allows stabilization of the reaction front further upstream, creating a wider operating window for self-sustained combustion.

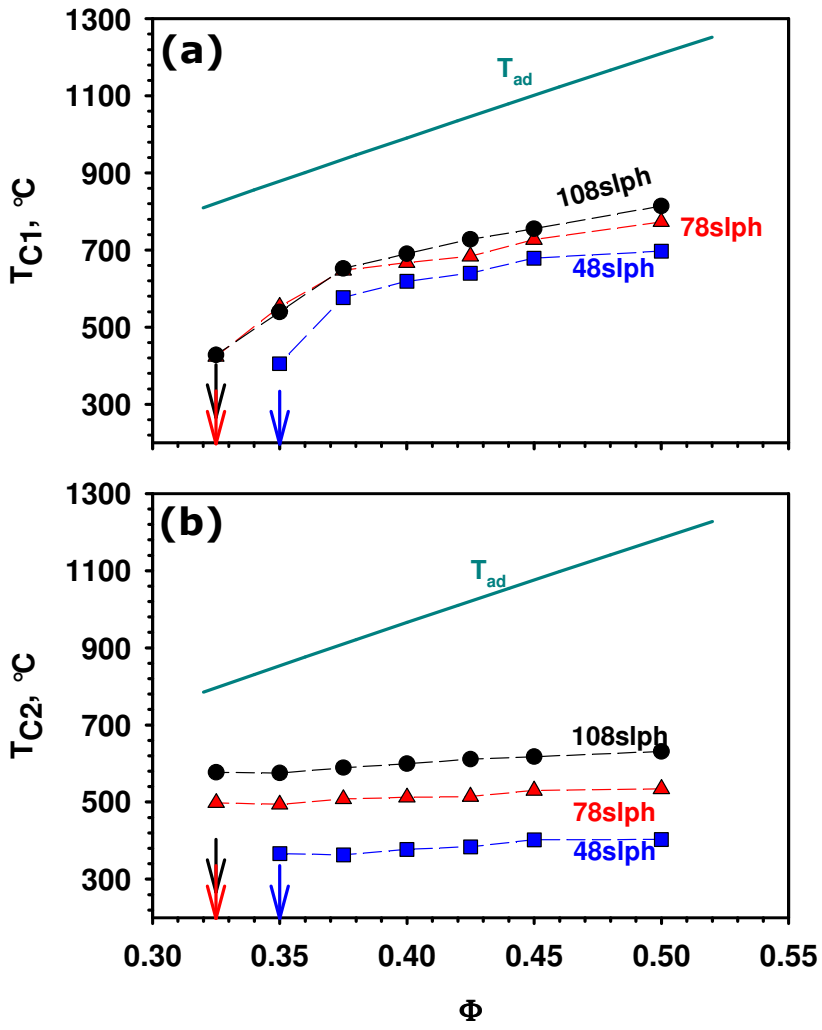

Figure 6.3 *Heat recirculation reactor (HRR): temperatures (a) near the inlet of the catalytic monolith (T_{C1}) and (b) the exit of the catalytic monolith (T_{C2}) along with extinction points (arrows) at different flow rates using the R1Pt400 catalyst. Points are experimental data and lines just guide the eye.*

Like the NRR, the reaction front downstream when decreasing the equivalence ratio: the near entrance temperature T_{C1} (Figure 6.3a) experiences a strong drop near quenching; for 78slph, for example, the T_{C1}'s drop is ~290 °C when varying Φ from 0.5 to quenching. In contrast, the temperature at the exit of the catalyst (T_{C2} in Figure 6.3b) does not significantly change with equivalence ratio: for 78slph, T_{C2}'s drop is only ~40°C.

In the HRR, increasing the total flow rate or decreasing the equivalence ratio of the fuel/air mixture does not affect the total fuel conversion. Figure 6.4 shows the propane conversion as a function of flow rate (Figure 6.4a) and equivalence ratio (Figure 6.4b) in autothermal combustion in the HRR for the R0.5PtLM400 catalyst. The results show that even with less amount of active catalyst, the fuel is completely converted for an equivalence ratio equal to 0.5, and its conversion

decreases only slightly with decreasing flow rate, remaining higher than 98% in all cases (Figure 6.4a). Figure 6.4a also shows that, in agreement with results discussed above for higher Pt content, the increase in flow rate is accompanied with an increase in the near exit temperature. Decreasing the flow rate below 36slph results in quenching as evidenced by a strong drop in both temperature and fuel conversion. Despite the longer residence time, the decrease of the flow rate is detrimental for the process because of the low power input compared to heat losses through the reactor wall (the latter are essentially determined from the maximum temperature reached by the catalyst, which changes slightly with varying flow rate). This particular instability mode occurs at nearly complete fuel conversion and, according to published simulations, is described as extinction (Kaisare et al., 2008).

When decreasing the equivalence ratio of the fuel/air mixture (Figure 6.4b), a more pronounced decrease of fuel conversion occurs especially at lower flow rates. The changes in the critical equivalence ratio are smaller than the composition increments employed here for a change to be detected accurately. The lower critical equivalence ratio with increasing Pt content (compare Figs. 6.3 and 6.4) indicates kinetic limitations near extinction.

The experimental results presented above demonstrate a different quenching mode in the HRR and NRR. In particular, blowout occurs in the NRR with increasing flow rate due to insufficient preheating, reaction front shift toward the exit, and a low contact time in the hot temperature zone. Under these conditions, most of the heat generated by combustion is lost through the exhaust gas. In the HRR, the recirculation channel preheats the incoming reactants. As a result, complete fuel conversion occurs even at higher flow rates. These experimental results underscore for the first time that heat recirculation may change the quenching mode from blowout (NRR) to extinction (HRR).

The above analysis is further confirmed by comparing the HRR and NRR results in Figure 6.5. As expected, the reaction zone in the HRR is upstream as evidenced from the higher inlet temperature (T_{C1}) and the lower exit temperature (T_{C2}) compared to those of the NRR. Heat recirculation allows stabilization of combustion upstream, prevents blowout, and allows self-sustained combustion of fuel leaner mixtures, as evidenced with the much lower Φ_C of the HRR.

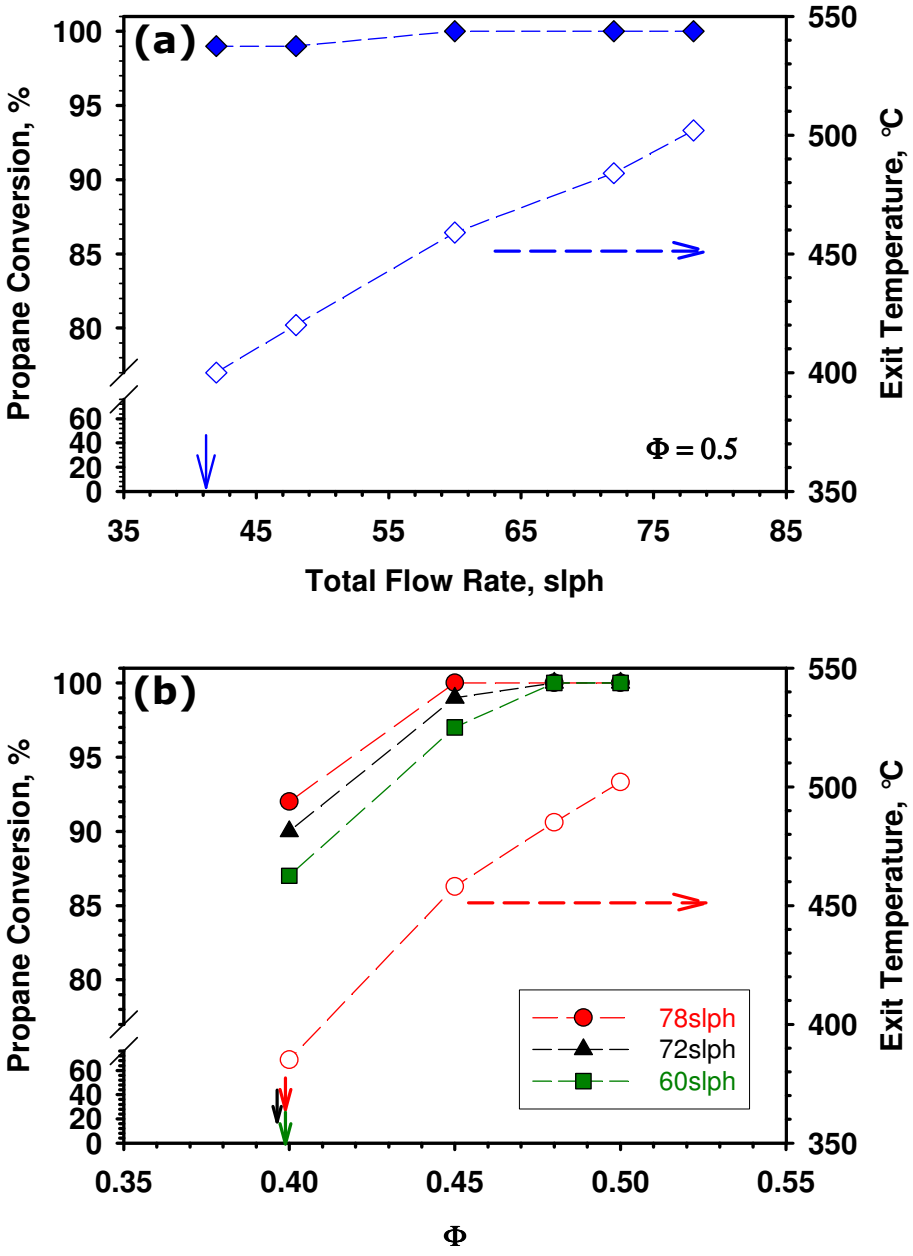

Figure 6.4 *Heat recirculation reactor (HRR) using the R0.5PtLM400 catalyst. Propane conversion (left axis) and near exit gas temperature (right axis) vs. (a) flow rate for an equivalence ratio of 0.5 and (b) equivalence ratio at different flow rates.*

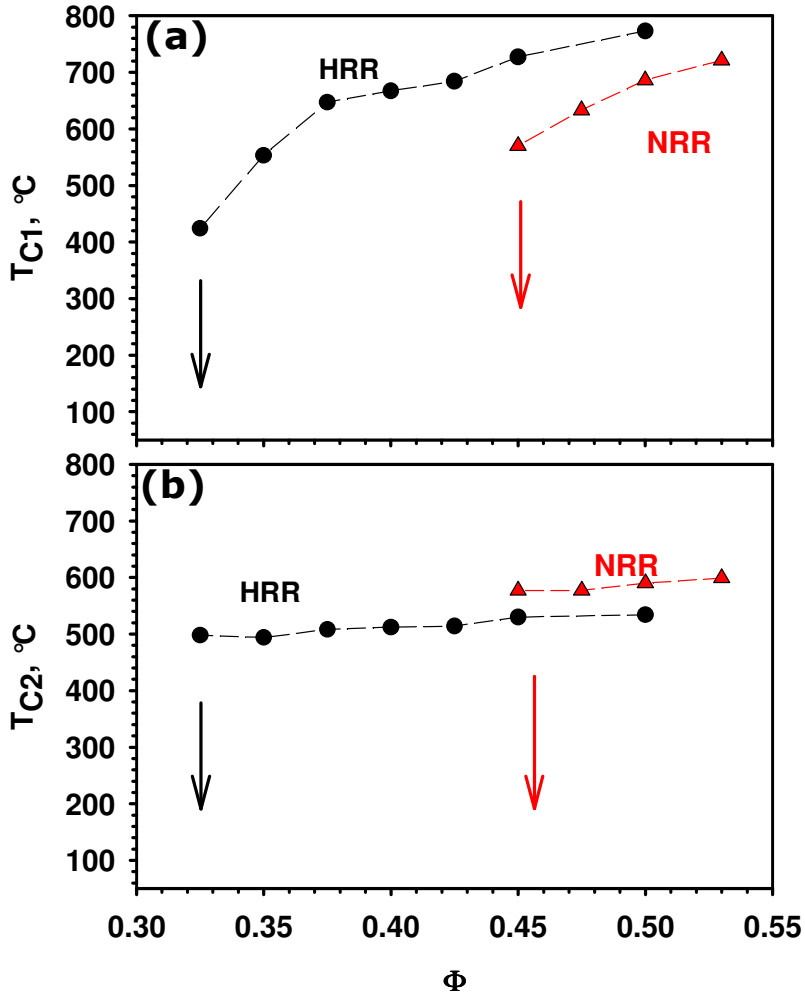

Figure 6.5 *Comparison between the heat recirculation reactor (HRR, black filled circles) and no-recirculation reactor (NRR, red filled triangles) using the R1Pt400 catalyst: (a) temperatures at the inlet (T_{C1}) and (b) at the exit of the catalytic monolith (T_{C2}) and extinction points at 78slph.*

6.2.2 Effect of thermal shields

Thermal shields are commonly used in high temperature combustion and partial oxidation to prevent heat losses via radiation and flashback (Cimino et al., 2001, Henning and Schmidt, 2002). A less obvious and discussed effect of thermal shields is that they increase the reactor exposed surface and, consequently, the heat losses. In microsystems, this enhanced surface area has a detrimental role in stability, at least of single channels (Kaisare and Vlachos, 2007). It is therefore unclear at what reactor scale thermal shields actually benefit reactor stability. In addition, the question raised is whether thermal shields are of any value in the HRR given that the recirculating channels behave effectively as heat traps.

In order to understand the effect of thermal shields on combustion stability, experiments were repeated by removing the shields (blank monoliths placed upstream and downstream the catalyst).

Figure 6.6 and Figure 6.7 compare respectively the HRR and NRR and results in terms of the measured temperatures (at the same position in all cases).

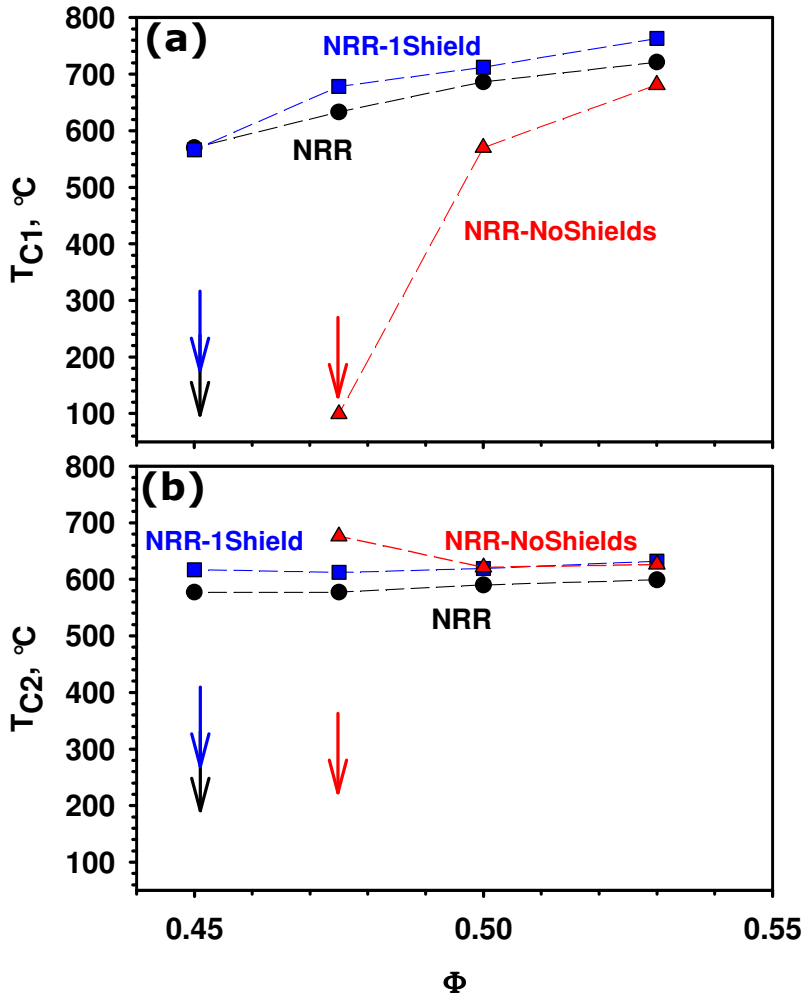

Figure 6.6 *Comparison between no-recirculation reactor (NRR) with and without thermal shields using the R1PT400 catalyst: (a) temperatures at the inlet (T_{C1}) and (b) at the exit of the catalytic monolith (T_{C2}) and extinction points at 78slph. NRR with both thermal shields (black filled circles); NRR with no shields (red filled triangles); NRR with only one thermal shield downstream (blue filled squares).*

Removing both thermal shields is detrimental for combustion stability in the NRR (filled black circles versus filled red triangles, see Figure 6.6). The critical equivalence ratio increases from approximately 0.45 (with both shields) to 0.48 (absence of shields). The higher inlet temperature (Figure 6.6a) and lower outlet temperature (Figure 6.6b) in the presence of shields suggests a significant role of the shields in allowing stabilization of the reaction front further upstream. Thermal shields upstream and downstream of the reactor may have multiple roles. A blank

monolith upstream of the catalyst could increase the pre-heating length improving, as a consequence, combustion efficiency and stability. At the same time, a blank monolith downstream of the catalyst can trap heat decreasing the heat losses through the exhaust gas. Both these effects could affect combustion. In order to understand which of the two shields prevails, combustion tests have been carried out by removing only one shield (upstream). The results of Figure 6.6a (filled blue squares) show that both the critical equivalence ratio and the temperatures are not significantly affected by the presence of only the blank monolith downstream of the catalyst: the slightly larger (up to ~50 °C) temperature lies within the range of the experimental error. On the basis of this result, one may conclude that the role of the thermal shields in improving the stability of combustion is to trap the heat, mainly by decreasing the sensible heat losses through the exit gas.

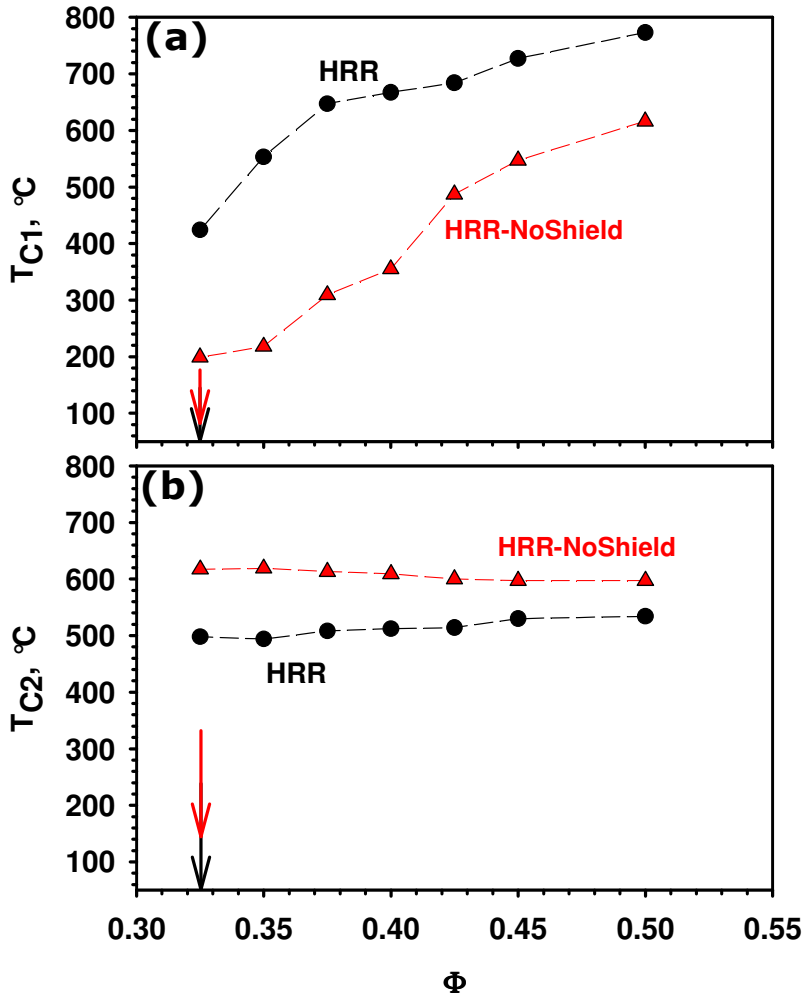

Figure 6.7 *Comparison between the heat recirculation reactor (HRR) with and without thermal shields using the R1Pt400 catalyst: (a) temperatures at the inlet (T_{C1}) and (b) at the exit of the catalytic monolith (T_{C2}) and extinction points at 78slph. HRR with both thermal shields (black filled circles); HRR with no shields (red filled triangles).*

For the HRR, shield removal shifts the reaction front downstream, as demonstrated from the higher entrance (Figure 6.7a) and lower exit temperatures (Figure 6.7b) in the presence of both thermal shields. Unlike the NRR, removal of both blank monoliths in the HRR does not affect the critical equivalence ratio (within the composition increment taken). This result is consistent with the role of the thermal shields previously described: in the HRR, most of the sensible heat is recovered through the recirculation channels, minimizing the role of shields in combustion stability.

6.2.3 Effect of the monolith cell density

The effect of monolith cell density on HRR stability has been investigated using the R1Pt catalysts. In particular 900 and 400 cpsi monoliths have been compared with the same overall burner dimensions. Figure 6.8 compares the near entrance temperatures of the two catalysts at autothermal conditions. The R1Pt900 (900 cpsi) substrate shows a critical equivalence ratio much smaller than that of the R1Pt400 (0.22 vs. 0.32) under the same experimental conditions. To further confirm the beneficial effect on combustion stability achieved with the higher cell density monolith, it is worth mentioning that is not possible to stabilize combustion in the case of $LaMnO_3/\gamma\text{-}Al_2O_3$ catalysts with 400 cpsi substrates while this is possible with 900 cpsi substrates (data not shown).

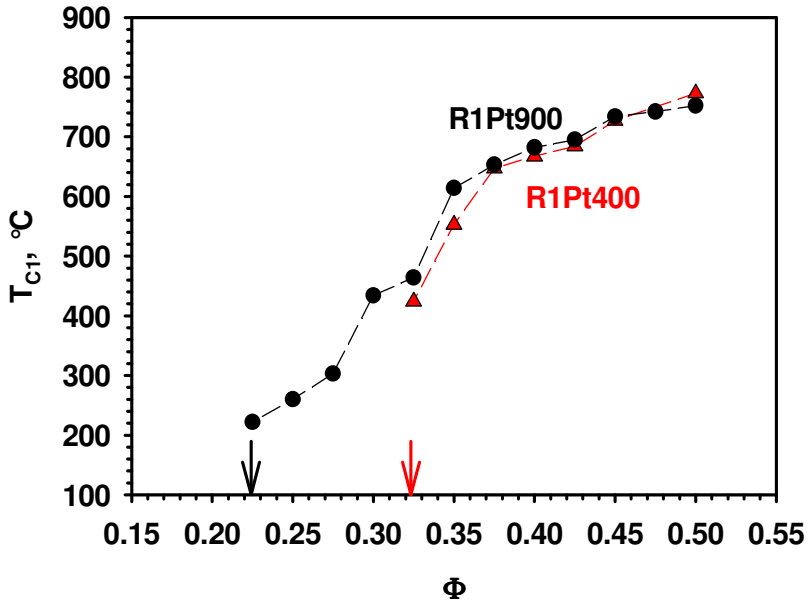

Figure 6.8 *Effect of monolith porosity on heat recirculation reactor (HRR) combustion stability in the case of R1Pt catalysts: temperature measurements at the inlet of the catalyst and extinction points at 78slph. R1Pt900 (black circles); R1Pt400 (red triangles).*

The reason for the enhanced stability could be related to the larger amount of catalyst deposited and/or the faster mass transfer due to narrower channels. It is interesting to note that the higher the

monolith density is, the lower the temperature near quenching is (e.g., T_{C1} ~200 °C vs. ~400°C for 900 and 400 cpsi monoliths, respectively). This finding may be important for low temperatures applications, e.g., integration of microburners with thermoelectrics.

6.2.4 Effect of active phase

Figure 6.9 shows the effect of different catalysts (R1Pt900, R0.5Pt900, R0.5PtLM900 and RLM900) on performance.

Pt/γ-Al_2O_3 catalysts (R1Pt900 and R0.5Pt900) exhibit the lowest Φ_C and the platinum loading affects significantly the operating range of autothermal propane/air combustion. By approximately doubling the noble metal loading on alumina, the critical equivalence ratio decreases from ~0.27 to 0.22. The inlet temperature (T_{C1}, in Figure 6.9) is approximately the same for equivalence ratios higher than 0.35, where complete fuel conversion is expected for both systems, regardless of the amount of Pt. For an equivalence ratio lower than 0.35, lower temperatures are observed in the 0.5-Pt-900 catalysts. This evidence could be attributed to the lower activity of the R0.5Pt900 catalyst compared to that of the R1Pt900, resulting in a lower generated power at the same equivalence ratio and consequently in a higher Φ_C.

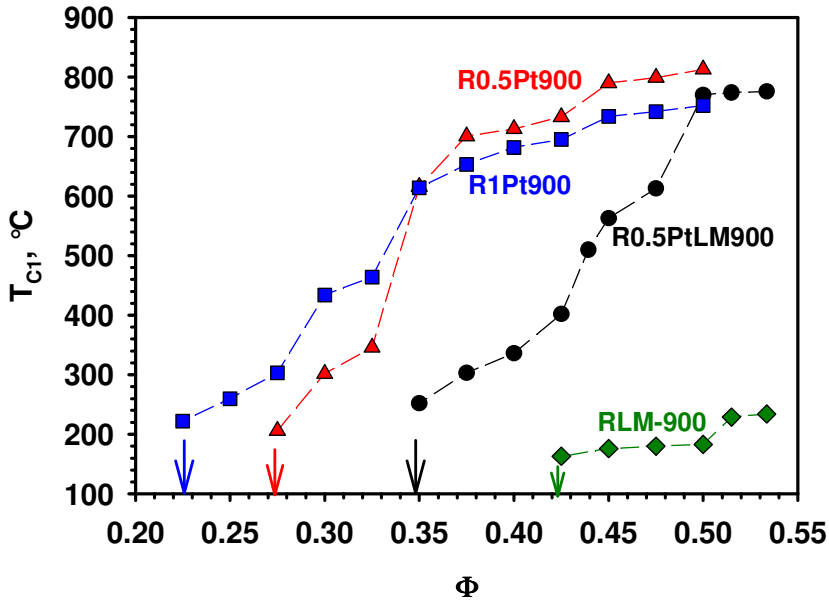

Figure 6.9 *Effect of the active phase on the heat recirculation reactor (HRR) combustion stability: temperatures at the inlet of the catalyst and extinction points at 78slph. RLM900 (green diamonds); R0.5PtLM900 (black circles); R1Pt900 (blue squares); R0.5Pt900 (red triangles).*

The RLM900 catalyst (green diamonds in Figure 6.9) results in lower reactor stability (critical equivalence ratio is ~0.42, much higher than that on Pt/γ-Al_2O_3 systems). Furthermore, for all

equivalence ratios, the inlet catalyst temperature is also significantly lower (for Φ = 0.5, by ~450°C) than that on Pt/γ-Al_2O_3. The lower intrinsic activity of perovskite leads to stabilization of the reaction zone much closer to the exit, leading a very low inlet temperature.

Figure 6.10 (black open circles) shows the thermal profile for the perovskite catalyst. T_{C1} is compared with the other temperature measurements performed on the external quartz tube of the HRR. In particular, the very high temperature measured at the end of the reactor, at the turn of the gas flow direction, highlights that the hottest zone for RLM900 is near the exit.

The addition of ~0.6 wt% Pt to perovskite (R0.5PtLM900, black circles in Figure 6.9) enhances the operating range of autothermal propane combustion compared to the RLM900 catalyst. In particular, the critical equivalence ratio decreases from 0.42 (un-promoted perovskite) to 0.35 (Pt-containing perovskite). Pt addition to the perovskite strongly increases T_{C1}, resulting in the reaction front moving upstream and, consequently, in a higher intrinsic activity. Figure 6.10 compares the HRR thermal profile for R0.5PtLM900 catalyst (open blue squares) and RLM900 (open green circles), providing further evidence of the change in the location of the reaction front.

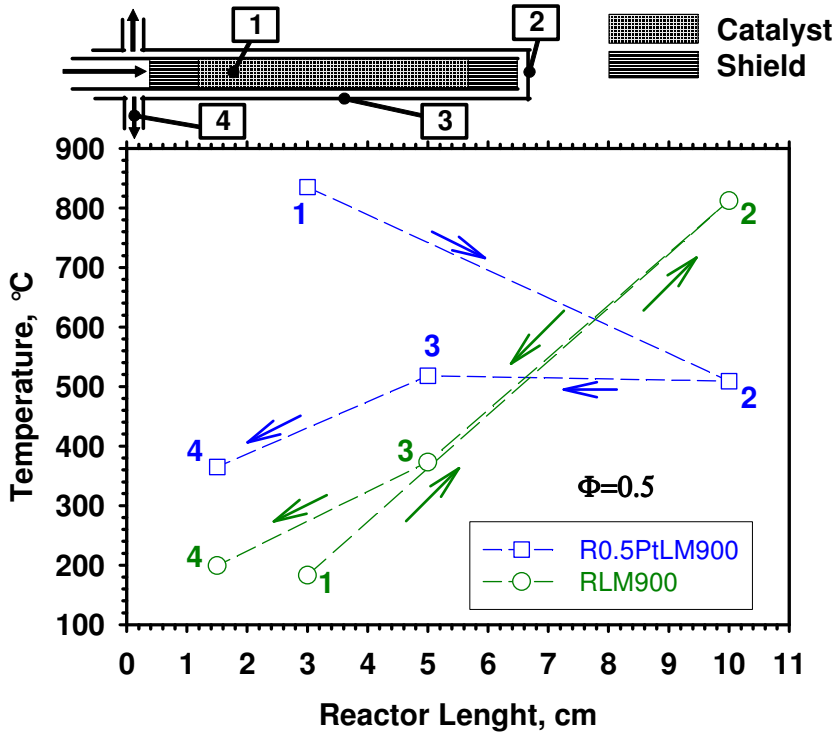

Figure 6.10 *Thermal profile along the heat recirculation reactor (HRR): comparison between RLM900 (green circles) and R0.5PtLM-900 (blue squares) at a total flow rate of 78slph and Φ=0.5. Temperature at the inlet of the catalyst (position 1), on external quartz tube at the turn of the gas flow direction (position 2), on external quartz tube at the catalyst (position 3), and the exit of the HRR (position 4).*

The maximum temperature in the R0.5PtLM900 catalyst, which is approximately the same in the promoted and un-promoted perovskites, has moved upstream. Furthermore, for an equivalence ratio ~0.5, the inlet temperature of the R0.5PtLM900 catalyst is comparable to that of Pt/γ-Al_2O_3 (Figure 6.9), resulting from complete conversion for all the Pt-based catalysts. For an equivalence ratio lower than 0.5, Pt-$LaMnO_3$ catalyst temperatures are lower than those of Pt/γ-Al_2O_3 with the same platinum loading, consistent with the larger Φ_C of the Pt-$LaMnO_3$ catalysts. Pt exhibits lower activity when dispersed on the perovskite matrix compared to alumina. Such a behaviour of the mixed phase catalyst has already been observed in the case of hydrogen oxidation (see Chapter 4) and was traced back to the different dispersion or migration of Pt inside the perovskite structure, effectively reducing the amount of noble metal available for reaction.

Finally, it is worth mentioning that for all the tested 900 cpsi catalysts, despite different values of Φ_C, the near entrance temperature before quenching is ~200 °C. This temperature may indicate a thermal threshold for self-sustainability of the process resulting from the balance of thermal power generated and heat loss through the reactor wall.

6.3 Performances of electricity generators

2pTER and 3pTER are tested using R1Pt900. As already reported in the Chapter 3, in these experiments thermal shields are not employed.

In the next two paragraphs the results are presented and discussed.

6.3.1 2pTER performances

In Figures 6.11, 6.12, 6.13 and 6.15 performances of propane fueled 2pTER generator are shown with varying the total flow rate. A fuel mixture is sent to the device with an equivalent ratio equal to 0.5 and a total flow rate varying in the range of Q_{TOT}=80÷150slph.

Once ignited fuel is efficiently converted in the reactor and high temperatures are sustained by the system (see Figure 6.11a). Due to the heat losses temperature level inside the catalyst is lower than that under adiabatic conditions. T_{C1} measured in the case of 2pTER is compared with that exhibited by HRR using R1Pt400. Even if the latter has been tested under different experimental conditions (a 400cpsi monolith is employed and thermal shields are used) by such a comparison it is possible to estimate the role on the thermal profile of thermoelectric integration with the combustor. In order to validate the above-mentioned affirmation it is worth noting that at Φ=0.5 (i.e., far from combustion quenching) thermal profile inside the reactor is not affected by the porosity of the monolith (see Figure 6.8). T_{C1} detected in 2pTER is significantly lower than that measured in the case of HRR (see Figure 6.11a). Considering a Q_{TOT}=78slph T_{C1} is 773 and 742°C respectively in

the case of HRR and 2pTER reactor, while at Q_{TOT}=108slph T_{C1} is respectively 814 and 755°C. Such a result reveals the inevitable enhancement in the heat losses shown by such a coupling. Still, analyzing T_{C1} trend in the case of 2pTER it is evident the presence of a maximum. For 80slph<Q_{TOT}<90slph, in fact, T_{C1} increases with the total flow rate while such a tendency is inverted at Q_{TOT}>90slph. This behaviour is due to the twofold effect of the flow rate that provides more input power but at the same time involves a decrease in the residence time (see Chapter 5). Specifically, in a range of low gas velocity, such as to guarantee a sufficient contact time, a temperature level enhancement is observed by increasing flow rate; nevertheless, in a range of gas velocity not more compatible with the total fuel conversion, a shift of the reaction zone towards the exit is observed thus causing a cooling of the reactor entrance. The presence of a maximum in T_{C1} exhibited by 2pTER with varying Q_{TOT} is consistent with the results obtained in the combustion test on MQR using C1PtLM900 catalyst (see Figure 5.4) and suggests a changing in the dynamics of combustion quenching from extinction (at low flow rate) to blowout (at high flow rate, Kaisare and Vlachos, 2007, Kaisare et al., 2008). On the contrary, the same dependence of T_{C1} didn't result in combustion tests on HRR (see Figure 6.3 and Figure 6.11a). Specifically, the inlet temperature monotonically increased with the total flow rare and, differently from tests on 2pTER, a maximum wasn't observed. Actually, HRR behaviour is consistent with a combustion quenching via extinction in the whole field of Q_{TOT} investigated. Such a result reveals that the integration of a thermoelectric module with HRR has caused a changing in the dynamics of combustion quenching. In particular, 2pTER compared to HRR is less robust as regards combustion stability and is more vulnerable to blowout.

The heat produced via combustion is transferred to thermoelectric module through the reactor walls and a temperature gradient is generated between the hot and cold junctions. In Figure 6.11b the temperatures of the hot and cold junctions of TEs are reported as a function of the flow rate. TEs temperature is significantly lower than that of the monolith thus evidencing the high resistance to heat transfer along the transverse direction of the device. In particular, under the investigated conditions T_{HOT} and T_{COLD} maximum values are respectively 175 and 117°C. The temperatures of thermoelectric junctions increase with Q_{TOT} due to the increase in the power released by combustion. Nevertheless, hot junction temperature increase is steeper than that exhibited by the cold one. T_{HOT}-T_{COLD}, in fact, increases with the flow rate and, specifically, it is 49 and 74°C respectively at Q_{TOT}=80 and Q_{TOT}=150slph (see Figure 6.11b).

The thermal gradient generated between the hot and cold side of the thermoelectric module is converted in an electrical potential according to Seebeck effect (see Chapter 1). Moreover, when the module is coupled in series with a resistive load a current, i and an electric power, given by

multiplying such a current by the electrical potential, are generated by the device (see Chapter 1 and 3). In Figure 6.12 the current, i and the electric power, P_{EL}, are shown as a function of the electrical potential, ΔV, with varying the total flow rate. Such a graph is obtained by changing the resistance of the load, R_L, thus simultaneously varying i and ΔV in the electrical circuit. In particular, by decreasing R_L, the detected electrical potential decreases too while the current increases. Analyzing Figure 6.12a, at Q_{TOT}=150slph the detected current is 450 and 22 mA respectively at the minimum and the maximum considered resistance of the load. Concerning ΔV, at the same R_L values it is respectively 0.2 and 2.2 V.

Considering Figure 6.12b, P_{EL} shows a typical bell-like shape. Moreover, by increasing Q_{TOT} the electrical power also increases due to the increase in the temperatures difference between the TEs hot and cold junctions. The maximum value of P_{EL} is not detected exactly in correspondence of R_L equal to the value of the internal resistance reported in literature ($R_{in}\approx4\Omega$, supplied by Hi-Z Technology, Inc. and $R_{in}\approx5.3\Omega$ measured by Federici et al., 2006); moreover, R_L at which a maximum electrical power is observed slightly changes with varying the flow rate of the fuel mixture. Actually, by changing Q_{TOT} the system temperature changes too, as it has already reported; however, a temperature variation affects the internal resistance of TEs thus altering R_L value corresponding to the maximum P_{EL}. In the present experimental campaign the maximum P_{EL} has been detected at R_L=4÷6Ω.

Table VI.2 *Performances of Propane fueled (Φ=0.5) 2pTER and 3pTER generators run under conditions guaranteeing maximum P_{EL}.*

	Q_{TOT} *slph*	T_{C1} *°C*	T_{HOT} *°C*	T_{COLD} *°C*	T_{HOT}-T_{COLD} *°C*	P_{EL} *W*	P_{INPUT} *W*	η *%*	ΔV *V*	i *mA*	R *Ω*	α *mV·K^{-1}*
2pTER												
Max P_{EL}	150	717	175	101	74	0.29	72	0.40	1.1	265	4.1	0.30
3pTER												
Max P_{EL}	110	697	158	93	65	0.20	52	0.38	1.1	186	5.8	0.34

In Table VI.2 are resumed the data measured in the case 2p-TER is run under conditions guaranteeing the maximum electric power developed. In particular, in this table is pointed out the Seebeck coefficient, α, exhibited in average by each thermocouple constituting HZ-2 module in the combustion tests. The measured value, $\alpha\approx0.30$, is roughly in agreement with α value reported in

literature for HZ-2 thermocouple ($\alpha \approx 0.28$, Federici et al., 2006) thus highlighting an acceptable experimental error in the values of the quantities measured.

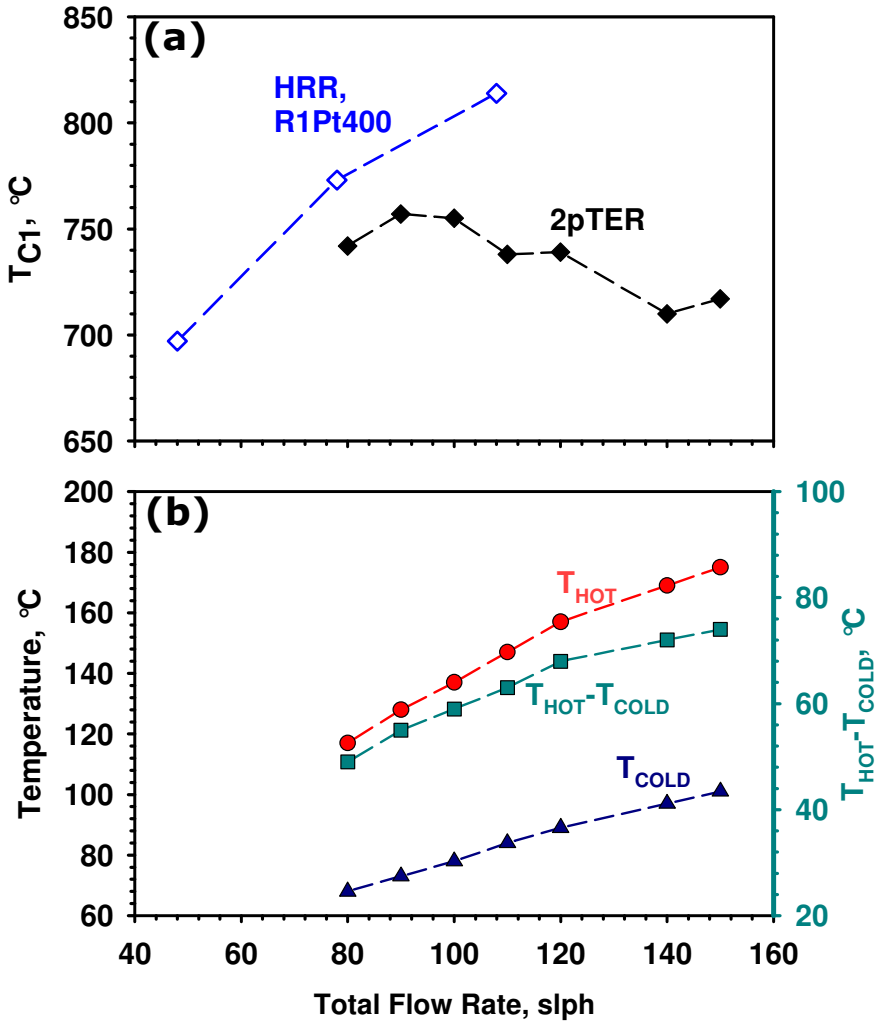

Figure 6.11 *Performances of propane fueled (Φ=0.5) 2pTER generator with varying Q_{TOT}=80÷150slph. (a) Temperature measured on the catalyst: T_1 in the case of 2pTER (filled black diamonds) and in the case of HRR using R1Pt400 catalyst (open blue diamonds); (b) Cold junction (dark blue filled triangles) and hot junction (red filled circles) temperatures (left axis); temperature difference between hot and cold junction (right axis, cyan filled squares).*

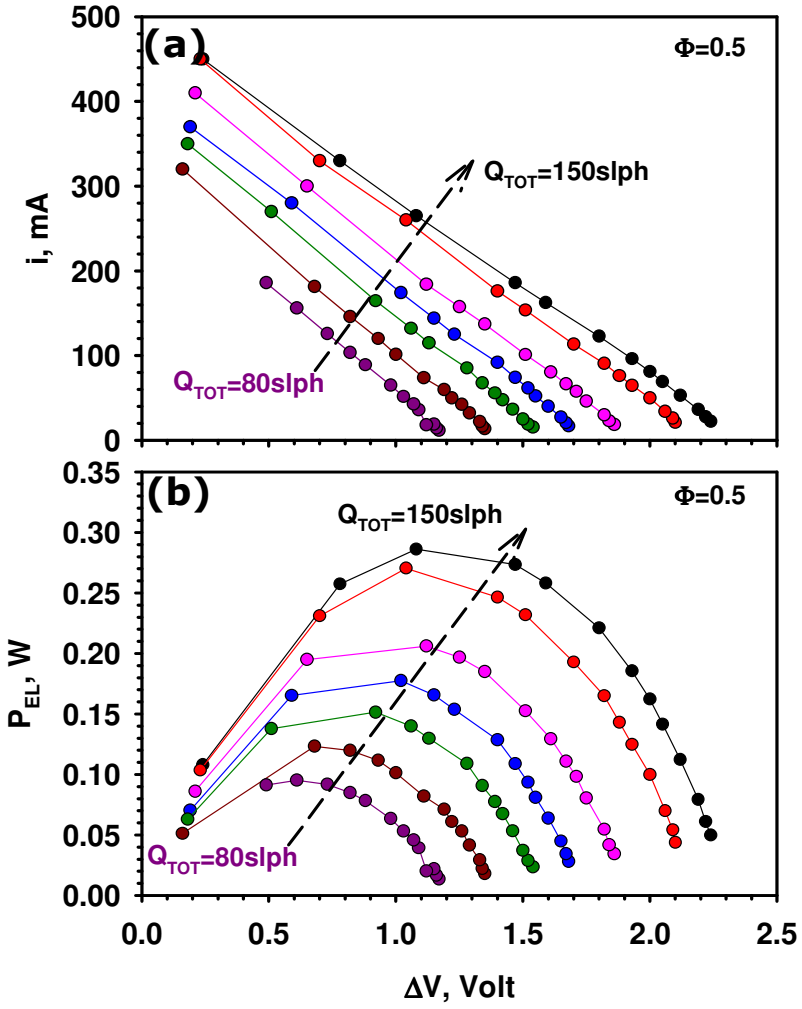

Figure 6.12 *Propane fueled (Φ=0.5) 2pTER generator performances. (a) Current in the electrical circuit and (b) electric power developed as a function of the potential differences at the ends of the rheostat with varying the total flow rate. Q_{TOT}=80slph (dark pink circles); Q_{TOT}=90slph (dark red circles); Q_{TOT}=100slph (dark green circles); Q_{TOT}=110slph (blue circles); Q_{TOT}=120slph (pink circles); Q_{TOT}=140slph (red circles); Q_{TOT}=150slph (black circles).*

In Figure 6.13 the maximum value of P_{EL} (in correspondence with R_L=4-6Ω) is reported as a function of the flow rate and it is compared with the total power input (obtained by multiplying the overall heating value of fuel mixture by the total flow rate). The ratio between P_{EL} and P_{INPUT} gives the the overall efficiency of the device, η, that is also shown (see the righ axis of Figure 6.13). As already reported, P_{EL} increases by increasing Q_{TOT}. In particular, it is approximately 0.1 and 0.3W respectively at Q_{TOT}=80 and Q_{TOT}=150slph. However, as it is expected, an increase in the total flow rate determines a linear increase in the input power; specifically P_{INPUT} is 38 and 72W respectively at Q_{TOT}=80 and Q_{TOT}=150slph, resulting in an overall efficiency that, at the same Q_{TOT}s, is respectively 0.24 and 0.4%. The enhancement of the overall efficiency is due to the steeper increase

(more than linear) in P_{EL} compared to that of P_{INPUT} by increasing the total flow rate. More specifically, this behaviour is found up to Q_{TOT}=140slph; further increasing the total flow rate the overall efficiency is unchanged attesting that under these conditions P_{EL} increases linearly with Q_{TOT}. Such a twofold dependance of P_{EL} on Q_{TOT} (more than linear at Q_{TOT}<140slph, almost linear at $Q_{TOT}\geq$140slph) is ascribed to the shift of the reaction front (i.e., the hottest temperature zone) towards the exit of the reactor with icreasing the total flow rate. Actually, at the highest Q_{TOT} the combustion hot zone may be pushed out from the sphere of action of thermoelectric thus involving a decrease in the in the generated electric power.

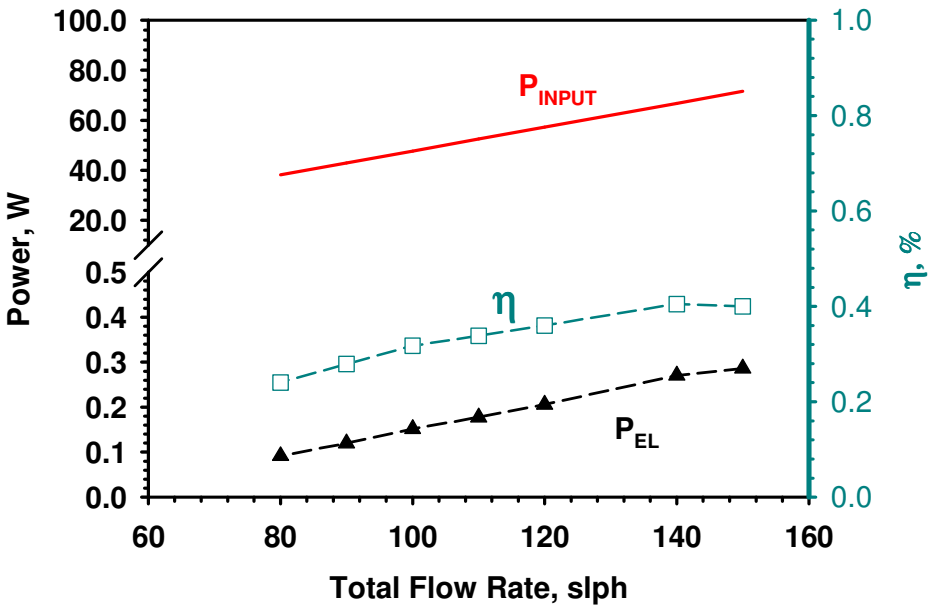

Figure 6.13 *Propane fueled (Φ=0.5) 2pTER generator performances. Overall device efficiency with varying the total flow rate. Input power (red line, left axis); Electric power developed at $R_L=R_{in}\approx 4\div 6\Omega$ (dark black triangles, left axis); Overall efficiency (open cyan squares, right axis).*

In Figure 6.14 the performances of 2pTER are reported with varying the equivalence ratio of the fuel mixture. In particular, compared to Φ=0.5 till now considered, the equivalence ratio is decreased maintaining the same total flow rate, Q_{TOT}=140slph. By decreasing Φ the input power decreases too. Despite of such a decrease, the produced electrical power is practically unchanged. This result is ascribable to the shift of the reaction front (i.e., the hottest temperature zone) towards the exit of the reactor with decreasing the equivalence ratio (see paragraph 6.2.1). Actually, the combustion reaction front moving along the combustor may stabilize in a region in which the heat exchange with thermoelectric module is more favourable thus determining a more efficient use of

the power released by combustion and of the fuel. The maximum efficiency is detected at Φ=0.4 and it is about 0.5%. Under these conditions, P_{EL}=0.27W, i=250mA and ΔV=1.1V.

Furthermore, it is not possible to sustain combustion at an equivalence ratio lower than Φ=0.4. Φ_C shown by 2pTER is thus much lower in comparison with that exhibited by HRR considering the same catalyst (i.e., Φ_C=0.22, see Figure 6.9). Even if HRR critical equivalence ratio was measured at different experimental conditions, specifically at a significantly lower total flow rate (i.e, Q_{TOT}=78slph) and with the use of thermal shields, the strongly lower Φ_C also confirms the worsening in combustion stability in consequence of the integration of TEs.

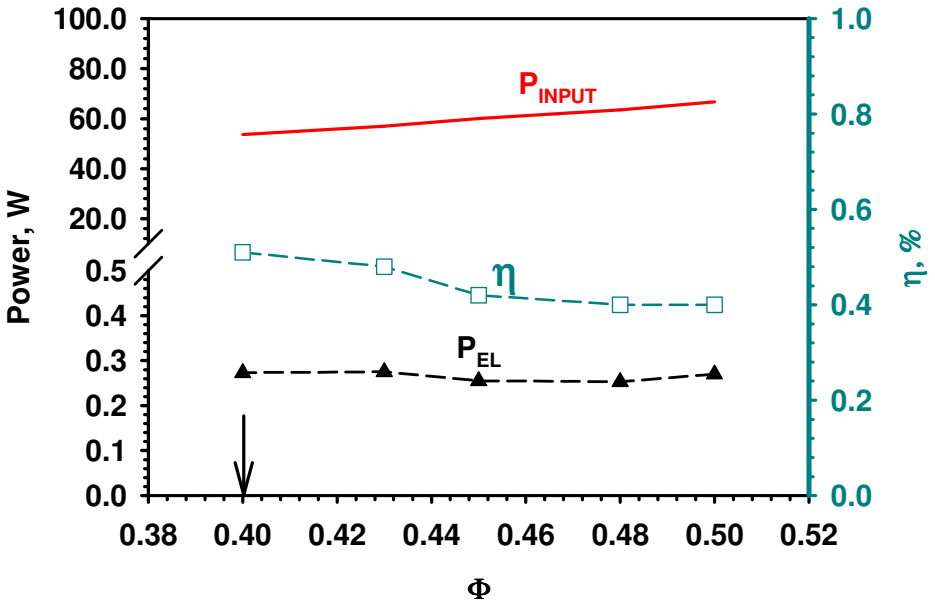

Figure 6.14 *Propane fueled (Q_{TOT}=140slph) 2pTER generator performances. Overall device efficiency with varying the equivalence ratio. Input power (red line, left axis); Electric power developed at R_L=R_{in}≈4÷6Ω (dark black triangles, left axis); Overall efficiency (open cyan squares, right axis).*

6.3.2 3pTER performances

2pTER performances show the feasibility of an electricity generator based on the coupling of a combustor with a thermoelectric module. However, the low electrical power developed compared to the total input power induces to find out a more efficient coupling configuration.

In Figure 6.15 the temperature of TEs hot junction is compared with that of the exhausted gas (gas exiting from the device) as a function of the total flow rate in the case of 2pTER generator. It is worth noting that T_{OUT} is significantly higher that T_{HOT}; in particular, T_{OUT} is 310 and 245°C at Q_{TOT}=150 and Q_{TOT}=100slph respectively and, in all the range investigated it is 150°C higher than

T_{HOT} on average. Such a behaviour points out that much sensible heat may be still transferred transversally to TEs and the electric power developed may ideally increase. In order to further decrease the sensible power of the exhausted gas in advantage of the power lost through the reactor walls the gas flow may be forced in an additional channel devoted to the counter current heat exchange thus constituting the 3pTER.

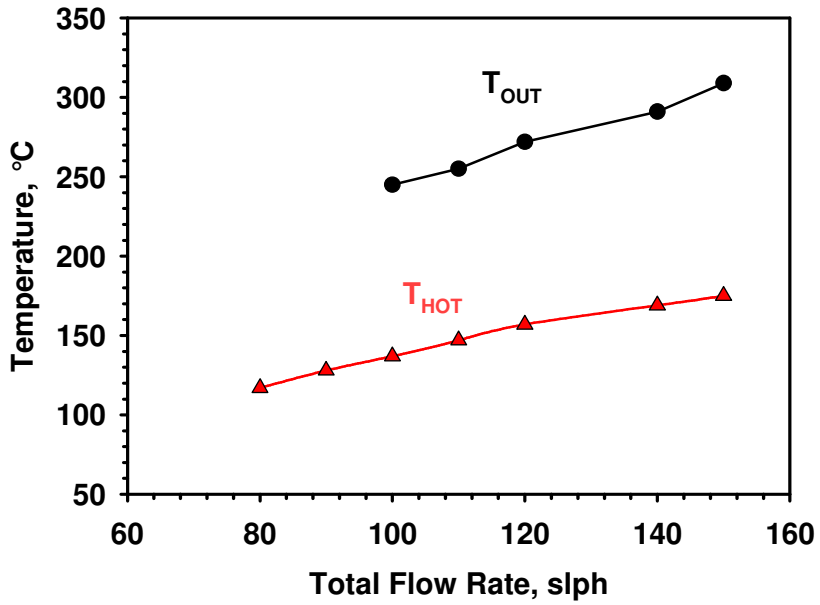

Figure 6.15 *Performances of propane fueled (Φ=0.5) 2pTER generator with varying Q_{TOT}=80÷150slph. Temperature measured at the exit of the reactor (filled black circles) and on TEs hot junction (red filled triangles).*

The same experiments previously discussed for 2pTER have been carried out on 3pTER. In Figures 6.16, 6.17 and 6.18 the performance of 3pTER are shown with varying the total flow rate of the fuel mixture. In particular, in Figure 6.16a the temperature measured at the inlet of the monolith is reported. Due to the heat losses temperature level inside the catalyst is lower than that expected under adiabatic conditions. Moreover, T_{C1} detected in 3pTER is significantly lower than that measured in the case of 2pTER under the same experimental conditions. In confirming with that, at Q_{TOT}=78slph T_{C1} is 692 and 742°C respectively in the case of 3pTER and 2pTER reactor, while at Q_{TOT}=110slph T_{C1} is respectively 697 and 755°C. Actually, 3pTER is a much more dissipative system compared to 2pTER. The former, in fact, is constituted by a much larger aluminum tube compared to that used in the case of 2pTER (in 3pTER Al tube is the external wall of the device, in 2pTER, instead, it is employed only to support TEs, see Chapter 3) thus exhibiting much higher heat losses. Moreover, analyzing T_{C1} trend also in the case of 3pTER it is evident the presence of a

maximum at around Q_{TOT}=90slph. Such a result confirms that the integration of a thermoelectric module with HRR causes a changing in the dynamics of combustion quenching and, more specifically, makes the combustion system more vulnerable as regards blowout.

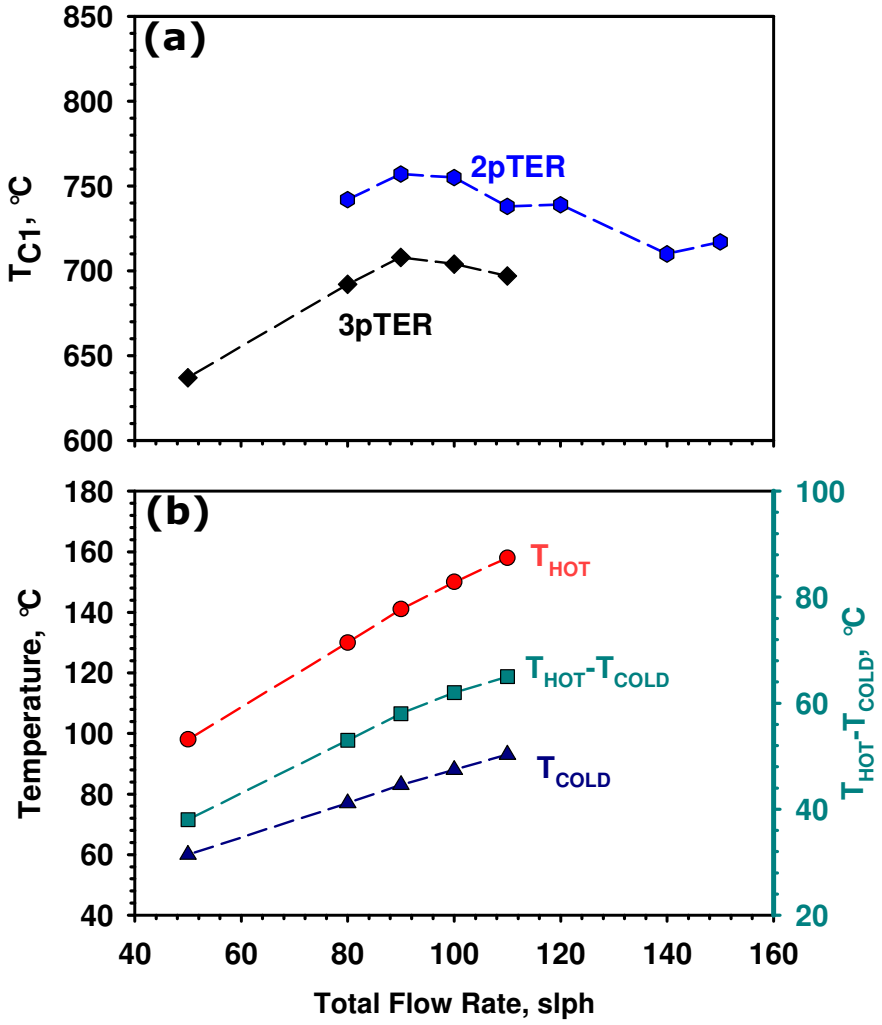

Figure 6.16 *Performances of propane fueled (Φ=0.5) 3pTER generator with varying Q_{TOT}=50÷110slph. (a) Temperature measured on the catalyst: T_1 in the case of 3pTER (filled black diamonds) and in the case of 2pTER (filled blue hexagons); (b) Cold junction (dark blue filled triangles) and hot junction (red filled circles) temperatures (left axis); temperature difference between hot and cold junction (right axis, cyan filled squares).*

In Figure 6.16b the temperatures of TEs hot and cold junctions are reported as a function of the flow rate in the case of 3pTER. Under the investigated conditions T_{HOT} and T_{COLD} maximum values are respectively 158 and 93°C. The temperatures of thermoelectric junctions increase with Q_{TOT} due to the increase in the power released by combustion. Nevertheless, hot junction temperature

increase is steeper than that exhibited by the cold one. T_{HOT}-T_{COLD}, in fact, increases with the flow rate and, specifically, it is 38 and 65°C respectively at Q_{TOT}=50 and Q_{TOT}=110slph (see Figure 6.16b).

In Figure 6.17 the current, i and the electric power, P_{EL}, are shown as a function of the electrical potential, ΔV, with varying the total flow rate. As reported previously, the simultaneous variation of i and ΔV is obtained by varying the resistance of the rheostat (R_L). Analyzing Figure 6.17a, at Q_{TOT}=110slph the detected current is 390 and 18 mA respectively at the minimum and the maximum considered resistance of the load. Concerning ΔV, at the same R_L values it is respectively 0.2 and 1.8 V.

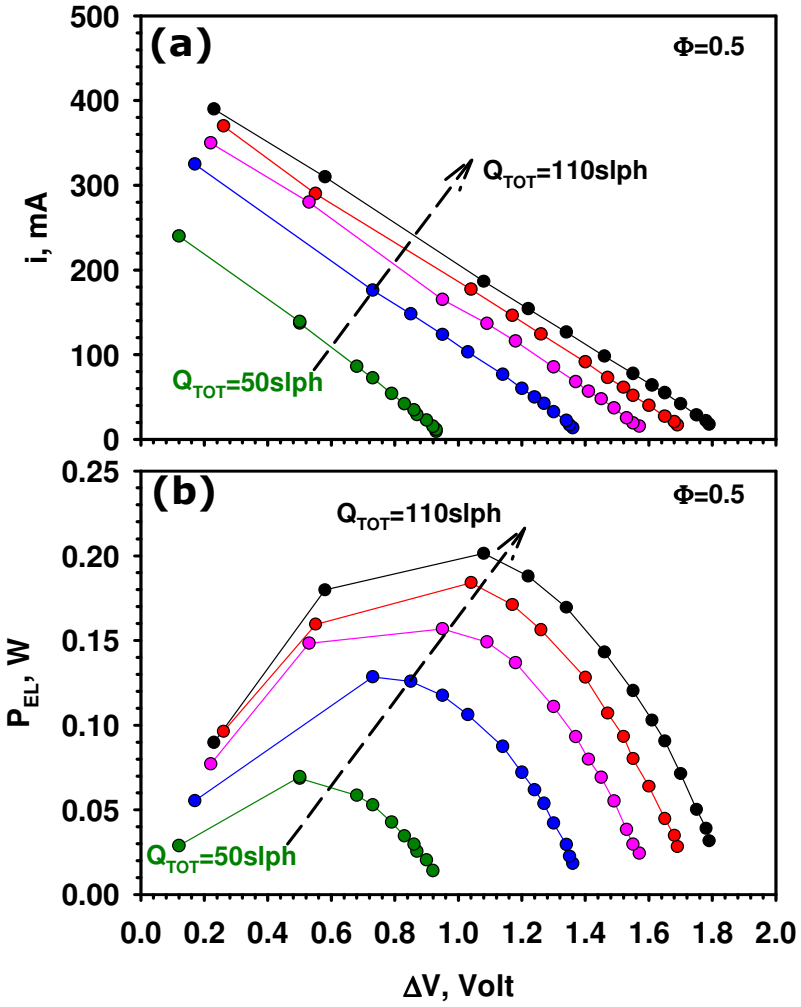

Figure 6.17 *Propane fueled (Φ=0.5) 3pTER generator performances. (a) Current in the electrical circuit and (b) electric power developed at the ends of the rheostat with varying the total flow rate. Q_{TOT}=50slph (dark green circles); Q_{TOT}=80slph (blue circles); Q_{TOT}=90slph (pink circles); Q_{TOT}=100slph (red circles); Q_{TOT}=110slph (black circles).*

Considering Figure 6.17b, as it is expected P_{EL} shows a typical bell-like shape (as already found for 2pTER generator 3pTER exhibits the highest P_{EL} in correspondence with R_L=4÷6Ω) and it increases by increasing Q_{TOT}. Resuming, the test performed on 3pTER generator have shown that the maximum P_{EL} is detected at the highest total flow rate investigated (Q_{TOT}=110slph) and it is P_{EL}=0.2W; under these conditions, i=186mA and ΔV=1.1V. In Table VI.2 the electrical performances of 3pTER are reported and compared with those exhibited by 2pTER.

In Figure 6.18 the maximum P_{EL} (in correspondence with R_L=4÷6Ω) and the overall efficiency obtained for 3pTER generator are reported as a function of the flow rate and they are compared with the corresponding values exhibited by 2pTER. Concerning 3pTER performances, as already reported, P_{EL} increases by increasing Q_{TOT}. In particular, it is approximately 0.07 and 0.20W respectively at Q_{TOT}=50 and Q_{TOT}=110slph. However, as it is expected, an increase in the total flow rate determines a linear increase in the input power; specifically P_{INPUT} is 24 and 52W respectively at Q_{TOT}=50 and Q_{TOT}=110slph (data not shown), resulting in an overall efficiency that, at the same Q_{TOT}s, is respectively 0.29 and 0.38%. The enhancement of the overall efficiency confirms that P_{EL} increases more than linearly (the increase is thus steeper than that exhibited by P_{INPUT}) by increasing the total flow rate. More specifically, this behaviour is found up to Q_{TOT}=100slph; further increasing the total flow rate the overall efficiency slightly decreases revealing that under these conditions P_{EL} increases less than linearly with Q_{TOT}. Resuming, the tests performed on 3pTER have shown that the highest efficiency is detected at Q_{TOT}=100slph and it is η=0.39%; under these conditions, P_{EL}=0.18W, i=260mA and ΔV=1.0V.

Comparing 2pTER and 3pTER performances (see Figure 6.18) it is worth noting that it is possible to distinguish two regions in dependence on the total flow rate. In particular at Q_{TOT}<110slph 3-pass generator shows higher electric power developed and overall efficiency while at Q_{TOT}>110slph 2-pass generator exhibits higher performances. Such a behaviour reveals that passing from a 2-pass to a 3-pass configuration is an effective tool to improve generator performances. Based on this result, 3pTER allows to increase the heat transferred to TEs through the reactor walls but maintaining exhausted gas temperature sufficiently high for an efficient thermal to electrical power conversion. However, the obtained result highlights another important issue in combustor-TEs coupling that was not taken into account up to now. As already reported, by increasing the number of reactor gas passes the heat transferred to TEs increases too due to the increase in the power lost through the reactor walls to the detriment of exhausted gas sensible power. However, the heat effectively transferred to TEs is a part of the total power lost trough the reactor walls (Federici et al., 2006): most of such a power is, in fact, transferred to the environment thus not involving any improvement in the generator performances but only causing a worsening in

combustion stability. As a consequence, even if 3pTER is ideally more efficient than 2pTER it is more vulnerable as regards blow out and it effectively exhibits higher performances only in a range of low flow rate.

Moreover, 3pTER shows a $\Phi_C \approx 0.5$, much lower than that detected in the case of 2pTER ($\Phi_C \approx 0.4$). Such an experimental evidence is a further confirmation of the lower robustness as regards combustion stability exhibited by 3pTER.

As a result, in order to find out an optimum configuration in the design of a electricity generator based on combustor-TEs coupling it is needed to consider the efficiency with which the power lost through the reactor walls is transferred to TEs rather than to the environment and its dependence on the number of reactor passes.

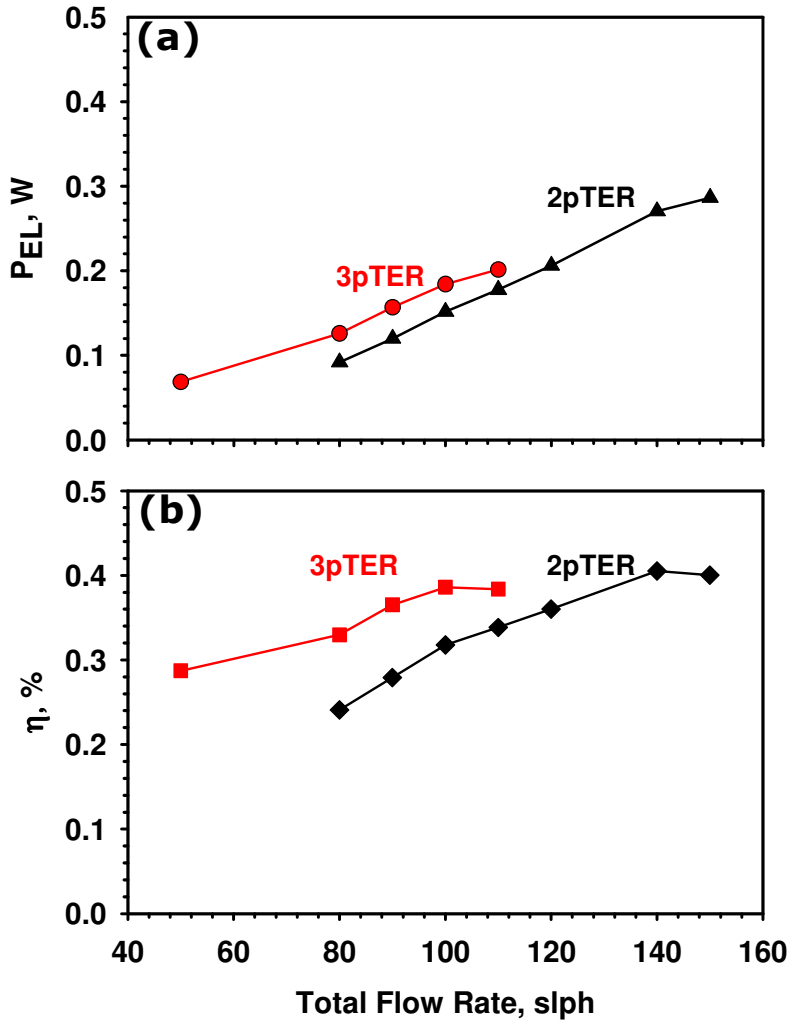

Figure 6.18 *Propane fueled (Φ=0.5) 3pTER generator performances with varying the total flow rate. (a) Maximum P_{EL} at $R_L=R_{in}\approx 4\div 6\Omega$; (b) overall device efficiency. P_{EL} obtained for 2pTER (filled black triangles) and for 3pTER (filled red circles); Overall efficiency obtained for 2pTER (filled black diamonds) and for 3pTER (filled red squares).*

CHAPTER 7

CONCLUSIONS

In the present Ph. D. thesis the main issues in catalytic micro-combustion have been experimentally explored. The study has dealt with the development of novel micro-structured combustors and has provided for an investigation on process efficiency, kinetics and operating windows. Hydrogen, propane and methane based fuels have been taken into account; moreover, hydrogen assisted combustion of methane is considered too. Platinum, perovskite and mixed phase γ-alumina supported catalysts have been investigated. Still, different reactors have been designed: particularly, single micro-channel and multi-channels monolithic reactors were employed respectively in isothermal and autothermal combustion tests. Such a study has constituted the background in the development of electricity generators constituted by catalytic microcombustors integrated with thermoelectric converters. Particularly, micropower generators constituted by novel 2 and 3-pass heat recirculation quartz micro-combustors are investigated.

Micro-structured catalytic reactors have been developed starting from high thermally stable and relatively cheap inert substrates in the shape of monoliths and platelets. Differently from monoliths whose employment in catalytic combustion is well-established, planar substrates constitute an innovative solution which is having a strong resonance in micro-system applications. A deposition technique of catalytic layers on platelets has been set up; it is found a good repeatability in the preparation of structured catalysts highly resistant and well anchored on substrate of different materials and specifically of α-alumina and FeCralloy.

The combustion tests have been carried out taking into account two different configurations. In a first kind of approach to the micro-combustion problem, thermal effects have been insulated from fluid dynamics, mass transfer and reactive phenomena, so that combustion has been studied under strongly diluted and temperature controlled conditions in isothermal planar reactors. For this kind of reactor configuration the fluid dynamics is well known and has revealed a fully developed laminar regime. Under these conditions mass transfer effects on the reaction rate have been evaluated showing the absence of interphase and interparticle diffusive limitations up to a maximum temperature of 800°C. In a second kind of approach to the problem, autothermal combustion tests have been performed in order to understand the role of heat fluxes on combustion efficiency and

stability, as well as the role of thermal shocks of repeated ignition-extinction/blow-out cycles on the catalytic micro-combustor stability and durability.

Concerning the active phase a great attention has been devoted to the development of relatively cheap catalyst formulations alternatively to noble metals catalysts that, despite of the high cost and the low chemical and thermal stability, are still widely studied. Supported perovskites, $LaMnO_3/Al_2O_3$ based catalysts have been the starting point due to the great chemical and thermal stability and low cost. However, novel catalysts consisting of perovskites promoted by a very low platinum amount have been investigated too, with the aim to enhance the mixed oxide activity but maintaining stability and inexpensiveness typical of perovskite. The most significant results are related to the higher activity of $LaMnO_3/Al_2O_3$ compared to that of Pt/Al_2O_3 in methane combustion; as a consequence, the promoting effect of platinum on perovskite is practically not observed at all, neither any enhancement in activity has been visible. On the contrary, Pt/Al_2O_3 catalysts have exhibited significantly higher activity than $LaMnO_3/Al_2O_3$ in hydrogen and propane combustion thus rendering productive the promotion of perovskite with small amounts of platinum. Under the investigated conditions hydrogen has been efficaciously converted at 200°C while total methane conversion has not been achieved up to at a maximum temperature of 800°C, under experimental conditions suggested by practical applications (flow-rates and thermal power developed). However, by co-burning methane and hydrogen a strong enhancement of CH_4 combustion rate has been measured and attributed to the activation of reactive paths in the homogeneous phase. Particularly, by replacing about 40% of the energetic CH_4 content with H_2 a total fuel conversion has been obtained at 800°C on unpromoted perovskite catalysts.

Autothermal experiments have revealed the strong non adiabaticity of microcombustors. Loss of combustion stability has occurred either via extinction or blowout. In extinction, occurring at low flow rates, stability is lost due to large heat losses compared to the power provided via combustion. In blowout, occurring at the high flow rates, quenching is due to the low residence time, resulting in incomplete fuel conversion and a considerable shift of the reaction front downstream. Experimental results have revealed that Non-Recirculating-quartz-micro-Reactor (NRR) for propane combustion has operated in the blowout regime and quenching has occurred due to lack of sufficient reactant preheating. On the contrary, Heat-Recirculating-quartz-micro-Reactor (HRR) has enlarged the operability limits of the process; in particular, heat recirculation has enhanced preheating of the incoming gases, allowing stabilization of the reaction front upstream and preventing blowout. The obtained results on quartz reactors have represented a relevant complement of another experimental study reported in literature on heat recirculation in metallic reactors; consistently with some

theoretical studies, it has been definitively confirmed that heat recovery is effective only in the limit of low conductivity materials.

On the other hand, the results of the present experimental campaign have shown that the enhancement of micro-combustor field of operability could be drastically affected by the type of fuel too. Particularly, the results have shown that higher is the fuel reactivity wider is the window of autothermal combustion. Propane combustion has exhibited a wide range of stability being sustained without an external preheating. On the contrary, because of the high chemical stability, methane combustion has shown a very narrow operating range. CH_4, in fact, is efficaciously burnt only by supplying heat to the combustor thus pre-heating reactants. Hydrogen assisted methane combustion has been considered as a possible strategy to enhance CH_4 combustion operating limits. Obtained results, in fact, have shown that this fuel is more reactive than methane. Hydrogen addiction to methane fuel produces a chemical synergy between the two fuel bringing about an enhancing in the methane combustion rate. Moreover, results have shown that hydrogen thermally assists methane combustion by lowering its catalytic ignition temperature. Despite of the higher reactivity of CH_4-H_2 compared to methane, it has been found that the addiction of H_2 to CH_4 fuel doesn't play a role on autothermal operation limits.

Propane fueled heat recirculating reactors constituted by Pt/Al_2O_3 active phase have been integrated with thermoelectric modules (TEs) thus showing the feasibility of electricity generators based on combustion. A net positive electrical power of the order of 0.2÷0.3 W has been developed being characterized by a maximum overall efficiency of 0.4%. The main issues involved in the integration of the catalytic combustor with thermoelectric elements (TEs) have been discussed. In particular, thermal management of the device has been studied in order to make as efficient as possible such a coupling. At this proposal, the performances of the generator have been evaluated in the case TEs are integrated with both a 2 and 3 pass combustors. A 2-pass generator has shown a low efficiency in the heat transfer from combustor to TEs. By increasing the number of reactor passes is an effective tool to increase efficiency but such a strategy also determines an increase in the process heat losses thus worsening operation limits of the electricity generator.

LITERATURE CITED

J. Ahn, C. Eastwood, L. Sitzki, P. Ronney; “Gas-phase and catalytic combustion in heat recirculating burner”; Proceedings of the Combustion Institute, vol. 30 (2005): pp. 2463-2472.

M. Alifanti, N. Blangenois, M. Florea, B. Delmon; “Supported Co-based perovskites as catalysts for total oxidation of methane”; Applied Catalysis A: General, vol. 280 (2005): pp. 255-265.

H. Arai e M. Machida; “Thermal stabilization of catalyst supports and their application to high-temperature catalytic combustion”; Applied catalyisis A: General, vol 138 (1996): pp. 161-176.

H. Arai, T. Yamada, K. Eguchi, T. Seiyama; "Catalytic combustion of metahane over various perovskite-type oxides"; Applied Catalysis, vol. 26 (1986): pp. 265-276.

S. Arnone, G. Busca, L. Lisi, F. Milella, G. Russo, M. Turco; “Catalytic combustion of methane over $LaMnO_3$ perovskite supported on La_2O_3 stabilized alumina, a comparative study with Mn_3O_4, Mn_3O_4- Al_2O_3 spinel oxides”; Proceedings of the Combustion Institute, vol. 27 (1998): pp. 2293-2299.

J. A. Barnard, J. N. Bradley; "Flame and Combustion"; Chapman and Hall, London New York (1985).

R. Byron Bird, Warren E Stewart, Edwin N. Lightfoot; “Transport Phenomena”. John Wiley & Sons, New York (1960).

A. I. Boukai, Y. Bunimovich, J. Tahir-Kheli, J.-K. Yu, W. A. Goddard III, J. R. Heath; “Silicon nanowires as efficient thermoelectric materials; vol. 451 (2008): pp. 168- 171.

C. Bozo, N. Guilhaume, E. Garbowsky, M. Primet; “Combustion of methane on CeO_2- ZrO_2 based catalysts”; Catalysis Today, vol. 59 (200): pp. 33-45.

T. V. Choudhary, S. Banerjee, V. R. Choudhary; “Catalysts for combustion of methane and lower alkanes”; Applied Catalysis A: General, vol. 234 (2002): pp. 1-23.

F. Cifà, P. Dinka, P. Viparelli, S. Lancione, G. Benedetti, P. L. Villa, M. Viviani, P. Nanni; "Catalysts based on $BaZrO_3$ with different elements incorporated in the structure I: $BaZr_{(1-x)}Pd_xO_3$ systems for total oxidation"; Applied Catalysis B: Environmental, vol. 46 (2003): pp. 463-471.

S. Cimino, L. Lisi, R. Pirone, G. Russo; “Dual-site Pd/perovskite monolithic catalysts for methane catalytic combustion”; Ind. Eng. Chem. Res., vol. 43 (2004): pp. 6670-6679.

S. Cimino, L. Lisi, R. Pirone, G. Russo, M. Turco; “Methane combustion on perovskite-based structured catalysts”; Catalysis Today, vol. 59 (2000): pp. 19-31.

S. Cimino, A. Di Benedetto, R. Pirone, G. Russo; “CO, H_2 or C_3H_8 assisted catalytic combustion of methane over supported $LaMnO_3$ monoliths”; Catalysis Today, vol. 83 (2003): pp. 33-43.

S. Cimino, A. Di Benedetto, R. Pirone, G. Russo; “Transient behaviour of perovskite-based monolithic reactors in the catalytic combustion of methane”; Catalysis Today, vol. 69 (2001): pp. 95-103.

S. Cimino, M. P. Casaletto, L. Lisi, G. Russo; "Pd-$LaMnO_3$ as dual site catalysts for methane combustion"; Applied Catalysis A: General, vol. 327 (2007): pp. 238-246.

A. Civera, G. Negro, S. Specchia, G. Saracco, V.Specchia; "Optimal compositional and structural design of a $LaMnO_3/ZrO_2$/Pd-based catalyst for methane combustion"; Catalysis Today, vol. 100 (2005): pp. 275-281.

P. Dagaut, A. Nicolle; "Experimental and detailed kinetic modelling study of hydrogen-enriched natural gas bled oxidation over extended temperature and equivalence ratio ranges"; Proceedings of the Combustion Institute 30 (2005): pp. 2631-2638.

B. De Collongue, E. Garbowski, M. Primet; "Catalytic combustion of methane over bulk and supported lanthanum chromium oxide (LaCrO3) perovskites"; Journal of the Chemical Society, Faraday Transactions, vol. 87(15) (1991): pp. 2493-2499.

O. Demoulin, I. Seunier, M. Navez, P. Ruiz; "Influence of the addiction of H_2 upon the behaviour and properties of a Pd (2 wt%)/γ-Al_2O_3 catalyst and a comparison with the case of the Pt-based catalyst"; Applied Catalysis A: General, vol. 300 (2006): pp. 41-49

W. Deng, J. F. Klemic, X. Li, M. A. Reed, A. Gomez; " Liquid fuel microcombustor using microfabricated multiplexed electrospray sources"; Proceedings of the Combustion Institute 31 (2007): pp. 2239-2246.

M. Derudi, A. Villani, R. Rota; "Sustainability of mild combustion of hydrogen-containing hybrid fuels"; Proceedings of the Combustion Institute, vol. 31 (2007): pp. 3393-3400.

O. Deutschmann, L. I. Maier, U. Riedel, A. H. Stroemman, R. W. Dibble; "Hydrogen assisted catalytic combustion of methane on platinum"; Catalysis Today, Vol. 59 (2000): pp. 141-150.

Z. H. Dughaish; "Lead telluride as thermoelectric material for thermoelectric power generation"; Physica B, vol. 322 (2002): pp. 205-253.

G. Ertl, H. Knoezinger, F. Schueth, J. Weitkamp; "Handbook of Heterogeneous Catalysis", Vol. 3. Wiley-VCH Verlag GmbH & Co. KGaA, Weinheim, Germany (2008).

L. Fabbrini, I. Rossetti, L. Forni; "La_2O_3 as primer for supporting $La_{0.9}Ce_{0.1}CoO_{3\pm\delta}$ on cordieritic honeycombs"; Applied Catalysis B: Environmental, vol. 56 (2005): pp. 221-227.

J. A. Federici, D. G. Norton, T. Bruggemann, K. W. Voit, E. D. Wetzel, D. G. Vlachos; "Catalytic microcombustors with integrated thermoelectric elements for portable power production"; Journal of Power Sources, Vol. 161 (2006): pp. 1469-1478.

J. A. Federici, D. G. Vlachos, A computational fluid dynamics study of propane/air microflame stability in a heat recirculation reactor. Combustion and Flame 153 (2008) 258-269

J. A. Federici, E. D. Wetzel, B. R. Geil, D. G. Vlachos; "Single channel and heat recirculation catalytic micro-burners: an experimental and computational fluid dynamics study"; Proc. Combust. Inst. 32 (accepted).

A. C. Fernandez-Pello; "Micro-power generation using combustion: issues and approaches"; Proceedings of the Combustion Institute, vol. 29 (2002): pp. 883-899.

L. Forni, I. Rosetti; "Catalytic combustion of hydrocarbons over perovskites"; Applied Catalysis B: Environmental, vol. 38 (2002): pp. 29-37.

P. Gélin, L. Urfels, M. Primet, E. Tena; "Complete oxidation of methane at low temperature over Pt and Pd catalysts for the abatement of lean-burnt natural gas fuelled vehicles emission: influence of water and sulphur containing compounds"; Catalysis Today, vol. 83 (2003): pp. 45-57.

L. Giebeler, D. Kiebling, G. Wendt; “LaMnO3 perovskite supported noble metal. Catalysts for the total oxidation of methane”; Chem. Eng. Technol., vol. 30 (7) (2007): pp. 889-894.

L. M. Goncalves, P. Alpuim, G. Min, D. M. Rowe, C. Couto, J. H. Correia; “Optimization of Bi2Te3 and Sb2Te3 thin films deposited by co-evaporation on polymide for thermoelectric applications”; Vacuum, vol. 82 (2008): pp: 1499-1502.

R. E Hayes, S. T. Kolaczkowski; “Introduction to Catalytic Combustion”. Gordon and Beach Science Publisher (1997).

A. I. Hochbaum, R. Chen, R. D. Delgado, W. Liang, E. C. Garnett, M. Najarian, A. Majumdar; “Enhanced thermoelectric performance of rough silicon nanowires”; Nature, vol. 451 (2008): pp. 163-167.

N. S. Kaisare, D. G. Vlachos, Optimal reactor dimensions for homogeneous combustion in small channels. Catalysis Today 120 (2007) 96-106

N S. Kaisare, D. G. Vlachos, Extending the region of stable homogeneous micro-combustion through forced unsteady operation. Proceedings of the Combustion Institute 31 (2007) 3293-3300

N. S. Kaisare, S. R. Deshmukh, D. G. Vlachos, Stability and performance of catalytic microreactors: simulations of propane catalytic combustion on Pt. Chemical Engineering Science 63 (2008) 1098-1116

S. Karagiannidis, J. Mantzaras, G. Jackson, K. Boulouchos; "Hetero/homogeneous combustion and stability maps in methane-fueled catalytic microreactor"; Proceedings of the Combustion Institute, vol. 31 (2007): pp. 3309-3317.

A. M. Karim, J. A. Federici, D.G. Vlachos; “Portable power production from methanol in an integrated thermoeletric/microreactor system”; Journal of Power Sources, vol. 179(1) (2008): pp. 113-120.

N. I. Kim, S. Aizumi, T. Yokomori, S. Kato, T. Fujimori, K. Maruta; "Development and scale effect of small swiss-roll combustors"; Proceedings of the Combustion Institute, vol. 31 (2007): pp. 3243-3250.

J. Kirchnerova, M. Alifanti, B. Delmon; “Evidence of phase cooperation in the $LaCoO_3$-CeO_2-Co_3O_4 catalytic system in relation to activity in methane combustion”; Applied Catalysis A: General, vol. 231 (2002): pp. 65-80.

J. Kirchnerova, D. Klvana; “Performance of $La_{1-x}Sr_xAl_{1-y-y'}Fe_yMg_{y'}O_{3-\delta}$ perovskites in methane combustion: effect of aluminium and magnesium content”; Catalysis Today, vol. 83 (2003): pp. 233-238.

B. Kucharczyk, W. Tylus; "Effec of Pd or Ag additive on the activity and stability of monolithic $LaCoO_3$ perovskites for catalytic combustion of methane"; Catalysis Today, vol. 90 (2004): pp. 121-126.

C. H. Kuo and P. D. Ronney; "Numerical modeling of non-adiabatic heat-recirculating combustors"; Proceedings of the Combustion Institute, vol. 31 (2007): pp. 3277-3284.

K. Kusakabe, S. Morooka, H. Maeda; “Development of a microchannel catalytic reactor system”; Korean J. Chem. Eng., vol. 18(3) (2001): pp. 271-276.

O. Levenspiel; "Chemical Reaction Engineering: second edition"; John Wiley & Sons, New York, Chichester, Brisbane, Toronto, Singapore (1962).

W. Liu, M. F. Stephanopoulos; “Total oxidation of carbon monoxide and methane over transition metal-fluorite oxide composite catalysts”; Journal of Catalysis, vol. 153 (1995): pp. 304-316.

M. Lyubovsky, L. L. Smith, M. Castaldi, H. Karim, B. Nentwick, S. Etemad, R. LaPierre, W. C. Pfefferle; "Catalytic combustion over platinum group catalysts: fuel-lean versus fuel-rich operation"; Catalysis Today, vol. 83 (2003): pp. 71-84.

L. Marchetti, L. Forni; “Catalytic combustion of methane over perovskites”; Applied Catalysis B: Environmental, vol. 15 (1998): pp. 179-187.

A. Mehra, X. Zhang, A. A. Ayon, I. A. Waitz, M. A. Schmidt, C. M. Spadaccini, A six-wafer combustion system for a silicon micro gas turbine engine. Journal of Microelectromechanical systems 9 (2000) 517-527

C. M. Miesse, R. I. Masel, , C. D. Jensen, M. A. Shannon, M. Short, Sub-millimeter scale combustion. A. I. Ch. E. Journal 50 No. 12 (2004) 3206-3213

A. Muhtaroglu, A. Yokochi, A. von Jouanne; “Integration of thermoelectrics and photovoltaics as auxiliary power sources in mobile computing applications”; Journal of Power Sources, vol. 177 (2008): pp. 239-246.

J. G. McCarty, M. Gusman, D. M. Lowe, D. L. Hildenbrand, K. N. Lau; "Stability of supported metal and supported metal oxide combustion catalysts"; Catalysis Today, Vol. 47 (1999): pp. 5-17.

D. G. Norton and D. G. Vlachos; "A CFD study of propane/air microflame stability"; Combustion and Flame, vol. 138 (2004): pp. 97-107.

D. G. Norton, E. D. Wetzel, D. G. Vlachos; "Fabrication of single-channel catalytic microburner: effect of confinement on the oxidation of hydrogen/air mixtures"; Ind. Eng. Chem. Res., vol. 43 (2004): pp. 4833-4840.

D. G. Norton and D. G. Vlachos; "Hydrogen assisted self-ignition of propane/air mixtutures in catalytic microburnes"; Proceedings of the Combustion Institute 30 (2005): pp. 2473-2480.

D. G. Norton, E. D. Wetzel, D. G. Vlachos; "Thermal management in catalytic microreactors"; Ind. Eng. Chem. Res., vol. 45 (2006): pp. 76-84.

M. O'Connel, A. K, Norman, C. F. Huttermann, M. A. Morris; “Catalytic oxidation over lanthanum-transition metal perovskite materials”; Catalysis Today, vol. 47 (1999): pp. 123-132.

D. R. Palo, J. D. Holladay, R. T. Rozmiarek, C. E. Guzman-Leong, Y. Wang, J. Hu, Y.-H. Chin, R. A. Dagle, E. G. Baker; “Development of a soldier portable fuel cell power system. Part I: A bread board methanol fuel processor”; Journal of power sources, vol. 108 (2002): pp. 28-34.

R. H. Perry, D. W. Green; “Perry’s chemical engineers’ handbook”; Mc Graw Hill (Seventh Edition).

S. Petrovic, L. Karanovic, P. K. Stefanov, M. Zdujic, A. Terlecki-Baricevic; "Catalytic combustion of methane over Pd-containing perovskite type oxides"; Applied Catalysis B: Environmental, vol. 58 (2005): pp. 133-141.

K.Qiu and A. C. S. Hayden; “Development of a thermoelectric self-powered residential heating system”; Journal of Power Sources, vol. 180 (2008): pp. 884-889.

S. B. Riffat, Xiaoli Ma; “Thermoelectrics: a review of present and potential applications”; Applied Thermal Engineering, vol. 23 (2003): pp. 913-935.

P. D. Ronney; "Analysis of non-adiabatic heat-recirculating combustors"; Combustion and Flame, vol. 135 (2003): pp. 421-439.

P. Sabia, M. de Joannon, S. Fierro, A. Tregrossi, A. Cavaliere; " Hydrogen-enriched methane mild combustion in a well-stirred reactor"; Experimental Thermal and Fluid Science, vol. 31 (2007): pp. 469-475.

G. Saracco, G. Scibilia, A. Iannibello, G. Baldi; “Methane combustion on Mg-doped $LaCrO_3$ perovskite catalysts”; Applied Catalysis B: Environmental, vol. 8 (1996): pp. 229-244.

G. Saracco, F. Geobaldo, G. Baldi; “Methane combustion on Mg-doped $LaCrO_3$ perovskite catalysts”; Applied Catalysis B: Environmental, vol. 20 (1999): pp. 277-288.

T. Seiyama; “Total oxidation of hydrocarbons on perovskite oxides”; Catalysis Reviews, vol. 34 (1992): pp. 281-300.

R. W. Schefer, D. M. Wicksall, A. K. Agrawal; "Combustion of hydrogen-enriched methane in a lean premixed swirl-stabilized burner"; Proceedings of the Combustion Institute 29 (2002): pp. 843-851.

C. M. Spadaccini, X. Zhang, C. P. Cadou, N. Miki, I. A. Waitz; "Preliminary development of a hydrocarbon-fueled catalytic micro-combustor"; Sensors and Actuators A, vol. 103 (2003): pp. 219-224.

Y. Suzuki, J. Saito, N. Kasagi; "Development of micro catalytic combustor with Pt/Al2O3 thin films"; JSME International Journal, Series B, vol. 47 (3) (2004): pp. 522-527.

L. G. Tejuca, J. L. G. Fierro, J. M. D. Tascon, Structure and reactivity of perovskite-type oxides. Advances in Catalysis 36 (1989) 237-328.

M. Uenishi, M. Tanigushi, H. Tanaka, M. Rimura, Y. Nishihata, J. Mizuki, T. Kobayashi; "Redox behaviour of palladium at star-up in the Perovskite-type $LaFePdO_x$ automotive catalysts showing a self-regenerative function"; Applied Catalysis B: Environmental, vol. 57 (2005): pp. 267-273.

M. Valentini, G. Groppi, C. Cristiani, M. Levi, E. Tronconi, P. Forzatti; "The deposition of γ-Al_2O_3 layers on ceramic and metallic supports for the preparation of structured catalysts"; Catalysis Today, vol. 69 (2001): pp. 307-314.

G. Veser; "Experimental and theoretical investigation of H_2 oxidation in a high-temperature catalytic microreactor"; Chemical Engineering Science, vol. 56 (2001): pp. 1265-1273.

J. Vican, B. F. Gajdeczko, F. L. Dryer, D. L. Milius, I. A. Aksay, R. A. Yetter; "Development of a microreactor as a thermal source for microelectromechanical systems power generation"; Proceedings of the Combustion Institute, vol. 29 (2002): pp. 909-916.

C. B. Vining; "Desperately seeking silicon"; Nature, vol. 451 (2008): pp. 132-133.

M. Wagner, G. Span, S. Holzer, T. Grasser; "Thermoelectric power generation using large-area Si/SiGe pn-junctions with varying Ge content"; Semicond. Sci. Technol., vol. 22 (2007): pp. S173-S176.

X. Wang, J. Zhu, H. Bau, R. J. Gorte; "Fabrication of micro-reactors using tape-casting methods"; Catalysis Letters, vol. 77, No. 4 (2001): pp. 173-177.

F. Weinberg; "Optimising heat recirculating combustion systems for thermoelectric converters"; Combustion and Flame, vol. 138 (2004): pp. 401-403.

F. J. Weinberg, D. M. Rowe, G. Min; "Novel high performance small-scale thermoelectric power generation employing regenerative combustion systems"; J. Phys. D: Appl. Phys. 35 (2002): pp. L61-L63.

Wierzba, A. Depiac; "Catalytic oxidation of lean homogeneus mixtures of hydrogen/hydrogen-methane in air"; International Journal of Hydrogen Energy, vol. 29 (2004): pp. 1303-1307.

W. M. Yang, S. K. Chou, C. Shu, Z. W. Li, H. Xue; "Study of catalytic combustion and its effect on microthermophotovoltaic power generator"; Journal of Physics D: Applied Physics, vol. 38 (2005): pp. 4252-4255.

W. M. Yang, S. K. Chou, C. Shu, Z. W. Li, H. Xue; "Development of microthemophotovoltaic system"; Applied Physics Letters, vol. 81-27 (2002): pp. 5255-5257.

S. Zhao, J. Zhang, D. Weng, X. Wu; "A method to form well-adhered γ-Al_2O_3 layers on FeCrAl metallic supports"; Surface and Coating Technology, Vol. 167 (2003): pp. 97-105.

M. F. M. Zwinkels, O. Haussner, P. Govind Menon, S. G. Jaras; "Preparation and characterization of $LaCrO_3$ and Cr_2O_3 methane combustion catalysts supported on $LaAl_{11}O_{18}$- and Al_2O_3- coated monoliths"; Catalysis Today, vol. 47 (1999): pp. 73-82.